VŠB – Technical University of Ostrava
Faculty of Electrical Engineering and Computer Science
Department of Telecommunications

New Approaches Using Cognitive Radio in Green Networking

PHD THESIS

2021 Hong Nhu Nguyen

VSB TECHNICAL UNIVERSITY OF OSTRAVA | FACULTY OF ELECTRICAL ENGINEERING AND COMPUTER SCIENCE

Department of Telecommunications
17. listopadu 2172/15, 708 00 Ostrava–Poruba, Czech Republic

Ph.D. Dissertation Thesis:

NEW APPROACHES USING COGNITIVE RADIO IN GREEN NETWORKING

Ostrava, 2021

Doctoral Study Program:
P1807 Computer Science, Communication Technology and Applied Mathematics

Doctoral Study Branch:
2601V018 Communication Technology

PhD. Student:
Hong Nhu Nguyen
VSB – Technical University of Ostrava
Faculty of Electrical Engineering and Computer Science
Department of Telecommunications
17. listopadu 2172/15, 708 00 Ostrava–Poruba, Czech Republic
nhu.hong.nguyen.st@vsb.cz

Supervisor:
Assoc. prof. Jaroslav Zdrálek
VSB – Technical University of Ostrava
Faculty of Electrical Engineering and Computer Science
Department of Telecommunications
17. listopadu 2172/15, 708 00 Ostrava–Poruba, Czech Republic
jaroslav.zdralek@vsb.cz

Declaration

I declare that I have written my doctoral thesis on the theme of "New Approaches Using Cognitive Radio in Green Networking" independently, under the guidance of the doctoral thesis supervisor and using the technical literature and other sources of information which are all quoted in the thesis and detailed in the list of literature at the end of the thesis. As the author of the doctoral thesis I furthermore declare that, as regards the creation of this doctoral thesis, I have not infringed any copyright. In particular, I have not unlawfully en-croached on anyone's personal and/or ownership rights and I am fully aware of the consequences in the case of breaking Regulation S 11 and the following of the Copyright Act No 121/2000Sb., and of the rights related to intellectual property right and changes in some Acts (Intellec-tual Property Act) and formulated in later regulations, inclusive of the possible consequences resulting from the provisions of Criminal Act No 40/2009 Sb., Section 2, Head VI, Part 4.

Ostrava, August 2021

Acknowledgements

First of all, I would like to express my sincere gratitude to my supervisor **Assoc. prof. Jaroslav Zdrálek** for supervising my doctoral study.

Special thanks go to **Dr. Dinh-Thuan Do** for his consultations and for always being very professional. He guided me into this challenging and interesting research and inspired me to explore the science with consistent encouragement and tremendous support.

I would like to take this opportunity to thank my dear friends Mr. Hung, Mr. Long and Mr Nam for their sincere support and friendship, and for the happy times, we spent together throughout our journey at the VSB - Technical University of Ostrava.

My thoughts also go to my extended family and friends, who deserve my gratitude for their help and support. I specifically want to thank my father, and brothers for always supporting and being there for me.

Most important, I would like to express my sincere thanks to my beloved wife Hong Phuoc, and to our sons Thinh and Phuc. Your unconditional love, sacrifice and, support have been endless sources of strength, and purpose in my life. I love my family.

Abstrakt

Zelené sítě jsou energeticky efektivní síťové architektury a považujeme je za základ bezdrátové komunikace optimalizující spotřebu energie. Tímto směrem se ubírají budoucí komunikační technologie, což znamená, že budou méně energeticky náročné a v některých případech dokonce energeticky soběstačné. Kognitivní rádiové (CR) sítě, kooperativní relay sítě a neortogonální vícenásobné přístupové (NOMA) techniky jsou považovány za účinný prostředek k usnadnění získávání energie (EH) a přidělování výkonového spektra pro minimalizaci celkového vysílacího výkonu, díky čemuž je bezdrátová komunikace zelenější.

Disertační práce se skládá ze tří výzkumných částí odpovídajících cílům. První cíl se zabývá modelem bezdrátového přenosu radiofrekvenční (RF) energie pro systémy D2D. Aby bylo možné získat více energie, jsou pro přenosovou D2D síť použity základnové stanice s více anténami a napájecím radiomajákem. Pro navržený model jsou odvozeny pravděpodobnosti výpadků, kdy tyto výrazy jsou v uzavřené formě. Dále jsou k ověření platnosti získaných teoretických výrazů použity nezávislé simulace. Ve druhém cíli jsou navrženy a zkoumány nové modely kooperativního systému. Aby bylo dosaženo druhého cíle, sekundární zdroj funguje jako relay uzel a využívá režim AF (Amplify and Forward), který slouží vzdáleným NOMA uživatelům za specifických interferenčních podmínek. Abychom poskytli podrobné zhodnocení výkonnostních metrik systému, odvodili jsme vztahy v uzavřené formě pro pravděpodobnost výpadků a průměrnou propustnost více uživatelů za přítomnosti interferenčních omezení. V posledním cíli disertační práce jsme navrhli nový systémový model pro hybridní satelitně-terestrickou kognitivní síť (HSTCN) založenou na neortogonálním vícenásobném přístupu (NOMA) propojující satelit a více terestrických uzlů. Zkoumána byla spolehlivost a zabezpečení přenosu s důrazem na minimalizaci celkového vysílacího výkonu. Pro dosažení třetího cíle jsme zkoumali následující výkonnostní faktory: pravděpodobnost výpadku, poškození hardwaru, pravděpodobnost zachycení a průměrnou propustnost. Pro tyto výkonnostní faktory jsou odvozeny v uzavřených formách nové výrazy. V neposlední řadě jsme rovněž simulovali nový systémový HSTCN model. Dosažené výsledky potvrdily, že nově navržené přístupy umožňují zohledňovat požadavky na kvalitu služeb a jsou použitelné v budoucích zelených sítích.

Klíčová slova: Kognitivní rádio, NOMA, hybridní satelitní a terestriální kognitivní sítě, získávání energie, pravděpodobnost výpadku, propustnost.

Abstract

The green networks are energy-efficient network architectures and we consider them as the basis of the wireless communication optimizing energy usage. Indeed, future communication technologies are moving in this direction, meaning that they will be less energy-intensive and, in some cases, even energy self-sufficient. Specifically, cognitive radio (CR) networks, cooperative relay networks, and non-orthogonal multiple access (NOMA) techniques have been considered as effective means to facilitate energy harvesting (EH) and a power spectrum allocation for the minimization of total transmit power, hence, making the wireless communication greener.

The dissertation consists of three research sections corresponding to the aims. The first aim deals with an radio frequency (RF) wireless energy transfer model for D2D systems. In order to harvest more energy, a multiple-antenna base station and a power beacon are adopted for the D2D transmission network. We derive expressions outage probability in closed-forms. Further, independent simulations are used to validate the exactness of the theoretical expressions. In the second aim, new cooperative system models are proposed and studied. To reach the second aim, the secondary source acts as a relay and employs Amplify and Forward (AF) mode to serve distant NOMA users under a given interference constraint. To provide a detailed examination of the system performance metrics, we derived closed-form formulas for the outage probability and average throughput of the multi-users in the presence of interference constraints. In the last aim of the dissertation, we designed a new system model for a hybrid satellite-terrestrial cognitive network (HSTCN) relying on NOMA interconnecting a satellite and multiple terrestrial nodes. Reliability and security of transmission were studied to minimize the total transmit power. To reach the third aim, we examined the following performance factors: outage probability, hardware impairment, intercept probability, and average throughput. The novel closed-forms expressions of these performance factors are derived. The last but not at least, we simulated the new HSTCN system model. The achieved results figured that the new proposed approaches make it possible to take into account service quality requirements and are applicable in future green networking.

Keywords: Cognitive radio, NOMA, hybrid satellite-terrestrial cognitive networks, energy harvesting, outage probability, throughput.

Contents

List of Figures

List of Tables

List of symbols and abbreviations

5G	–	Fifth Generation
6G	–	Sixth Generation
AF	–	Amplify-and-Forward
ASC	–	Average Secrecy Capacity
AWGN	–	Additive White Gaussian Noise
BPCU	–	Bit per Channel Use
BER	–	Bit Error Rate
BF	–	Beamforming
CRNs	–	Cognitive Relay Networks
CCI	–	Co-Channel Interference
CDF	–	Cumulative Density Function
CHSTRN	–	Cognitive Hybrid Satellite-Terrestrial Relaying Network
CR	–	Cognitive Radio
CSI	–	Channel State Information
CUE	–	Current User Equipment
D2D	–	Device-to-Device
DF	–	Decode-and-Forward
DSA	–	Dynamic Spectrum Access
EC	–	Ergodic Capacity
ERs	–	Energy Receivers
EH	–	Energy Harvesting
FD	–	Full-Duplex
HSAT	–	Hybrid Satellite-Aerial-Terrestrial
HD	–	Half-Duplex
HI	–	Hardware Impairment
HSTCN	–	Hybrid Satellite-Terrestrial Cognitive Networks
IoT	–	Internet of Things
IT	–	Information Transmission
IP	–	Intercept Probability
LMS	–	Land Mobile Satellite
LoS	–	Line-of-Sight
LTE	–	Long Term Evolution
MAC	–	Medium Access Control
MIMO	–	Multiple-Input Multiple-Output
MISO	–	Multiple-Input Single-Output
MRC	–	Maximal Ratio Combining

MUs	–	Mobile Users
NLoS	–	Non Line-of-Sight
NOMA	–	Non-Orthogonal Multiple Access
OMA	–	Orthogonal Multiple Access
OP	–	Outage Probability
OWR	–	One-Way Relaying
PB	–	Power Beacon
PDF	–	Probability Density Function
PLS	–	Physical-Layer Security
PN	–	Primary Network
PSR	–	Power Splitting-based Relaying
PU	–	Primary User
QoS	–	Quality of Service
RF	–	Radio Frequency
RS	–	Relay Selection
RV	–	Random Variable
SATINs	–	Satellite-Aerial-Terrestrial Integrated Networks
SDUs	–	Secondary Destination Users
SER	–	Symbol Error Rate
SN	–	Secondary Network
SNR	–	Signal Noise Ratio
SU	–	Secondary User
SINR	–	Signal Interference plus Noise Ratio
SISO	–	Single-Input Single-Output
SOP	–	Secrecy Outage Probability
SWIPT	–	Simultaneous Wireless Information and Power Transfer
TPSR	–	Time-Switching and Power Splitting
TWR	–	Two-Way Relaying
TWRN	–	Two-Way Relaying Network
TWFD	–	Two-Way Full Duplex
TSR	–	Time Switching-based Relaying
TWR	–	Two-Way Relaying
UAV	–	Unmanned Aerial Vehicle
WPNR	–	Wireless Powered NOMA Relaying
WPT	–	Wireless Power Transfer

1 Introduction

1.1 Motivation and Goals

Soon, EH wireless networks are expected to introduce several transformative changes in wireless networking [3]. While conventional wireless devices are powered with batteries, energy in EH wireless devices may be continuously and stably supplied by available radio frequency (RF) sources over the air [4]. Advanced relay networks suffer from energy depletion problems as a result of relaying activities and user mobility. A prospective approach therefore is to apply EH technologies to relay networks.

The thesis will examine amplify-and-forward (AF) and decode-and-forward (DF) protocols in both full-duplex (FD) and Half-duplex (HD) relay networks which apply EH, in which relay nodes without batteries harvest energy from the received RF signals from a source node and use the harvested energy to forward the source information to destination node. Time-switching-based relaying (TSR) and power-splitting-based relaying (PSR) [5] will be studied as EH relaying protocols.

CR [6, 7] and cooperative communication techniques will be applied extensively in the research to explore improvements for the effective use of wireless radio resources. The two following problems will be addressed:

- Exploration of the power spectrum in wireless communication networks.
- Opportunistic exploitation and identification of spectrum holes [8] which are momentarily unused by the licensed owners of the spectrum.

To facilitate massive connectivity, even more advantages can be achieved by employing multiple access for mobile users, especially if the network allocates resources to users by dividing the total radio resources according to orthogonal multiple access (OMA) and non-orthogonal multiple access (NOMA). Interference can be eliminated under the OMA scheme, while NOMA employs a successive interference cancellation (SIC) technique to mitigate interference from other users' signals [9]. By exploiting the users' channel asymmetries, NOMA can significantly enhance the SE and thereby reduce transmission latency [10–13]. The authors in [14] showed that the achievable rate region in the NOMA uplink is improved in comparison with OMA. This type of analysis has been adopted in wireless powered communications (WPC) networks. In [15], the main results showed that NOMA's advantage is improved user fairness and that it grants more benefits than OMA. The results also demonstrated that NOMA's downlink and uplink performance is better than OMA because it solves the problem of joint maximization of the downlink/uplink rates while ensuring fairness between users [16].

The development of hybrid satellite-terrestrial relay networks (HSTRNs) is one of the driving forces in revolutionizing satellite communications in the modern era. In HSTRNs, satellite communications and terrestrial networks are integrated to provide useful services in broadcasting,

navigation and disaster relief [17]. To enhance coverage, much research has also been directed towards these networks in employing cooperative relaying techniques [18, 19]. Recently, cognitive radio assisted NOMA has become an important component to improve spectrum utilization efficiency in HSTRNs [20]. This prompts a promising architecture, referred to as a NOMA-based cognitive HSTRN [21]; this type of network allows a secondary terrestrial network to share the spectrum with the primary satellite network. Consequently, the use of HSTRNs are becoming more important in the seamless integration of terrestrial cellular and satellite communications.

1.2 Purpose of the Research

- A survey and exploration of wireless relay network models for EH and information transmission strategies.
- Investigation of the integration of NOMA with CR into a holistic system, i.e. a cognitive NOMA network, for more intelligent spectrum sharing. I discussed open challenges and research directions on the implementation of cognitive NOMA networks.
- Analysis of the performance and throughput of these types of systems through equations describing the probability of instantaneous channels.
- Simulation and evaluation of the performance and throughput of the systems.

1.3 Dissertation Thesis Structure

This dissertation is organized as follows:

- Chapter 1 Introduction
- Chapter 2 Presents the background of the dissertation.
- Chapter 3 Shows the State-of-the-Art.
- Chapter 4 Determines the aims of the proposed research.
- Chapter 5 Investigation and proposal of the system model energy harvesting and information transmission for wireless relaying network models.
- Chapter 6 Proposal of cooperative relaying network using CR-NOMA and proposal of calculating and analyzing to enhance power spectrum distribution efficiency of users in wireless communication.
- Chapter 7 Design of reliable and secure transmission in multiple antennas hybrid satellite-terrestrial cognitive networks relying on NOMA to further strengthen power distribution efficiency of integrated network.

- Last but not least, chapter 8 contains a conclusion and future work plans. The references and candidate's published results cited are at the end of the dissertation.

2 Background

This chapter aims to present some concepts and technologies that give better understanding for my work. The first concepts are about wireless power transmission (WPT), and simultaneous wireless power and information transmission (SWIPT). As a next step, in order to minimize the shortage of wireless communication spectrum, my work aims to the combination of the concepts of cooperative communication techniques and cognitive radio networks with the aim of increasing spectrum efficiency and system throughput is provided. Furthermore, an integrated system model between satellite and terrestrial is proposed in this chapter, which presents new ideas into the wireless communication system. In overall, this is the essential knowledge to understand my research that will be worked on later in this dissertation.

2.1 Cognitive Radio Network

2.1.1 Cognitive radio Definition

In a study of J. Mitola in 1999, CR Technology was presented [6]. CR is a form of wireless communication in which the working status of communication channels is detected, and immediately moved into vacant channels while preventing occupied ones. This both improves the function of available RF spectrum and decreases interference for other users. There have been many different academies and regulatory bodies giving different definitions of CR since it was introduced.

- *Mitola gives more detailed definition of the CR as in* [22]: Wireless individual digital assistants and the related networks has enough computing power about radio resources, and related computer-to-computer communications, to discover user needs as a function of use context and to support radio resources and wireless services most applicable to those needs.

- *In 2005, CR was defined by S. Haykin as in* [7]: The cognitive radio is defined as an intelligent wireless communication system that uses a building-by-building understanding method to learn from its environment and adjust its internal states to statistical variations when RF ex-citations come by changing correspondingly in particular operating parameters in real time to achieve high dependability and efficient use of the radio spectrum.

- *Wikipedia:* Cognitive radio is a paradigm for wireless communication in which either a network or a wireless node changes its transmission or reception parameters to communicate efficiently, avoiding interference with licensed or unlicensed users. This alteration of parameters is based on the active monitoring of several factors in the external and internal radio environment, such as radio frequency spectrum, user behavior, and network state.

2.1.2 Spectrum Sharing techniques

The emergence of multi-utility new wireless products and services has resulted in a huge increase in demand for spectrum resources in recent years, bringing many challenges for service providers and regulators. However, the Federal Communications Commission (FCC) Spectrum Policy Task Force has made measurements using actual spectrum which show that at any given time and place, most of the authorized spectrum will not work. In such a framework, secondary (unauthorized) systems coexist with primary (authorized) user systems and access spectrum on a sharing basis. This unused or underused spectrum of certain service providers or authorized users is known as "spectrum hole" [23].

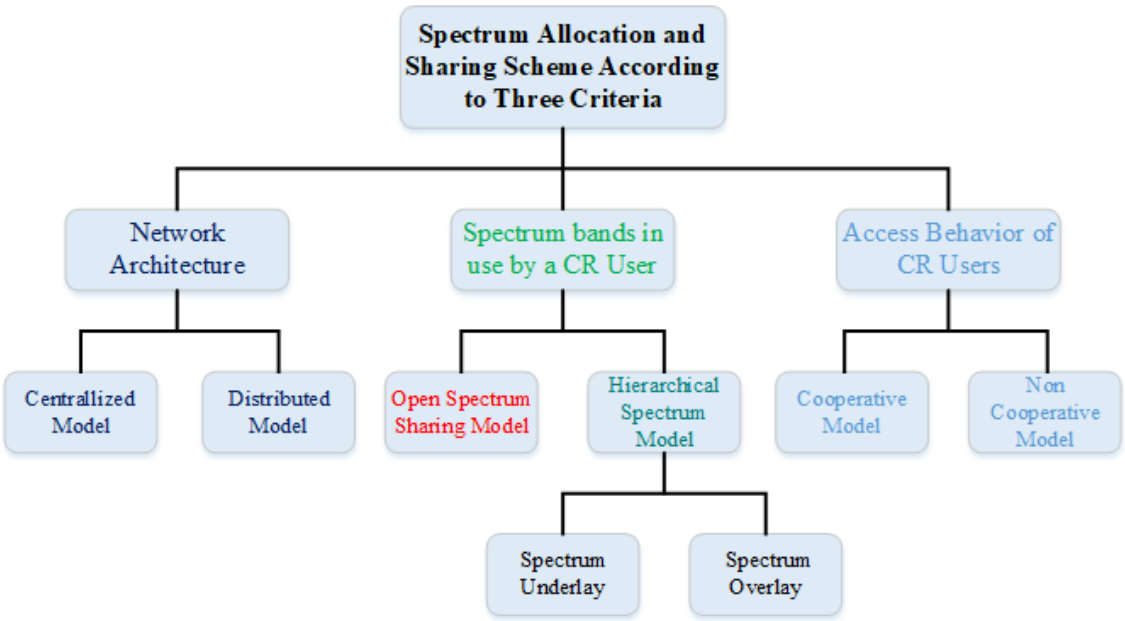

Figure 2.1: Spectrum sharing in Cognitive Radio Network

.

2.1.2.1 Spectrum sensing

The cognitive radio network has an important task of scanning the entire frequency band for the presence of a primary user called a spectral sensor, and it can perform either locally by a single cognitive user or collectively by a group of cognitive users. Spectral sensing techniques enable to be aware of the surrounding environment. Cognitive users utilize unused spectrum bands flexibly by allowing spectrum sensing. In order to detect and record the activity of the primary and secondary users, energy detection, matched filter detection, and cyclostationary feature detection are utilized.

Furthermore, to determine their suitability for communication, the available frequency bands are examined. In order to determine the most suitable frequency range, possible characteristics

such as signal-to-noise ratio (SNR), link error ratio, delay, noise, and hold time can be utilized. When a suitable frequency band is obtained, the cognitive users transmission in that frequency band will take place. If a cognitive user detects a primary user's transmission, it must clear the corresponding band and search for an unused band, which is known as spectrum distribution. Cognitive radio networks will be vulnerable due to the delays involved in spectrum distribution. A cognitive radio transceiver examines unused spectrum or spectrum holes and using an accessing method without interfering with the primary user's transmissions.

2.1.2.2 Spectrum analysis

The spectrum sensor uses the obtained information to plan spectrum access by unauthorized users. Therefore, unauthorized user communication requests are also used to optimize the transmission parameters. The information from the spectrum sensor is examined to estimate interference, time availability, and collision anticipation with authorized users due to sensor failure. After optimizing system performance, spectrum access decisions were made in order to maximize throughput by unauthorized users and limiting interference caused to authorized users below the target threshold.

2.1.2.3 Spectrum sharing

Base on a cognitive medium access control (MAC) protocol, spectrum access is used to prevent collision with the authorized users as well as with other unauthorized users. The DSA method remarkably enhances the function of frequency bands and improves the performance of communication systems. The DSA approach in cognitive radio technology has an important advantage of sharing spectrum, which enables for efficient and fair spectrum distribution or scheduling solutions between authorized and cognitive users. Thanks to the spectrum sharing model, the radio spectrum can be shared simultaneously between the main user network and the cognitive network. Moreover, unauthorized or cognitive users may expectantly access the radio spectrum if it has no users or is not fully utilized by primary users. The unauthorized users are also allowed to access the spectrum provided that the interference level at the primary receiver is kept below a defined threshold so as not to disrupt the primary user's ongoing communication.

2.1.2.4 Spectrum mobility

Spectrum mobility shows the ability of a cognitive radio user to change the operating frequency range. When an authorized user first accesses a radio channel occupied by an unauthorized user, the unauthorized user may switch to an inactive band. The protocol parameters at other layers in the protocol stack are regulated to accommodate the new operating frequency band during this spectrum handover. Spectrum distribution ensure that data transmission by unauthorized users can go on in the new spectrum band. Spectrum mobility enables cognitive radio users to switch to unused frequency bands if a primary user is present during ongoing cognitive radio communication.

2.1.3 Cognitive Radio Network Architecture

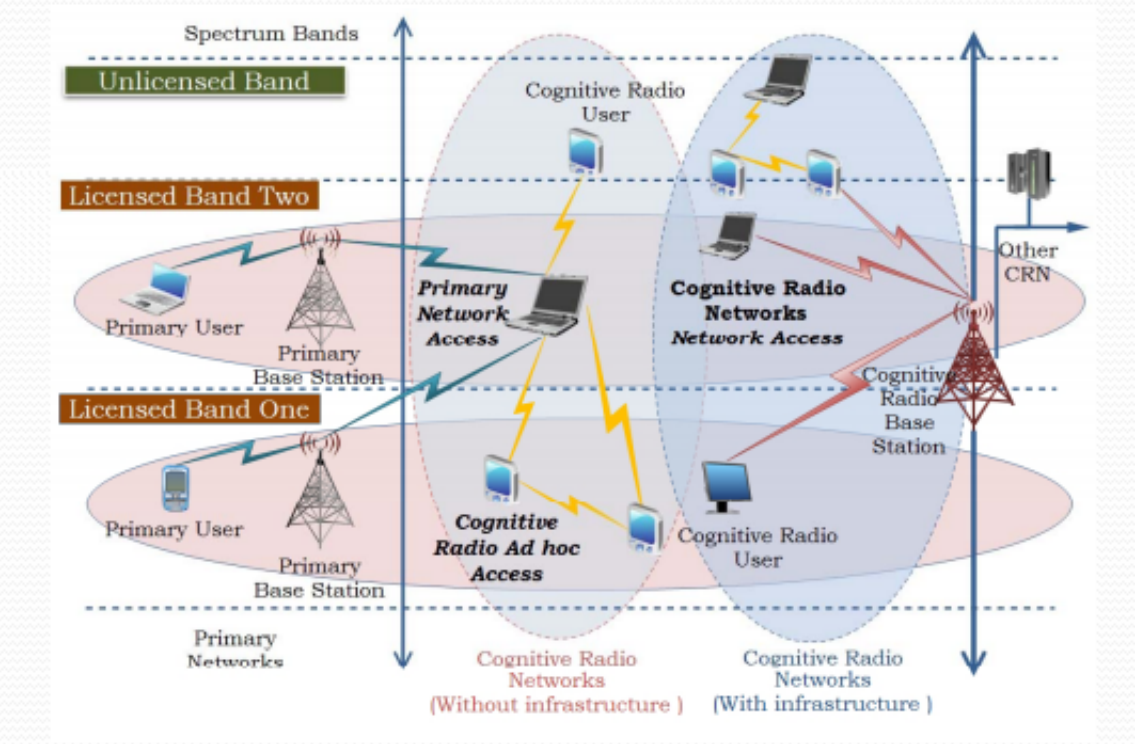

Figure 2.2: Cognitive Radio Architecture [1]

.

Cognitive radio networks with dynamic spectrum access (DSA) techniques can accept either cooperative or non-cooperative network architectures. Each cognitive node in a non-cooperative cognitive radio network architecture make its own decision. Furthermore, in the centralized, collaborative cognitive radio network architecture, a joined server has a database of spectrum availability and accesses information from cognitive users. As a result, spectrum management is simpler and allows efficient spectrum sharing. The dynamic spectrum access techniques in a collaborative but assigned cognitive radio network architecture depend on equivalent actions to attain performance that is related to universally excellent performance.

- **MAC layer**: The spectrum sensing and making decisions activity regarding spectrum access on a channel. Other important MAC layer tasks contain synchronizing transmission parameters between transmitter and receiver, facilitating negotiation between primary and cognitive users, and assisting spectrum trading functions.
- **Network layer**: The network layer's primary tasks contain topology construction, addressing, and routing. Under topology construction, spectrum detection, neighbor discovery, and topology management are examined.

- **Transport layer**: The transport layer is in charge of flow and congestion control, which is influenced by MAC protocol performance and spectrum mobility.

2.2 Integrated Networks Satellite-Terrestrial

Satellite-to-terrestrial integrated network combines with satellite network and terrestrial network, providing smooth and global Internet access. It is a significant technological opportunity and challenge for the future growth of hybrid networks. Satellite network access is one of the effective ways to achieve global connectivity, especially for far-distance areas where modern telecommunications infrastructure is difficult to access. Consequently, it is necessary to study a new type of integrated terrestrial-satellite network architecture and its protocol system based on the available Internet architecture. The future integrated wireless communications will bring together not only people but also things, data, applications, smart cities, and transportation in an intelligent, integrated, and seamless networked society, Internet of things, Industry 4.0, automotive and transportation sectors, e-Health, and factories of the future The integrated wireless communication of the future will bring not only people but also everything of the future (Figure 2.3).

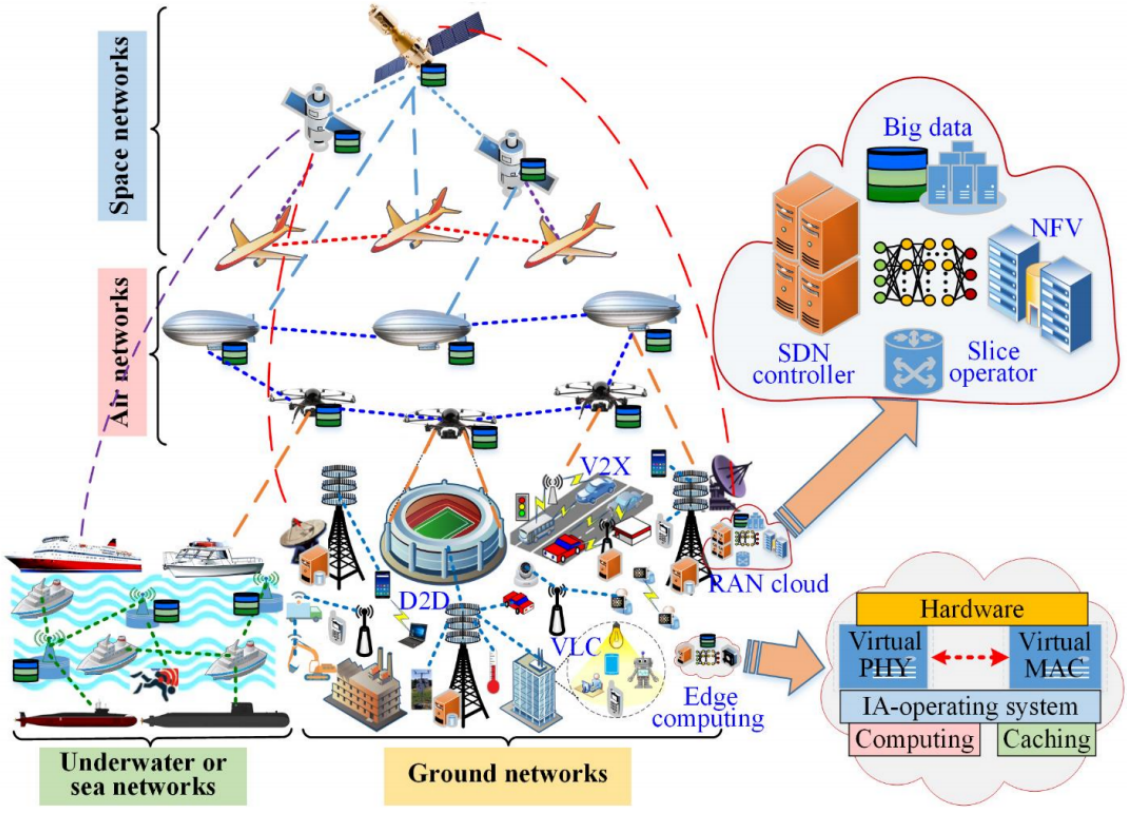

Figure 2.3: Integrated Satellite-Terrestrial architecture [2]

.

Satellites are relay stations in space for the transmission of voice, video, and data communications. They are ideally suited to meet the global communications requirements of military, government, and commercial organizations because they provide economical, scalable, and highly reliable transmission services that easily reach multiple sites over vast geographic areas.

- Fixed Satellite Services (FSS) uses ground equipment at set locations to receive and transmit satellite signals. FSS satellites support the majority of the nation and international services.
- Mobile Satellite Services (MSS) uses a variety of transportable receiver and transmitter equipment to provide communication services for terrestrial mobile, sea, and air customers.
- Broadcast Satellite Services (BSS) offers high transmission power for reception using minimal terrestrial equipment. BSS is best known for television and broadband applications services.

The downlink is the link from a satellite down to one or more terrestrial stations or receivers in satellite telecommunication, and the uplink is the link from the terrestrial station up to the satellite. The following Table 2.1 shows the major frequency bands used for satellite links.

Table 2.1: The main frequency bands used for satellite and mobile links.

Communication	**Frequency Band**	**Dowlink Frequency Range**	**Uplink Frequency Range**
Satellite	C	3,700 – 4,200 MHz	5,925 – 6,425 MHz
Satellite	K_u	11,7 – 12,2 GHz	14,0 – 14,5 GHz
Satellite	K_a	17,7 – 21,2 GHz	27,5 – 31,0 GHz
Mobile	GSM-900	1805 - 1880 MHz	1710 - 1785 MHz
Mobile	GSM-1800	935 - 960 MHz	890 - 915 MHz

2.3 Radio Frequency Energy Harvesting

Along with the explosive growth of the wireless communication industry and the development of the green revolution, the change in power supply in wireless communication related to the energy consumption of wireless networks and devices has attracted a great deal of attention from the academic and industrial research communities. On the other hand, taking the place of batteries for low-cost devices in power-constrained networks is either inaccessible or high-priced. Energy harvesting is considered as an emerging solution of great interest to solve these problems, because it provides power to mobile devices by collecting energy from the surrounding environment (solar energy, wind, vibration, thermoelectric effect, ambient radio energy, etc.). The use of energy-collecting nodes is a hopeful approach to improve the energy efficiency of wireless communication systems. The Figure 2.3 illustrates the main components of energy and spectrum collecting of wireless communication systems [24].

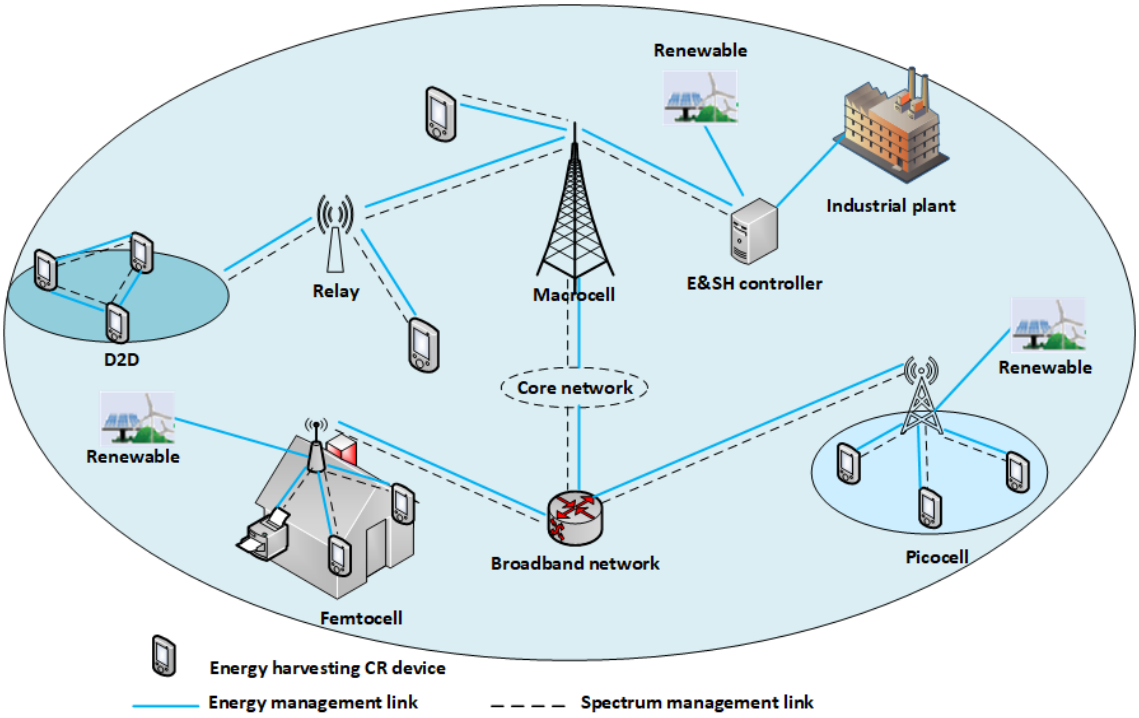

Figure 2.4: Energy harvesting cognitive radio architecture

.

In Figure 2.4, The devices harvest energy from BS (the dashed line) and the information transmission components (the line) to connect the system presented. It should be noted that each node in the EH and IT is provided with a separate RF energy receiver and corresponding RF transceiver. Therefore, both EH and information transmission can be performed simultaneously. Thus, there are two realistic designs for relay node EH and information transmission of wireless communication. Authors strictly studied performance analysis of these two EH strategies [25,26]. This section describes the basic system model for EH in a HD relay network with two EH and information transmission protocols.

2.3.1 Time switching-based relay protocol (TSR)

In Figure 2.5, TS receiver model switches between EH and information decoding mode at relay are presented. T is the block time in which a certain block of information is transmitted from the source node to the destination node, and α is the fraction of the block time during which the relay harvests energy from the source signal, where $0 \leq \alpha \leq 1$. The first interval corresponds to the EH phase, while the remaining block time $(1-\alpha)T$ is used for information transmission such that half, i.e. $(1-\alpha)T/2$, is used for the source-to-relay information transmission and half is used for the relay-to-destination information transmission.

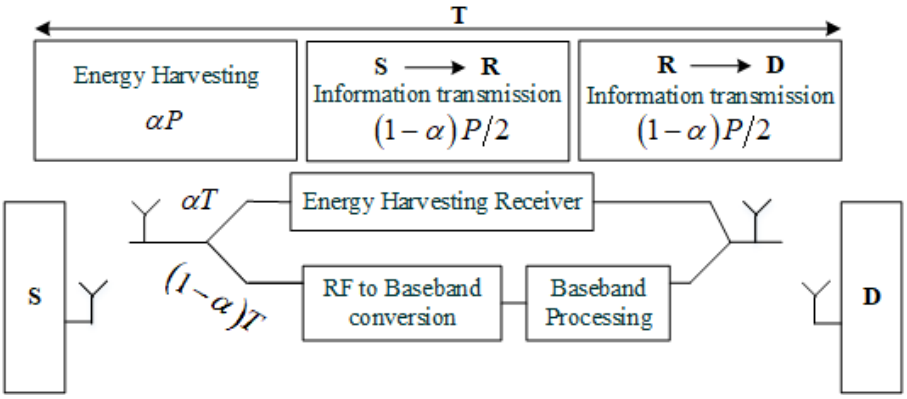

Figure 2.5: EH and data transmission processes in the TSR.

The received signal at the relay node in second phase can be expressed as

$$y_R = hx_R + n_R, \tag{2.1}$$

where h is the BS to relay channel gain, d_1 is the BS to relay distance, P_S is the transmitted power from the BS, $E\left\{|x_R|^2\right\} = 1$, where $E\{.\}$ is the expectation operator and $|.|$ is the absolute value operator, n_R is the zero-mean additive white Gaussian noise (AWGN) with variance $\sigma^2_{n_R}$. E_h during energy harvesting time αT is given by

$$E_h = \frac{\eta P_S |h|^2}{d_1^m} \alpha T, \tag{2.2}$$

where d_1 is the BS to relay distance, P_S is the transmitted power from the BS, m is the path loss exponent, $0 < \eta < 1$ is the energy conversion efficiency which depends on the rectification process and the energy harvesting circuitry.

The transmitted power from the relay node, P_R is given by

$$P_R = \frac{2\eta P_S |h|^2 \alpha}{d_1^m (1-\alpha)}. \tag{2.3}$$

2.3.2 Power splitting-based relay protocol (PSR)

The PSR protocol and block diagram for EH and information processing at the relay are presented in Figure 2.6. T is the total block of relay information transmission. The first $T/2$ interval is used for the source-to-relay information transmission and the remaining half, $T/2$ is used for the relay-to-destination information transmission. During the first half of the block time, the fraction of the received signal power, εP_S is used for EH, while the remaining received power, $(1-\varepsilon) P_S$ is used for the source-to-relay information transmission, where $0 \leq \varepsilon \leq 1$.

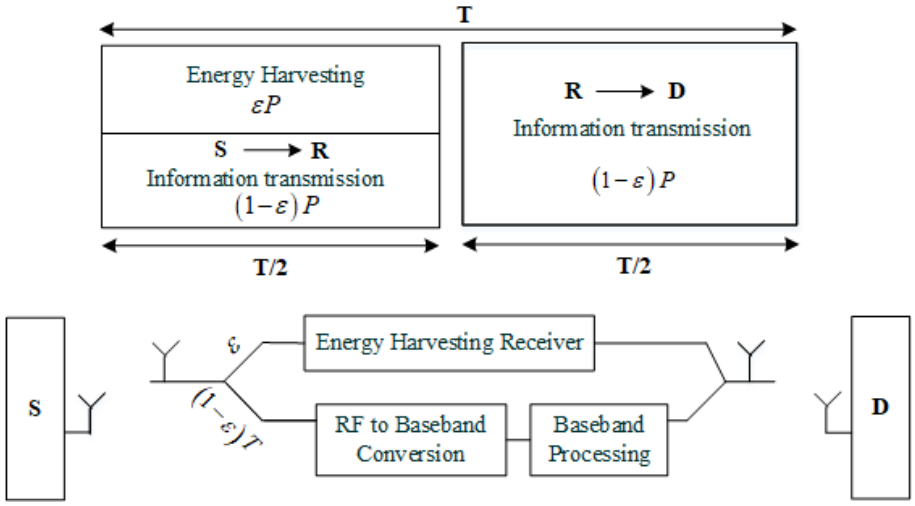

Figure 2.6: EH and data transmission processes in the PSR.

The power splitter splits the received signal in ε: $1-\varepsilon$ proportion, such that the portion of the received signal, $\sqrt{\varepsilon}x_R$ is sent to the energy harvesting receiver and the remaining signal strength, $\sqrt{1-\varepsilon}x_R$ drives the information receiver. E_h at the relay is given by

$$E_h = \frac{\eta\varepsilon P_S|h|^2}{d_1^m}(T/2), \tag{2.4}$$

where the energy is harvested at the relay during half of the block time, $T/2$, and $0 < \eta < 1$ is the energy conversion efficiency.

The transmitted power from the relay node, P_R is given by

$$P_R = \frac{\eta\varepsilon P_S|h|^2}{d_1^m}. \tag{2.5}$$

2.3.3 Energy harvesting in NOMA-enabled relay systems: two SIC modes and performance evaluation

The results are achieved by applying TSR, PSR protocols of RF energy harvesting, and information transmission with harvest energy at relay node from BS and power beacon to improve the performance of wireless communication [25, 26]. **[NHN06]**, **[NHN08]**, **[NHN09]**.

In this section, we deployed to design and perform analysis of a new system model using a relaying model, energy harvesting, and NOMA network. It is called such topology as wireless powered NOMA relaying (WPNR). In the proposed model, NOMA was investigated in two cases including single successive interference cancellation (SIC) and dual SIC. Moreover, the SWIPT technology can be employed to feed energy to relays that intend to serve far NOMA users. In particular, exact outage probability expressions are provided to performance evaluation **[NHN08]**.

We examined the wireless communication system depicted in Figure 2.7. The base station is indicated by BS (assigned wireless power transfer capability), the two relays are indicated by R_1 and R_2 and can be approached using NOMA, and the two remote users are indicated by U_1 and U_2. The separated Rayleigh channel factors between the BS and R_1 and R_2 are h_{R_1} and h_{R_2}. Between R_1 and U_1 and R_2 and U_2, these factors are h_{U_1} and h_{U_2}, respectively. Two SIC modes are deployed here: dual SIC is required at link $BS - R_1 - U_1$, while a single SIC is assigned at link $BS - R_2 - U_2$.

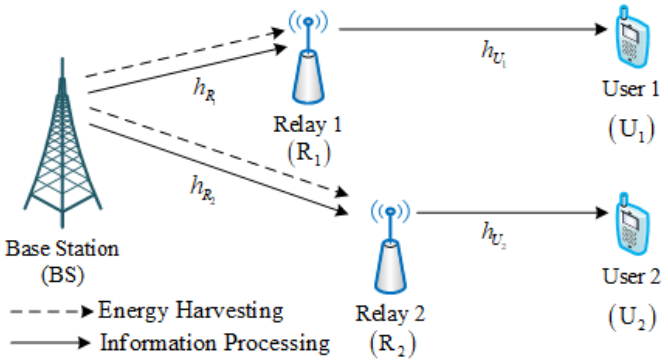

Figure 2.7: System model for EH NOMA network.

SWIPT technology is employed to feed energy to relays which will serve distant NOMA users [25].

First, the BS transmits a superimposed NOMA signal $\left(\sum_{i\in 1,2} x_i a_i\right)$ to R_1 and R_2 with power distribution fractions a_1 and a_2, respectively, where $a_1 < a_2$ and $a_1^2 + a_2^2 = 1$. The received signal at relay R_1 and R_2, respectively is given as

$$y_{R_1}^{T_1} = \sqrt{a_1 P} x_1 h_{R_1} + \sqrt{a_2 P} x_2 h_{R_1} + n_{R_1}, \tag{2.6}$$

and

$$y_{R_2}^{T_1} = \sqrt{a_1 P} x_1 h_{R_2} + \sqrt{a_2 P} x_2 h_{R_2} + n_{R_2}, \tag{2.7}$$

In this case, x_1 and x_2 are signal intended for U1 and U2, respectively, $n_{R_1} \sim CN\left(0, \sigma_{R_1}^2\right)$ and $n_{R_2} \sim CN\left(0, \sigma_{R_2}^2\right)$ define the additive white Gaussian noise (AWGN) at R_1 and R_2 with equivalent variance $\sigma_{R_1}^2 = \sigma_{R_2}^2 = \sigma^2$.

In order to deploy the relay structure, the two relays in WPNR harvest energy from the signals x_e transmitted by the BS in the second phase with $E\left\{|x_e|^2\right\} = 1$. When R_1 is closer BS than R_2, it harvests more energy than R_2. This unbalance is verified by R_1 consumes more energy to analyze data and transmits it to U_1. All of the powers harvested in this phase as follows

$$P_{R_1}^{T_1} = \frac{\eta P \alpha |h_{R_1}|^2}{3}, \tag{2.8}$$

and

$$P_{R_2}^{T_2} = \frac{\eta P \alpha |h_{R_2}|^2}{3}, \tag{2.9}$$

where $0 < \eta < 1$ stands for the efficiency coefficient of the energy conversion process, $0 < \alpha < 1$ the percentage of energy harvesting, and P denotes the transmission power of the source BS.

3 State-of-the-Art

As we step deeper into the twenty-first century, the need to strengthen network capacity is due to the increasing demand of users. This can be realized thanks to the emerging fifth-generation (5G) cellular network. In [27], the authors paid attention to the 5G network architecture including the device-to-device (D2D) communication and massive Multiple-Input Multiple-Output (MIMO) technology. Cooperative communication [28] relies on the broadcast nature of wireless communications to allow nodes to assist each other in attaining the same advantages as those offered by MIMO systems [29]. Various cooperative techniques have been widely investigated since the turn of the century. In [30, 31], several basic cooperative protocols were evaluated for their power-saving, diversity order, and outage probability parameters. Relay network, optimal resource allocation, and network-coded cooperation were investigated in [32,33]. Recent studies, an emerging of technologies that help to enhance the performance of wireless networks were considered, such as the spectrum sharing with cognitive radio (CR), full-duplex (FD), half-duplex (HD), cloud, ultra-dense networks, millimeter-wave solutions, interference management, and multi-radio access technology association. On the other hand, network capacity enhancement can be done with the distribution of small cell base stations (e.g., micro, pico, and femto) beneath the common macro cell base stations (BS), i.e., heterogeneous networks (HetNet) [34,35]. Recent years have witnessed the growth of self-sustaining wireless networks to reduce the dependency on conventional stable power sources for the ease of deployment and lower environmental impact. The first goal is to explore radio frequency (RF) energy harvesting solutions in wireless communication environments. This solution is possible to support the transceiver of the system ensures quality transmit information of the better. In particular, the authors [36] performed an overview study on the energy harvesting (EH) technology and discussed it from various perspectives including the sources of energy, EH protocols, energy scheduling, energy optimization, EH implementation, etc. When we use ambient RF signals with new sources for EH, a suitable method of harvesting energy is simultaneous wireless information and power transfer (SWIPT) through the collection of energy from ambient RF signals [37]. Accordingly, this assists in improving the efficiency of the available energy consumption in the wireless device and the cost-effectiveness of its operation [38]. After studying the elements mentioned above, I will analyze the spatial design of future wireless networks in relation to outage probability (OP) and energy efficiency in a D2D network-enabled with EH and consider a system in a large-scale heterogeneous cellular network with an energy-limited D2D transmitter.

The second goal research focuses on examining the benefit of power spectrum optimization in wireless communication in which remote radio units are deployed to serve mobile users in areas with high data traffic demand. CR has been identified as a promising solution for spectrum scarcity, and its core idea is dynamic spectrum access. It can dynamically utilize the idle spectrum without affecting the rights of primary users so that multiple services or users can share a part of the spectrum [39]. With the provision of cognitive radios (CRs), the underuti-

lized spectrum resources can be exploited to gain more bandwidth for the bandwidth-hungry applications [40]. CR-based Internet of Things (IoT) system is an effective step toward a world of smart technology. Efficient spectrum sensing and sharing are the main functional components of the CR-based IoT [41]. Next-generation wireless networks are expected to support extremely high data rates and radically new applications, which require a new wireless radio technology paradigm. In which machine learning is one of the most promising artificial intelligence tools, conceived to support smart radio terminals [42]. To support multiple users, the NOMA technique can allocate the total radio resources to different users [43]. NOMA manages the interference by utilizing the successive interference cancellation (SIC) technique. NOMA can significantly improve spectrum efficiency by exploiting user channel asymmetry and also alleviate transmission latency [9–12]. The authors in [44] have studied an underlay CR-NOMA relaying network, where a secondary source communicates with multiple NOMA secondary destination users (SDUs) by means of a detect-and-forward secondary relay under imperfect channel state information conditions. In [13] The authors proposed NOMA for the uplink of WPC networks. In [45], it is shown that NOMA can significantly improve user fairness in both downlink and uplink [14, 15]. The proposed system model shows the CR-NOMA's superiority compared with cooperative OMA in [46]. The security energy efficiency (SEE) is investigated in a two-way FD relay-assisted CR-NOMA networks to improve system energy efficiency [47]. Motivated by the results in [48], I will propose a system model and formulate the received signal at the SU to extract the data signal using the SINR or SNR. The OP of the SU will be analyzed in detail in terms of the SINR and SNR probabilities. The results will consider CR-NOMA in terms of the OP, average throughput in providing fairness to the end-users.

Unexpected large-scale events quickly make the terrestrial network overloaded, paralyzed, or destroyed. Therefore, it is highly demanded to build an emergency network that can be deployed rapidly, offer a high data rate, and extend area coverage. The third goal approach is to consider the secure performance of hybrid satellite-terrestrial cognitive networks (HSTCNs) using NOMA in the contexts of multiple-antenna and cooperative spectrum sharing. The indexes evaluate to minimize the total transmit power of the system, including spectrum allocation efficiency, information security investigated. The emergence of aerial platforms, especially the low altitude platforms (LAPs), indicates a stable and reliable direction for developing an emergency network. Hybrid satellite-aerial-terrestrial (HSAT) networks can provide effective services rather than traditional infrastructures during emergencies [49]. Furthermore, with the rapid development of marine activities, there has been an increasing number of IoT devices on the ocean. Besides, the integrated satellite-terrestrial to support maritime field considered. The authors compute dynamic electromagnetic propagation environment, geometrically limited available BS sites and rigorous service demands from mission-critical applications [50]. The integration of terrestrial and satellite components has been widely studied to take advantage of both sides and enable seamless broadband coverage. In [51], the authors presented research to uncovering the complete picture of HSTNs. They regard the HSTN as a combination of basic cooperative models that

contain the main traits of satellite-terrestrial integration to envision an agile, smart, and secure HSTN for the sixth-generation (6G) IoT.

To accommodate the explosive demands of IoT within the crowded spectrum, CR-based satellite-aerial-terrestrial integrated network (SATINs) where spectrum sharing is enabled among satellite, aerial, and terrestrial network segments and devote to efficient resource management have been researched in [52]. In the article [53], the authors introduce the cooperative NOMA (C-NOMA) scheme into a two-layer geostationary Earth orbit/low Earth orbit satellite network in a frequency coexistence scenario. To applying a multi-branch optimal transmitting beamforming/receiving combination strategy, an upper bound of signal to noise (SNR) was investigated [54]. However, expected massive connectivity in future communication networks will face issues associated with spectrum scarcity. In this regard, integrating CR and NOMA techniques into satellite-terrestrial networks is considered a promising remedy [55]. Furthermore, efficient resource management mechanisms should be proposed to provide a complete system analysis for this promising architecture. Towards this direction, the authors in [56] focus on power management in cognitive satellite-terrestrial systems, where the satellite system has the role of the cognitive system. Mainly, the security of the system is essential interested. In [57,58], the authors propose to employ a multi-antenna base station (BS) as a source of green interference to enhance secure transmission in the satellite network. In [59, 60], the authors studied HSTRNs in which the satellite dispatched information to a destination through multiple relays. At the same time, an eavesdropper attempted to intercept the transmissions from both the satellite and relays. The authors explored the context of single-relay and multi-relay selection and round-robin scheduling schemes to address the physical-layer security (PLS) of this proposed HSTRN through the adoption of a DF relay scheme. The studies in [61, 62] investigated secure transmission for HSTRNs in which the terrestrial base station served as a green interference resource to enhance the security of the satellite link. The authors adopted a stochastic model for the channel state information uncertainty and proposed a secure and robust BF framework to minimize the transmit power while satisfying a range of outage (probabilistic) constraints at the satellite user and terrestrial user locations [63].

4 Research Aims

This section lists the aims and a plan of the research in my thesis. The aims consider the different techniques applied to the physical layer and two models which include Rayleigh, Rician and Nakagami-m channels. The performance metrics are varied and include OP performance based on satisfying required data rates, secrecy performance in terms of IP, the practical factors resulting from potential hardware impairments, and the average throughput of the system, which will be modeled as Gaussian random variables. Additionally, I will analyze a hybrid satellite-terrestrial system model.

4.1 Aim 1: Study and proposal of a D2D communication system model with energy harvesting and information transmission for various wireless relaying network models

Radio frequency (RF) energy transfer and harvesting techniques have recently become alternative methods of powering next-generation wireless networks. As a contribution to the development of EH techniques, I investigate the models for collecting energy in wireless communication networks from the authors [25, 26].

- In a comparison of TSR and the PSR protocols, the authors showed through numerical analysis that in delay-limited transmission mode, the throughput performance of the TSR protocol is superior to the PSR protocol at higher transmission rates, at a relatively lower SNR and a lower EH efficiency.
- My contributions are an EH solution which employs a relaying scheme with the benefit of WPT , and performance improvements in an IoT network for two distant users who need the assistance of a WPT-assisted relay [64]. SWIPT technology can also be employed to feed energy to relays designed to serve distant NOMA users [16].

The results of the effect of EH parameters, included as the TS factor and PS factor [25], motivated me to study D2D networks which use WPT and SWIPT technology for EH and information transmission. For the first aim, my thesis will propose a mathematical system model for D2D communication provided by an EH-assisted relay. To improve energy consumption and prolong the lifetime of a wireless communication network, I will compute the OP from the SNR and power allocation parameters. The mathematical model and the effects of the network parameters on the OP and the average throughput will be validate with simulations to corroborate the exactness of the derived expressions.

4.2 Aim 2: Study of a cooperative relaying system model which uses CR-NOMA to enhance the spectrum power allocation strategy for wireless communications users

The authors in [65] evaluated OP as a performance metric for secondary NOMA users. A comparison of the derived OP results for CR-NOMA and the results for CR-OMA showed that CR-NOMA outperformed CR-OMA. In [66], the authors investigated the transmit quality of the AF and DF forwarding protocols in cooperative relay networks which use CR-NOMA. Over the past decade, cooperative relay networks have received much attention from scientists [67] because of their potential to enhance the quality of communications and meet the enormous demand of mobile users.

In the second aim, my dissertation will propose a new cooperative NOMA system model for underlay cognitive radio networks with perfect and imperfect SIC techniques. I will examine the received signal at the SU, which can extract the data signal from the SINR or SNR. I will explore end-to-end closed-form expressions to determine the OP and compare the OP of two users in a CR-NOMA network to determine the power spectrum allocation fairness for users and enhance the performance of wireless communication. I will also investigate the effect of various channels, and carefully analyze the transceiver parameters which relate to the reliability and performance of the communication mentioned above through mathematical analyses and numerical simulations.

4.3 Aim 3: Design of new system model for hybrid satellite-terrestrial cognitive networks relaying on NOMA to optimize the performance of integrated networks between satellite and terrestrial networks

Integrated networks which use CR-NOMA have not been extensively studied in the literature. To the best of my knowledge, no previous research examining the security performance of NOMA-HSTCNs in the context of multiple antennas and cooperative spectrum sharing has been conducted. However, secure transmission in HSTRNs has already been introduced to the community by the authors in [58, 59, 61]. The metrics of NOMA-HSTCNs are the purpose of future research and the third aim of my dissertation. In this aim, I will conduct an exhaustive analysis of reliability and security performance metrics for integrated system NOMA-HSTCNs.

For the third aim, I will study a new model linking satellite and multiple terrestrial nodes in HSTCNs relaying on NOMA. In this scenario, a satellite equipped with multiple antennas sends information to multi-antenna destinations through the base station, which acts as a relay, to achieve long distance communication. I will investigate the effects of hardware impairments on the reliability and security of NOMA-HSTCN systems. The practical factors of hardware impairments will be studied fully. I will examine the closed-form analytical expressions of the OP and IP as important performance metrics, and analyze the limitation of OP in the high SNR region to optimize the performance of integrated networks and minimize total transmit

power. The achieved outcomes in this part of the research will be verified with independent numerical simulation methods. I will also analyze the results and show that as the level of hardware impairment increases, the user's OP reduces significantly and the IP decreases. The different trends of curves in terms of the OP are caused by the power allocation parameters. I will investigate the severity of performance degradation according to several factors, which include the power allocation ratio, the transmit SNR at the source, and the channel quality.

5 Energy harvesting-based D2D communication in cellular networks: Mathematical modeling and analysis

In this chapter, the first goal of my dissertation with the results was achieved. I applied available RF EH protocols, including TSR, PSR, with energy harvesting and information transmission device-to-device (D2D) communications to enhance system reliability. I clarify the first aim that is mentioned in section 4.1 with publications published. **[NHN04]**, **[NHN10]**, **[NHN15]**

5.1 Device-to-Device Network with MISO Scheme for Wireless Power Transfer: Outage Performance Analysis

In this section, we considered an RF wireless energy transfer model for a D2D system with two transmission schemes and a multiple-input single-output (MISO) model in transmitting nearby users. Especially, to harvest more energy, a multiple-antenna power beacon (PB) is used to the robust D2D transmission network and enhance successful communication in a short distance. Therefore, this energy can maintain operation in small devices efficiently. As a result, we derived some expressions from analyzing outage probability by matching Monte-Carlo and analytical simulations to validate the exactness **[NHN15]**.

5.1.1 Introduction

With the growth of Internet and smart devices, investigating more spectral effective energy consuming wireless technique becomes more important. Wireless Power Transfer (WPT) is very promising in energy transfer and long run consuming. Moreover, the advancement of wireless charging technology has given a practical solution for these applications [68]. RF signals definitely can help in WPT [37, 69] to transmit energy to low power consuming devices for charging.

On the other hand, most of the current studies in the RFEH model focused on using RF signal transferred from the base station (BS). However, the RF-EH capability is reduced partly due to the overall loss between BS and EH users. PB for wireless energy transfer in [70–73] can adopt a devoted power supply for RF-EH. Therefore, the EH heterogeneous network (EHHN) is a solution to increase the productivity of RF-EH. However, because the PB and BS are at the same cell in EHHN, the information transmitting of PB can prevent the Information-Decoding (ID) users near the PB. Therefore, it's really necessary to research the distance problem in EHHN [71] and performance and improvement of PB [72, 73]. With a lot of antennas on PB, the intervention during transmission in EHHN can be reduced like in multiple-input-multiple-output (MIMO) or multiple-input-single-output (MISO) systems with RF-EH. However, how to transmit the energy beamforming excellently is still a problem that has not been widely discovered.

This section concerns the short D2D communications which not only improve network spectral and energy efficiency but also extend cellular coverage [74]. Otherwise, D2D devices using RF wireless energy can extend the endurance of D2D devices and broaden the scale of D2D network. The D2D communications were studied. However, due to the distance problem, the transmit power of UEs is inadequate and signal energy from BSs and the collected energy is not strong enough for D2D communications. Therefore, it's necessary to find system performance of D2D with help of the harvested energy amount from the PB.

5.1.2 System model

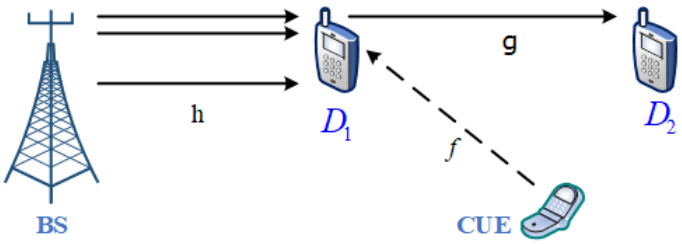

Figure 5.1: System model for MISO applied in D2D network.

The system model is described in Figure 5.1, the source D_1 connects with the destination D_2 in D2D scenario can be examined under help of wireless power from the beacon source. In this case, the BS expenditure multiple transmit antennas for energy transfer, while the near device and far device use single antenna for signal reception. It is assumed that power splitting protocol [37, 68, 69] for wireless power transfer to the self-power device due to its simplicity. It worth noting that the outside energy charging through PB-assisted wireless power transfer is required to overcome energy shortage and to prolong lifetime of D2D transmission link. In particular, N antennas are equipped in the PB while a single antenna design is provided for both D_2. All of the channel state connection information between PB and D_1 is expected to know at the PB. By sending the pilot message from the source, the channel can be predicted, and such a scheme is solved by using a channel estimation algorithm.

We considered power splitting relaying protocol, i.e. during the first phase of duration εP, where $0 < \varepsilon < 1$ stands for power percentage for energy transfer and P is transmit power at the PB, D_1 (i.e., energy harvesting device) collects energy from the PB to use for direct communicate with D_2 which is non-energy harvesting device. Such a two-stage communication protocol has also been researched in previous works, where it was so-called as the "harvest-then-transmit" protocol. We now study two independent cases relying on the interference from CUE.

In D2D networks, there are two basic modes. In the first mode, two devices can communicate directly without the help of BS. In the second mode, BS works as a relay to forward signal from

one device to another. In this section, we only examine the first mode to evaluate impacts of wireless power transfer.

5.1.2.1 D2D transmission without impact of CUE

For the pure D2D case, during the energy collecting phase, the received signal at can be formulated as

$$y_{D_1} = \sqrt{P}\mathbf{h}\mathbf{x}_s + w_{D_1}, \tag{5.1}$$

where P is the transmit power at the PB, $\mathbf{x}_s$ is an $N \times 1$ signal vector, and w_{D_1} is the additive white Gaussian noise (AWGN) with $E\left\{w_{D_1} w_{D_1}^*\right\} = N_0$.

With the short power transfer distance, the line-of-sight path is probably to occur between the PB and D_1. Therefore, applying the Rician allocation to model the PB to D_1 channel is reasonable. However, the complex Rician declining Probability Density Function (PDF) causes a big difficulty for the following analysis. Otherwise, the Nakagami-m fading distribution gives a very excellent estimation to the Rician allocation. Therefore, we apply the Nakagami-m fading to model the PB to D_1 channel in this paper in order to make the analysis easier. Hence, the elements of $\mathbf{h} = [h_i], i = 1, ..., N$, are considered to be independent and identically distributed (i.i.d.) with consistently allocated phase and the intensity, $x = [h_i]$, following a Nakagami-m

$$p(x) = \frac{2}{\Gamma(m)}\left(\frac{m}{\Omega}\right)^m x^{2m-1} e^{\left(-\frac{m}{\Omega}\right)x^2}, x \geq 0, \tag{5.2}$$

in which $\Gamma(\cdot)$ indicates the Gamma function, $m = \frac{E^2[x^2]}{\mathrm{var}[x^2]}$, and $\Omega = E\left[x^2\right]$. If there is no general loss, we set $\Omega = 1$.

Because the PB is attached with multiple antennas, energy beamforming is employed to enhance the capability of energy transfer, i.e.,

$$\mathbf{x}_s = \mathbf{w}s_e, \tag{5.3}$$

where $\mathbf{w}$ is the BF vector with $\|\mathbf{w}\|^2 = 1$ and s_e is the signal that contains the power energy that needs to be transmitted.

As BS has multiple antennas, the BS can use following strategies for antenna usage by deploying beamforming for transmissions. The beamforming approach applied in channel gains is that following Gamma distribution. We denote $\mathbf{h}$ as the fading column vector (size of this vector is based on the number of antennas of PB) between PB and its desired/beamformed user (near D2D device). We allocate Rayleigh distribution for each entity of $\mathbf{h}$. Under the transmit beamforming, the transmitter will multiply the information signal with beamforming vector before transmitting $\mathbf{x}_s$ in (5.3) above

$$\mathbf{w} = \frac{\mathbf{h}^\dagger}{\|\mathbf{h}\|}. \tag{5.4}$$

As such, the total received energy at the end of the first phase corresponding with the harvested ε percentage of transmit power can be calculated as [68]

$$E_n = \eta\varepsilon\|\mathbf{h}\|^2 P, \tag{5.5}$$

where $0 < \eta < 1$ is the energy conversion efficiency and T is block time. Then, the transmit power at D_1 can be expressed by

$$P_{D_1} = \eta\varepsilon\|\mathbf{h}\|^2 P. \tag{5.6}$$

In the second phase, thanks to the energy collected during the initial phase, D_1 will use this energy to transmit the signal to D_2 . Thus, the received signal at D_2 is shown as follows

$$y_{D_1-D_2} = \eta\varepsilon\|\mathbf{h}\|^2 P g s_0 + w_{D_2}, \tag{5.7}$$

in which, $g \sim \mathcal{CN}(0, \lambda_g)$ denotes the Rayleigh fading channel coefficient of the link $D_1 \to D_2$, s_0 is the signal that contains the data information while x_{02} serves as energy bearing signal to D_2, and $w_{D_2} \sim \mathcal{CN}(0, N_0)$, is the additive white Gaussian noise (AWGN).

Hence, the end-to-end signal to noise ratio (SNR) for can be calculated as

$$\gamma_{D_1-D_2} = \frac{\eta\varepsilon\|\mathbf{h}\|^2|g|^2 P}{N_0}. \tag{5.8}$$

5.1.2.2 D2D transmission with impact of CUE

In such mode, we determine D2D transmission with impact of CUE. In such model, to satisfying high quality for the system performance, the D_1 device does not transmit energy to other device. In the existing work, we study the assumption that each D2D link with impact of at least one nearby CUE. In the existence of CUE, the received signal during first phase is given as

$$y_{D_1} = \sqrt{P}\mathbf{h}x_{D_1} + \sqrt{P_I} f s_1 + w_{D_1}, \tag{5.9}$$

where P_I is the transmit power of the interferer (i.e. CUE), f is the interference channel coefficient, s_1 is the transmit signal of the CUE. The total received energy at the end of the first phase can be independently computed as

$$E_I = \eta\varepsilon\|\mathbf{h}\|^2 P + \delta \approx \eta\varepsilon\|\mathbf{h}\|^2 P, \tag{5.10}$$

where δ denotes as energy collected from the CUE. Unfortunately, amount of such energy is very small compared with the power from the PB. Hence, in this model we eliminate impact of

EH from the CUE. In the second phase, D_1 transmits the signal to D_2, the received signal y_{D_2} at D_2 is given by

$$y_{D_2} = \eta\varepsilon\|\mathbf{h}\|^2 P g s_0 + \sqrt{P_I} f s_1 + w_{D_2}, \tag{5.11}$$

As a result, the end-to-end signal to interference plus noise (SINR) can be calculated

$$\gamma_I = \frac{\eta\varepsilon g\|\mathbf{h}\|^2 \frac{P}{N_0}}{1 + \frac{P_I|f|^2}{N_0}} \tag{5.12}$$

It is assumed that we determine estimated value of the interference from CUE, i.e., $\varphi = P_I E\left\{|f|^2\right\}/N_0$

$$\gamma_I = \eta\varepsilon_1 g\|\mathbf{h}\|^2 \frac{P}{N_0} \tag{5.13}$$

where we denote $\varepsilon_1 = \varepsilon/(1+\varphi)$.

5.1.3 Outage Performance Analysis

Outage Performance of MISO D2D Without Impact of CUE. We call P_{out} as the outage probability. Such outage event can be defined as

$$P_{out} = \Pr(\gamma_I < \gamma_0), \tag{5.14}$$

Theory 1: The outage probability of such D2D link at the target rate R_0 can be formulated as [75]

$$P_{out} = \frac{2m^{\frac{Nm}{2}}\left(\frac{N_0}{\eta P}\gamma_0\right)^{\frac{Nm}{2}}}{\Gamma(Nm)} K_{Nm}\left(2\sqrt{m\frac{N_0}{\eta P}\gamma_0}\right), \tag{5.15}$$

where $\Gamma(x)$ is the Gamma function [[76], Eq. (8.310)], $K_n(.)$ is the modified Bessel function of the second kind [76], Eq. (8.432)], $\varphi = \frac{N_0}{\eta\varepsilon P(\alpha-\gamma_0+\alpha\gamma_0)}$,$\gamma_0 = 2^{R_0} - 1$ is the threshold SNR and R_0 denotes the target rate of source.

Proof:

The system's outage probability can be described as follows

$$P_{out} = \Pr(\gamma_I < \gamma_0) = \Pr\left(\|\mathbf{h}\|^2|g|^2 < \frac{N_0}{\eta P}\gamma_0\right). \tag{5.16}$$

In such case, it is required the condition on power splitting factor as $\varepsilon > \gamma_{th}/\left(\gamma_{th}+1\right)$. It is worth noting that $\|\mathbf{h}\|^2$ is a Gamma random variable with PDF given by

$$p(x) = \frac{m^{\frac{Nm}{2}}}{\Gamma\left(Nm\right)}\left(\frac{N_0}{\eta P}\gamma_0\right)^{\frac{Nm-1}{2}} e^{-mx}, \quad for \quad x \geq 0 \tag{5.17}$$

It is noted that the cumulative distribution function (CDF) of $\|\mathbf{h}\|^2|g|^2$ can be achieved by achieved by with some mathematical manipulations. Nevertheless, the consequential expression concerns multiple summaries. Here we employ a little contrasting approach to acquire an easy different (CDF) the following expression [75].

Conditioned on $\|\mathbf{h}\|^2$, the CDF $\|\mathbf{h}\|^2|g|^2$ is given by

$$F(x|\,\|\mathbf{h}\|) = 1 - e^{-\frac{x}{\|\mathbf{h}\|}}. \tag{5.18}$$

To this end, averaging over $\|\mathbf{h}\|^2$, the absolute CDF of such function can be calculated as

$$F(x) = 1 - \frac{2mx^{\frac{Nm}{2}}}{\Gamma\left(Nm\right)} K_{Nm}\left(2\sqrt{xm}\right). \tag{5.19}$$

It will be obtained the expected result after simple manipulations is given in Theory 1.

5.1.4 Numerical and Simulation Results

Simulations are accomplished for system performance evaluation in MATLAB to obtain the role of parameters that have affected D2D networks in analytical and simulation results. The important parameters for the simulations are provided in each illustration. In this part, the results of Monte Carlo imitation are introduced to confirm the analytical expressions from the previous sections. All the simulation results are gained by averaging over 10^6 independent trials. Unless stated differently, the following set of parameters were employed in simulations: $R_0 = 1\,(bps/Hz)$ so the target SNR threshold is given by $\gamma_0 = 2^{2R_0} - 1 = 3$. The energy conversion efficiency is set to be $\eta = 0.4$, $\varphi = 0.05$ and $\rho = P/N_0$ is denoted as transmit SNR, while the Nakagami-m parameter is set to be $m = 4$, which correlates to a Rician factor of $K = 3 + \sqrt{12}$. For simplicity, the distances between the PB and D_1, D_1 and D_2 are set to be unit.

Figure 5.2 shows the outage probability of D2D link under free-interference from the CUE when the BS use transmit beamforming for the near device which use energy harvesting capability for D2D link transmission. The more antenna equipped at the PB outperforms the case uses lower number of antenna in high SNR regime. Such performance gap related to the number of antenna can be seen clearly at high SNR value. In the low SNR, energy for signal processing cannot lead to large impacts on outage performance while more energy for better signal communication between two D2D users.

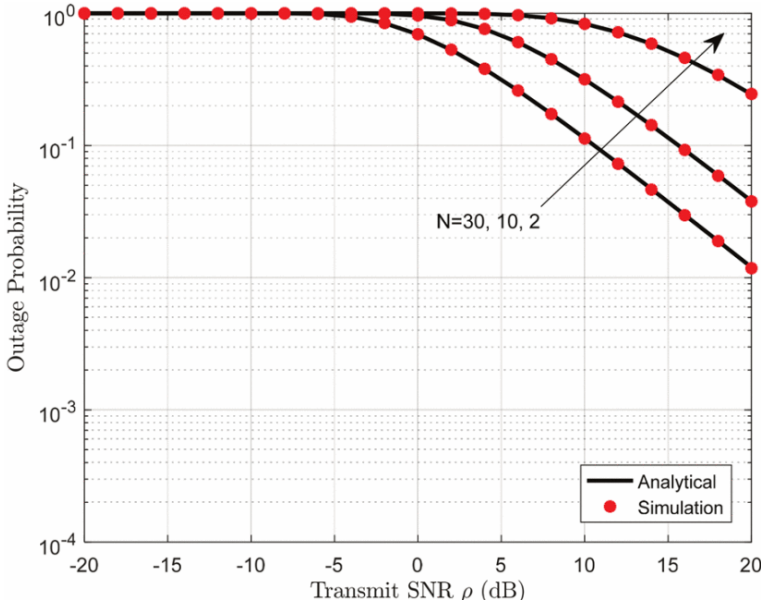

Figure 5.2: Outage performance for MISO D2D network with difference number of antenna of PB

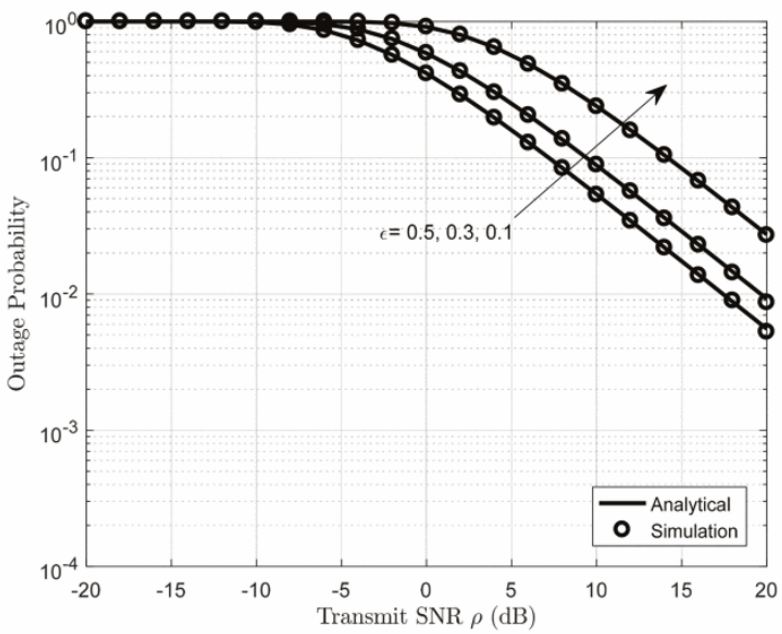

Figure 5.3: The outage performance versus the transmit SNR as varying harvested power percentage

Figure 5.3 demonstrates the outage performance as varying power percentage of energy harvesting from the PB where can be enhanced quality of short distance transmission of D2D. In this case we do not consider impact of CUE's interference signal. In both figures, adding

more energy to the PB can considerably enhance the achievable outage performance. When the transmit power is low, the advantage of putting more antennas rapidly declines. Moreover, the analytical result maintains efficiently tight with Monte-Carlo simulation in various parameter of energy harvesting and the number of antenna.

5.1.5 Conclusion

In this section, we introduced a multi-antenna PB design and the outage probability is evaluated in D2D link. The results of the study are verified by simulation and it shows that the proposed PB regime obtained the reasonable performance to applied in wireless D2D network. In future, the proposed scheme will be extended to multiple antenna D2D users where can be able to signal transfer and harvest energy BF from the PB. We also can further investigate the other system performance such as the throughput of the concerned MISO D2D approach.

5.2 Enabling D2D Transmission Mode With Energy Harvesting and Information Transfer in Heterogeneous Networks

The concept of EH-assisted relay has been introduced to support the relaying transmission using D2D communications for enhancing communication reliability. Motivated by the recent advance in HetNet using relaying techniques, we considered D2D communication provided by EH-assisted relay where a forward signal from a BS to the conventional cellular user (non-D2D user) and D2D user. We first derived the outage probability by considering the SNR and power allocation parameters and propose the transmission mode for the D2D link and non-D2D link. After deriving the outage probability of the D2D-HetNet, we explored the effects of the network parameters on the outage probability and throughput [**NHN04**].

5.2.1 Introduction

Today, the need to strengthen the network capacity via the distribution of small cell base stations (BSs) (e.g., micro, pico, and femto) underlying the common macrocell BSs, namely, HetNet, is increasingly growing up. More and more BSs can be supported by HetNet to be distributed in a good location to prevent interference. This provided us a lot of development about network sufficiency and power employing in comparison with macro BSs. Nevertheless, many problems have arisen, such as load balancing, traffic management, operation, and maintenance. BSs network scope also has issues like capacity with low power consumption; therefore, wireless EH plays a very important role for green networking for 5G world using infrastructures having sufficient and green energy in HetNet [34, 35]. When using ambient RF signals with a new source for EH, one of the appropriate ways to harvest energy is SWIPT by collecting energy from ambient RF signals [37]. Accordingly, this helps to make the wireless device's available energy consumption more efficient, and the operation cost reduced [38].

The HetNet helps build up the network capacity through reusing a greater space [3], but this results in the increased interference [4, 77, 78]. When BSs were distributed heavily, HetNet becomes more attractive for efficient RF-SWIPT. Then the gap between the mobile user (MU) and the BS in HetNet is much closer than inhomogeneous macrocell networks. Furthermore, the total interference in HetNet could be an additional energy source with full frequency reuse. Therefore, the SWIPT technique with self-maintaining and inexpensive characteristics employing the interference in HetNet can increase the spectrum and energy efficiency.

Although the above details are very vital and made a stable infrastructure for promoting new D2D and K-tier network technologies, the effect of hardware damage in such networks with D2D capability is less well evaluated. After studying mentioned results in [79], we analyze the design space of future wireless networks about outage performance and energy efficiency for the D2D networks to which EH enables. On the other hand, in this paper, the system in large-scale heterogeneous cellular networks with an energy-limited D2D transmitter will be considered. At first, the D2D transmitter collects energy from BSs.

5.2.2 System Model and Protocol Description

We considered a scenario of D2D communications underlay a cellular network that is shown in Figure 5.4, where D_2 intends to exchange information with D_4 in D2D link and D_2 transmit signal from BS to regular cellular user D_3. In this paper, we consider K-tier communication (i.e., considering two tiers) which is assigned for D2D in the first tier and non-D2D transmission mode in the second tier.

5.2.2.1 System Model

In this section, we considered a HetNet, in which the second tier services primary user D_3 by considering the BS wants to transfer information to the primary user D_3. It is noted that in such a case, D_3 is assigned as a non-D2D user. Meanwhile, the D2D user D_2 wants to transfer its own information which intended for the other D2D user D_4. Therefore, D_2 not only forwards to the user in tier 2 but also delivers the information in tier 1 simultaneously. As a result, D_2 plays the role of relay node, and it requires more energy to serve this duty. In particular, the relay D_2 has the ability to scavenge energy from the received signals. Furthermore, the operation of all devices in HD, and every device has one signal antenna.

In Figure 5.5, we present a parameter $\alpha_1^2 \left(0 \leq \alpha_1^2 \leq 1\right)$ denoting the fraction of the block time allocated for EH in the block time $T/2$ with T denoted as block time for signal frame processing, node D_2 is assumed as EH relaying node which uses PSR protocol [25, 35, 37, 38]. We assume that all of the channels are quasi-static fading channels, following Rayleigh fading. Let $g_{12}, g_{23}, g_{14}, g_{24}$ denote as the channel coefficients between BS and D_2, D_2 and D_3, BS and D_4, D_2 and D_4 in the concerned block time, respectively. Also, the channels are modeled as follows: $g_{ij} \sim CN\left(0, \Phi_{ij}\right)$ for $ij = 1, 2, ..., 4$. In addition, the transmitted power of BS which is

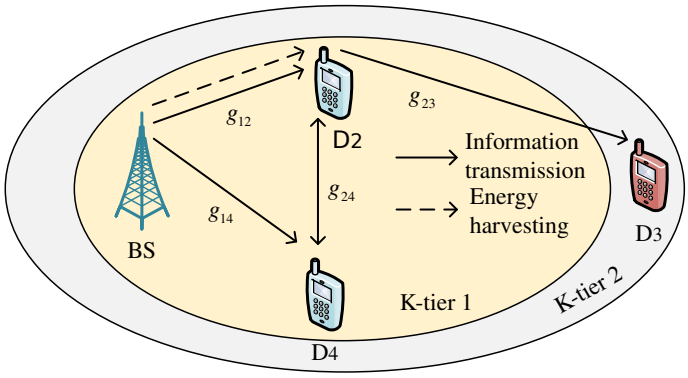

Figure 5.4: The structure of two-tier networks for D2D applications.

equipped a fixed power supply, i.e. power grid P_{S_1}, whereas there is no fixed energy supply for D_2 and it thus needs to harvest energy from the received signals.

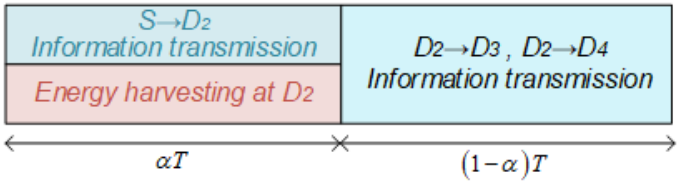

Figure 5.5: Illustration of the key parameters in the PSR protocol for EH and information processing at D_2.

5.2.2.2 The K-Tier Network Structure

In Figure 5.4, we show the structure of a two-tier network, in which the first tier includes D2D users D_2 and D_4, while D_3 is considered as in a conventional cellular user. In this paper, the EH-assisted device D_2 deploys a fraction of power to transmit the primary information from source BS to the normal cellular user and then uses remaining power to transmit signal for D2D link. It is worth noting that each user only detaches related signal and we concern other signals as the unwanted interferers.

5.2.2.3 Energy Harvesting and Information Transfer Procedure

In the system model of PS-assisted EH and information transfer protocol includes two phases which are shown in Figure 5.4 and it is applied as PSR protocol [25]. In phase 1, the BS transmits its information to D_2, EH of node D_2 and D_4 depends on the EH time of the block time and fraction of information split which is signed by α_1 and α_2, respectively, while power allocation of the second link (including non-D2D and D2D link) is denoted as $\alpha_3\,(0 < \alpha_1 < 1; 0 \leq \alpha_2 \leq 1; 0 \leq \alpha_3 \leq 1)$. In principle of PSR, PS1 is transferred the harvested signal at the relay D_2 and the total block time denoted by T, from which half of the time, $T/2$

is occupied for information processing at the first hop of the BS to relay D_2 and the remaining half, $T/2$ is used for the relay to destination D_3, D_4. In particular, the fraction of the received signal power, $\alpha_1 P_{S_1}$ is used for EH and the remaining received power, $(1-\alpha_1)P_{S_1}$ is used for the source to relay information transmission.

In this scenario, the received signals at D_2 can be expressed as:

$$y_{D_2} = \sqrt{P_{S_1}} g_{12} x_1 + n_{D_2} \tag{5.30}$$

$$y_{D_4} = \sqrt{P_{S_1}} g_{14} x_1 + n_{D_4} \tag{5.31}$$

Here, x_1 is the primary signal intended for D_3 in the different tier. It is assumed that $\mathrm{E}\left\{|x_1|^2\right\} = 1$, where $\mathrm{E}\{.\}$ is the expectation operator and $|.|$ is the absolute value operator, and noted that distance of each link is installed as simulation results in the next section.

Applying PSR protocol in EH, the transmitted power at D_2 after EH is shown as

$$P_{D_2} = \eta \alpha_1^2 P_{S_1} |g_{12}|^2 \tag{5.32}$$

where $0 \leq \eta \leq 1$ depicts the energy conversion efficiency and it depends on the rectifier and the EH. Similarly, D_4 can be fed by wireless power transfer from the BS. It can be computed the stored energy at the node D_4 is shown as

$$E_h = \frac{1}{2} \eta \alpha_2^2 P_{S_1} |g_{14}|^2 \tag{5.33}$$

During the phase 2, after EH, D_2 amplifies $\sqrt{1-\alpha_1^2} y_{D_2}$ together with the D2D-assisted information x_2, then forwards it to D_4. Interestingly, we assume that the relay D_2 in phase 2 can split its transmitted power into two parts: $P_{D_2} = \alpha_3^2 P_{D_2} + (1-\alpha_3^2) P_{D_2}$ for normal link (non-D2D) and D2D link. Thus, we have the broadcasting information at D_2 is given by

$$x_{D_2} = \underbrace{G\sqrt{P_{D_2}{\alpha_3}^2}\left(\sqrt{1-\alpha_1^2} y_{D_2} + n_{b1}\right)}_{non-D2D\ signal} + \underbrace{\sqrt{(1-\alpha_3^2)P_{D_2}} x_2,}_{D2D\ signal} \tag{5.34}$$

where x_2 is the unit-power transmitted information intended for D_4, $n_{b1} \sim CN\left(0, \sigma_{b1}^2\right)$ denotes the white Gaussian noise introduced by the signal conversion from passband to baseband at D_2. The amplifier factor G of D_2 is given by

$$G = \frac{1}{\sqrt{\left(1-\alpha_1^2\right)\left(P_{S_1}|g_{12}|^2 + \sigma_1^2\right) + \sigma_{b1}^2}} \approx \frac{1}{\sqrt{\left(1-\alpha_1^2\right) P_{S_1}|g_{12}|^2}}. \tag{5.35}$$

At the primary receiver D_3, we obtained the received signal at destination D_3, D_4, respectively, as below

$$y_{D_3} = g_{23}x_{D_2} + n_{D_3}, \quad \textit{and} \quad y_{D_4} = g_{24}x_2 + n_{D_4}, \tag{5.36}$$

where $n_{D_3} \sim CN(0, \sigma^2_{D_3})$, and $n_{D_4} \sim CN(0, \sigma^2_{D_4})$ represents the additive white Gaussian noise (AWGN) introduced at D_3 and D_4, respectively. Here, D_4 want to detach to signal x_1 where does not appear interference from the secondary signal x_2. At D_3, to decode signal x_1, the Signal-to-Interferences-plus-Noise Ratio (SINR) of D_3 can be calculated by

$$\gamma_{D_3} = \frac{\eta\alpha_1^2\alpha_3^2 P_{S_1}|g_{12}|^2|g_{23}|^2\alpha_3^2}{1-\alpha_3^2} \times \frac{1}{\frac{\eta\alpha_1^2|g_{23}|^2\alpha_3^2}{1-\alpha}\left(\sigma^2_{D_2}\alpha_3^2 + \frac{\sigma^2_{b1}\alpha_3^2}{(1-\alpha_1^2)} + (1-\alpha_3^2)\,P_{S_1}|g_{12}|^2\right) + \sigma^2_{D_3}}. \tag{5.37}$$

At the secondary receiver D_4, the received signal from the source along with the information intended for D_4 can be written as

$$\begin{aligned} y_{D_4} &= g_{24}x_{D_2} + n_{D_4} \\ &= \sqrt{(1-\alpha_1^2)\,\alpha_3^2 P_{D_2} P_{S_1}}Gg_{12}g_{24}x_1 + \sqrt{(1-\alpha_1^2)\,P_{D_2}}Gg_{24}n_{D_3} \\ &+ \sqrt{P_{D_2}}\alpha_3 Gg_{24}n_{b1}x_2 + \sqrt{(1-\alpha_3^2)\,P_{D_2}}Gg_{24} + n_{D_4}. \end{aligned} \tag{5.38}$$

On the other hand, when $\alpha_2 = 1$, the BS only transfer power to the D2D user. It means that all the harvested power is allocated to harvest energy during all time and no information processing in the link BS-D_4. This leads to a result that D_3 and D_4 have the primary interference to treat x_1 as interference and after D_3 and D_4 decode the secondary information x_1.

It is noted that $\alpha_2^2 = 1$, it can be computed the SNR expression as below

$$\gamma_{D_4} = \frac{\frac{\eta\alpha_1^2(1-\alpha_3^2)P_{S_1}|g_{12}|^2|g_{24}|^2\alpha_3}{1-\alpha_3}}{\beta_1\left[P_{S_1}|g_{12}|^2\alpha_3^2 + \sigma^2_{D_2}\alpha_3 + \frac{\sigma^2_{b1}\alpha_3}{(1-\alpha_1^2)}\right] + \sigma^2_{D_4}}, \tag{5.39}$$

where

$$\beta_1 = \frac{\eta\alpha_1^2|g_{24}|^2\alpha_3}{(1-\alpha_3)}. \tag{5.40}$$

We assume that the antenna noise power is zero, i.e. $\sigma^2_{D_2} = \sigma^2_{D3} = 0$. Thus, we have $\sigma^2_{D3} = \sigma^2_{D4} = \sigma^2_{b1} = \sigma^2_0$ as a result from (5.37), (5.39). We can rewrite the received SNR of the node D_3 and D_4 as follows

$$\gamma_{D_3} = \frac{\frac{\eta\alpha_1^2\alpha_3^2 P_{S_1}|g_{12}|^2|g_{23}|^2\alpha_3}{(1-\alpha_3)}}{\frac{\eta\alpha_1^2\alpha_3^2\sigma_0^2|g_{23}|^2\alpha_3}{(1-\alpha_3)(1-\alpha_1^2)} + \frac{\eta\alpha_1^2(1-\alpha_3^2)P_{S_1}|g_{12}|^2|g_{23}|^2}{(1-\alpha_3)\alpha_3^{-1}} + \sigma_0^2}. \tag{5.41}$$

Similarly, SNR at device D_4 can be expressed by

$$\gamma_{D_4} = \frac{\frac{\eta\alpha_1^2(1-\alpha_3^2)P_{S_1}|g_{12}|^2|g_{24}|^2\alpha_3}{(1-\alpha_3)}}{\frac{\eta\alpha_1^2|g_{24}|^2\alpha_3}{(1-\alpha_3)}\left(P_{S_1}|g_{12}|^2\alpha_3^2+\frac{\sigma_0^2}{(1-\alpha_1^2)}\alpha_3\right)+\sigma_0^2}. \tag{5.42}$$

Accordingly, from formula of the obtained SNR of the non-D2D user D_3 and the D2D user D_4, we can calculate the instantaneous rate at D_3 and D_4 as follows

$$R_{D_3} = \frac{1}{2}\log_2\left(1-\gamma_{D_3}\right); \qquad R_{D_4} = \tfrac{1}{2}\log_2\left(1-\gamma_{D_4}\right). \tag{5.43}$$

5.2.3 Outage Probability and Throughput Analysis

5.2.3.1 Outage Probability

The OP is defined that the data rate of the D2D user D_3 and the cellular user D_4 falls below the predetermined threshold target rate. Therefore, the OP for a given target rate F_i is given by

$$P_{out}(\Gamma_i < F_i) = \Pr(\gamma_i < f_i), \tag{5.44}$$

where $i = D_3$ or $i = D_4$. Here, we set $f_i = 2^{2F_i} - 1$. F_i is the fixed source transmission. According to (5.44), we have the following propositions.

Proposition 1 Let denote

$$\lambda = \frac{\alpha_3}{1-\alpha_3}, \tag{5.45}$$

$$l = \frac{\eta\alpha_1^2\alpha_3^2P_{S_1}}{\sigma_0^2}\lambda \tag{5.46}$$

$$m = \frac{\eta\alpha_1^2\left(1-\alpha_3^2\right)P_{s_1}\lambda}{\sigma_0^2}, \tag{5.47}$$

$$k = \frac{\eta\alpha_1^2\alpha_3^2\lambda}{(1-\alpha_1^2)}. \tag{5.48}$$

The OP of D_3 can be expressed as

$$P_{out}^{D_3} = 1-\exp\left\{-\frac{kf_{D_3}}{\Phi_1(l-mf_{D_3})}\right\}\sqrt{\frac{4f_{D_3}}{\Phi_1\Phi_2(l-mf_{D_3})}}K_1\left\{\sqrt{\frac{4f_{D_3}}{\Phi_1\Phi_2(l-mf_{D_3})}}\right\}, \tag{5.49}$$

where $K_1(.)$ is the modified Bessel function of the second kind. Interestingly in this section, the OP of D_4 can be calculated as **Proposition 1**

Proof: Let $X = |g_{12}|^2$, $Y = |g_{23}|^2$ and define

$$N = \frac{qXY}{\omega XY + gY + 1}, \tag{5.50}$$

where we use the definition the CDF of N (i.e. $F_N(n)$)can be easily derived through some algebraic manipulation. Finding out, we have $P_{out}^{D_3} = F_N(f_{D_3})$. The detailed derivation can be seen in [79].

Because of the secondary interference from the information transmission processing in the SN and the receiver antenna, the signal converts from pass-band to base-band at the secondary user D_2. It is quite easy to obtain from Eq. (44) that $\lim_{P_{S_1}\to\infty} \gamma_{D_3} = \frac{\alpha_3^2}{1-\alpha_3^2}$

Therefore, $\gamma_{D_3} \to \frac{\alpha_3^2}{1-\alpha_3^2}$ the outage event of the secondary user D_3 occurs all the time if $f_{D_3} \geq \frac{\alpha_3^2}{1-\alpha_3^2}$ and the α_3^2 factor is chosen exactly, the equation $P_{out}^{D_3} = 1$ will happen.

The OP of secondary user D_4 can be written as following expression (5.51).

In this case, the SU can not remove the primary interference from BS when $\alpha_2^2 = 1$, yielding $\lim_{P_{S_1}\to\infty} \gamma_{D_4} = \frac{1-\alpha_3^2}{\alpha_3^2}$. As a result, we can calculate the exact expression of $P_{out}^{D_4}$. Likewise, we have $P_{out}^{D_4} = 1$ if $f_{D_4} \geq \frac{(1-\alpha_3^2)}{\alpha_3^2} \approx \frac{1-\alpha_3^2}{\alpha_3^2}$ and $\alpha_2^2 = 1$. This indicates a difficult problem how to choose the factor α_3^2 to satisfy this condition. Note that, when the α_3^2 decreases, $P_{out}^{D_4}$ decreases, but results in $P_{out}^{D_3}$ increasing. Otherwise, if the α_3^2 decreases, $P_{out}^{D_4}$ increases, but results in $P_{out}^{D_3}$ decreasing.

$$P_{out}^{D_4} = \Pr\left[\gamma_{D_4} < f_{D_4}\right] = \Pr\left[\frac{m\left|g_{12}\right|^2|g_{24}|^2}{\left(l\left|g_{12}\right|^2|g_{24}|^2 + k\frac{1}{\alpha_3^2}|g_{24}|^2 + 1\right)} < f_{D_4}\right]. \tag{5.51}$$

5.2.3.2 Throughput Analysis

Proposition 1 Derives the OP at the D_3 and D_4, respectively. In this section, we consider both the secondary and primary network. The throughput at D_3 and D_4 is given by

$$\tau_m = \left(1 - P_{out}^m\right) R_m, \tag{5.52}$$

where achievable throughput τ_m with m is D_3 or D_4. Here, the transmitter communicates with fixed rate R_m $(bps.Hz^{-1})$. This number illustrates effective communication capability from the source node to the destination node in the block of time T seconds.

5.2.4 Numerical Results

In this section, we considered outage performance of D2D link and non-D2D link with the help of EH-assisted relay node D_2 to transfer information to D2D user in tier 1 and non-D2D in tier 2. We verify the accuracy of the proposed expressions by the simulation to demonstrate the performance of the proposed wireless EH and information transfer in HetNet. In the simulation,

we set the distances of each link which are normalized. Let d_1 denote the distance between BS and D_2, the distance between D_2 and D_3 are denoted by d_2. Similarly, we define d_3 as the distance between BS and D_4, and the distance between D_2 and D_4 represented by d_4, and hence the average channel gains as $\Phi_1 = 1/d_1$, $\Phi_2 = 1/d_2$, and $\Phi_3 = 1/d_3$, $\Phi_4 = 1/d_4$, for g_{12}, g_{23}, g_{14} and g_{24}, respectively.

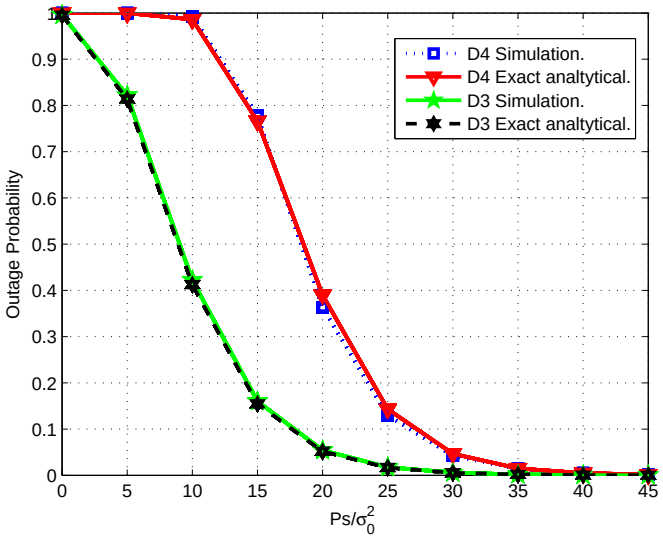

Figure 5.6: Simulation based and analytical OP at D_3, D_4. Here, $R_{D_3} = R_{D_4} = 3(bps.Hz^{-1})$; $d_1 = d_2 = 0.5; d_3 = 0.75\,; \alpha_1 = 0.62; \alpha_3 = 0.58$.

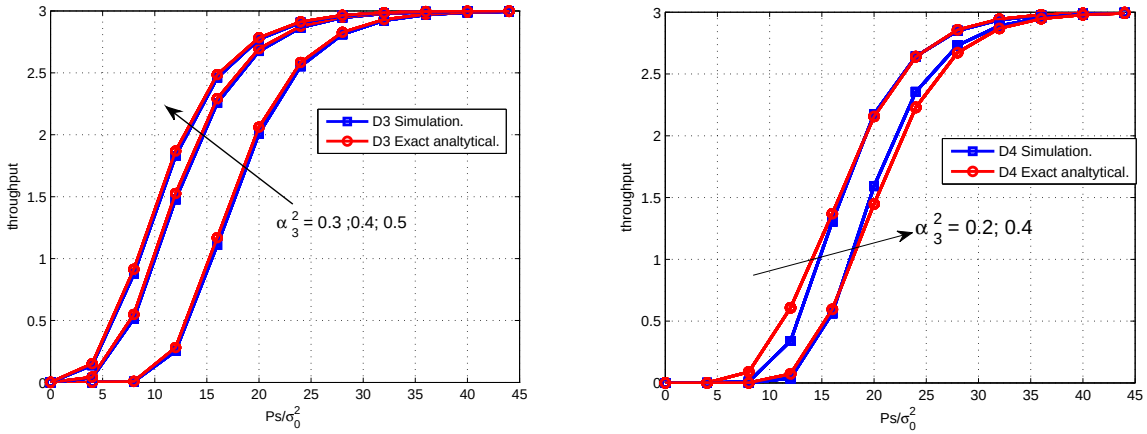

(a) at D_3. Here, $R_{D_3} = R_{D_4} = 3(bps.Hz^{-1})$; $d_1 = d_2 = 0.5; d_3 = 0.75\,; \alpha_1 = 0.92; \alpha_3 = 0.58$ and D_4.

(b) at D_4. Here, $R_{D_3} = R_{D_4} = 3(bps.Hz^{-1})$; $d_1 = 0.6; d_2 = 0.4; d_3 = 0.75\,; \alpha_1 = 0.62; \alpha_3 = 0.7$.

Figure 5.7: Simulation based and analytical throughput at D_3 and D_4.

In Figure 5.7a, we compare the result of simulation and exactly analysis at D_3 in case of the

increase from 0.3 to 0.5 of α_3^2 , we can see the throughput which will be better when the power allocation coefficient of the second link (including link assigned for non-D2D and D2D link), .i.e. α_3^2 increases to 0.5, we obtain the highest throughput among concerned values. Besides, the simulation and exactly analysis have the same result. Similarly, the throughput at node D_4 is considered in Figure 5.7b, the throughput is low and it increases very slowly at SNR from 0dB to 10dB, but it increases quickly at SNR from 15dB to 45dB. Furthermore, when α_3^2 increases, the throughput at node D_4 will increase very slowly.

5.2.5 Conclusion

This section has developed a tractable analytical framework for evaluating outage of D2D and non-D2D links in a general K-tier heterogeneous cellular network. In particular, we have obtained simple expressions for the non-D2D user in terms of outage probability. The numerical results based on the analysis show that RF EH can enable technology to power cellular devices. In addition, the simulation results validate the derived expressions, which are efficiently computed numerically.

5.3 Outage Probability of CR-NOMA Schemes with Multiple Antennas Selection and Power Transfer Approach

This section has been extended from published contents with D2D communication. We investigated the outage performance of CR-NOMA schemes in decode-and-forward (DF) relay systems Device-to-Device (D2D) with antenna selection. We proposed the power beacon (B), which can feed energy to the relay device node to further support the transmission from the source to the destination. To this end, closed-form expressions for the outage probabilities at user are derived. An asymptotic analysis at a high signal-to-noise ratio (SNR) is carried out to provide additional insights into the system performance **[NHN10]**.

5.3.1 Introduction

CR has been noticed remarkably thanks to its ability to improve spectrum utilization [7]. In the context as CR is proposed to the 5G mobile networks, both the primary users, including a BS and mobile users served by the BS and the secondary users (mobile users non-served by the BS, can coexist together in a same licensed system [80]. NOMA has been key as a promising solution to achieve higher spectrum efficiency in the 5G wireless networks [1]. Thanks to technical improvements of superposition coding and SIC in NOMA, multiple users can be served in the same resource block.

Cooperative NOMA is proposed in [81] to improve reception reliability. The performance of cooperative NOMA is investigated in [82, 83]. The achievable rate of the cooperative NOMA is studied in [82]. Considering imperfect SIC, the ergodic sum capacity of the cooperative NOMA is investigated where two sources communicate with their corresponding destinations

via a standard relay [84]. Cooperative NOMA is applied in a cognitive radio network to enhance spectrum efficiency [85]. Approximated expressions for the outage probability are derived for a cooperative NOMA in an underlay cognitive radio network where one secondary user is selected as a relay [86]. In [18], the OP and the ergodic capacity of cooperative NOMA in an underlay CRN are derived, assuming that the primary source's interference is considered a constant, which is not realistic in practice.

Recently, EH wireless networks are expected to introduce several transformative changes in wireless networking. So, a prospective approach is to apply EH technologies to relay networks. RF EH is used [25]. The relaying networks have been widely studied by introducing flexible, sustainable, and stable energy supply devices in such networks [87–90]. In [88], renewable energy is considered a solution to employing dense small cell base stations (SBSs) to adapt to the increasing demand for communication services. In [90], system throughput can be enhanced by utilizing the optimal channel selection method and the harvested RF energy. The CR sensor networks benefit from RF EH.

5.3.2 System model

We considered a cooperative NOMA system in an underlay CRN consisting of a primary destination PD , a power beacon B, a secondary source with multiple antennas $N\,(n = 1, \ldots, N)$, and two secondary destinations D_1, D_2 as shown in Figure 2.7. Assume that there is a direct path between BS and the secondary destination D_2. Suppose that each node has a single antenna and operates in half-duplex mode to transmit the signal to the secondary destinations according to NOMA principle. A transmission frame of the network consists of two equal length phases. In the first phase, BS transmits a signal to D_1, D_2. In the second phase, D_1 transmits the re-encoded signal to the secondary destinations only if the received signal at D_1 is decoded successfully and D_1 harvests energy from B, and then uses this energy to transmit signals [10]. Wireless channels denoted as in Fig. 1 in such a system relying on NOMA are subjected to Rayleigh flat fading plus additive white Gaussian noise. The complex channel coefficients for the links $BS \to D_1$, $BS \to D_2$, $BS \to PD$, $B \to D_1$, $D_1 \to PD$, $D_1 \to D_2$ are represented by $|h_{1n}|^2 \sim CN\,(0, \lambda_{1n})$, $|h_{2n}|^2 \sim CN\,(0, \lambda_{2n})$, $|h_{p1}|^2 \sim CN\,(0, \lambda_{p1})$, $|h_b|^2 \sim CN\,(0, \lambda_b)$, $|h_{p2}|^2 \sim CN\,(0, \lambda_{p2})$, $|h_3|^2 \sim CN\,(0, \lambda_3)$, respectively.

In the first phase, the received signal at $BS \to D_1$ is given by

$$y_{D_1} = \sqrt{P_{BS}} h_{1n}\,(a_1 x_1 + a_2 x_2) + n_{D_1}, \tag{5.53}$$

where P_{BS} is the transmit power of BS, $x_i\,(i = 1, 2)$ is the information symbol for D_i, a_i is the power allocation coefficient for s_i with $a_1 + a_2 = 1$ and $a_1 < a_2$, and n_{D_1} is the AWGN at $BS \to D_1$ with $n_{D_1} \sim CN\,(0, N_0)$.

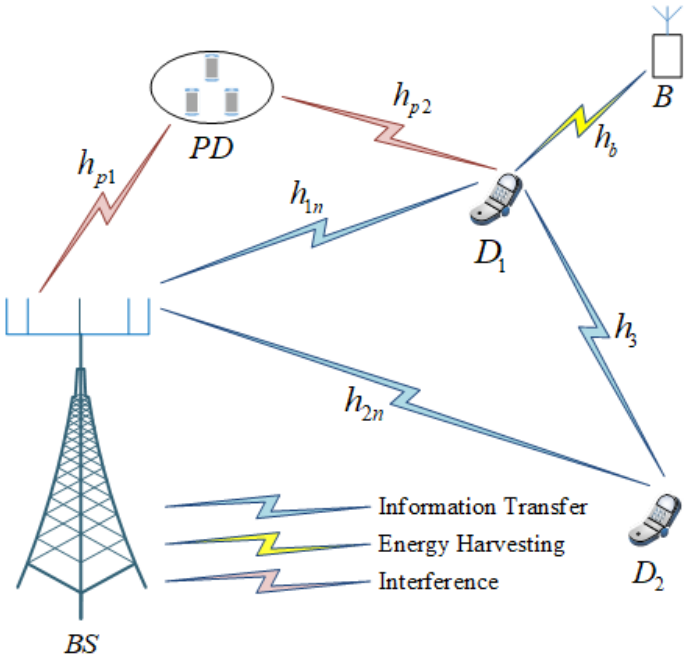

Figure 5.8: System model of power beacon-assisted CR-NOMA.

The signal to interference plus noise ratio (SINR) to decode x_2 at $BS \rightarrow D_1$ is given by

$$\gamma_{D_1}^{(x_2)} = \frac{a_2 P_{BS}|h_{1n}|^2}{a_1 P_{BS}|h_{1n}|^2 + N_0}. \tag{5.54}$$

After imperfect SIC, the SINR to decode x_1 is given by

$$\gamma_{D_1}^{(x_1)} = \frac{a_1 P_{BS}|h_{1n}|^2}{N_0}. \tag{5.55}$$

The observation $BS \rightarrow D_2$ for the direct link is written as

$$y_{BS-D_2} = \sqrt{P_{BS}} h_{2n} \left(a_1 x_1 + a_2 x_2\right) + n_{D_2}, \tag{5.56}$$

where n_{D_2} is the AWGN at with $n_{D_2} \sim CN\left(0, N_0\right)$.

The received SINR at D_2 to detect for the direct link is given by

$$\gamma_{BS-D_2}^{(x_2)} = \frac{a_2 P_{BS}|h_{2n}|^2}{a_1 P_{BS}|h_{2n}|^2 + N_0}. \tag{5.57}$$

In the second phase, since DF relaying protocol is invoked in D_1, we assume that D_1 can DF the signal x_2 to successfully for relaying the link from D_1 to D_2.

$$y_{D_1-D_2} = \sqrt{P_{D_1}} h_3 x_2 + N_{D_2}, \tag{5.58}$$

where P_{D_1} is the transmit power of D_1.

Therefore, calculating SNR to detect x_2, which is transmitted in the second hop from user D_1 to user D_2, is given as

$$\gamma_{D_1-D_2}^{(x_2)} = \frac{P_{D_1}|h_3|^2}{N_0}. \tag{5.59}$$

The chosen antenna can be selected to strengthen the $BS \rightarrow D_i$,$(i = 1, 2)$ link as follows [19]:

$$K^* = \arg \underbrace{\max}_{K=1,\ldots,N} \left(|h_{in}|^2\right). \tag{5.60}$$

The CDF and PDF related to selected channels are given as [91]

$$F_{|h_{in}|^2}(x) = 1 - \sum_{n=1}^{N} \binom{N}{n} (-1)^{n-1} \exp\left(-\frac{nx}{\lambda_{in}}\right), \tag{5.61}$$

and

$$f_{|h_{in}|^2}(x) = \sum_{n=1}^{N} \binom{N}{n} (-1)^{n-1} \frac{n}{\lambda_{in}} \exp\left(-\frac{nx}{\lambda_{in}}\right). \tag{5.62}$$

In the considered system, the relay D_1 harvests energy from a power beacon. The operation of the second stage of signal processing is supported by harvests energy at D_1. At EH phase, the time switching (TS) based EH technique is applied. In a transmission block time T(in which a block of information is sent from the beacon to the relay), the relay takes αT to harvest energy from the beacon, in which is the EH time fraction that depends on the schedule of B. The time slot $(1-\alpha)T$ is then divided into two equal time slots for the BS to D_1 and $D_1 \rightarrow D_2$ transmissions. Therefore, the energy harvested at D_1 is given as [10]

$$EH_{D_1} = \eta P_B \alpha T |h_b|^2, \tag{5.63}$$

where $0 < \eta < 1$ is the efficiency coefficient of the energy conversion process, $0 < \alpha < 1$ is the percentage of EH, is the transmit power of the beacon, assuming that these power beacons have the same power level, respectively. Under the assumption that the processing energy at D_1 is negligible, the transmit power of D_1 is written as following [10]:

$$P_{D_1}^{EH} = \frac{2\eta P_B \alpha |h_b|^2}{(1-\alpha)}. \tag{5.64}$$

In order to guarantee the quality of service requirement for PB, interference power at PB must be kept below a tolerable interference constraint H. The transmit power of BS and D_1 are limited by and $P_{D_1} \leq \min\left\{P_{D_1}^{EH}, P_{D_1}^{\max}, \frac{H}{|h_{p2}|^2}\right\}$ [92,93]. Respectively, where $P_{BS}^{\max}$ and $P_{D_1}^{\max}$ are the maximum available power of BS and D_1 respectively.

5.3.3 Outage Probability analysis

5.3.3.1 The outage probability of D_1

According to NOMA protocol, the complementary events of the outage at D_1 can be explained as: D_1 can detect as well as its own message x_1. From the above description, the outage probability D_1 is expressed as [94]

$$\begin{aligned} OP_1 &= \Pr\left(\min\left(\gamma_{D_1*}^{(x_2)}, \gamma_{D_1*}^{(x_1)}\right) < \gamma_1\right) \\ &= 1 - \Pr\left(|h_{1n*}|^2 > \tfrac{\gamma_1 N_0}{(a_2 - \gamma_1 a_1) P_{BS}}, |h_{1n*}|^2 > \tfrac{N_0 \gamma_1}{a_1 P_{BS}}\right) = 1 - \underbrace{\Pr\left(|h_{1n*}|^2 > \frac{\xi}{P_{BS}}\right)}_{A}, \end{aligned} \tag{5.65}$$

where $\gamma_1 = 2^{2R_i} - 1$, $i = (1, 2)$ with R_i being the target rate at D_i to detect x_i.

Theorem 1. The closed-form expression for the outage probability D_1 is given by

$$\begin{aligned} OP_1 = 1 &- \sum_{n=1}^{N} \binom{N}{n} (-1)^{n-1} \exp\left(-\tfrac{n\xi}{P_{BS}^{\max} \lambda_{1n}}\right) \times \left[1 - \sum_{n=1}^{N} \binom{N}{n} (-1)^{n-1} \exp\left(-\tfrac{nH}{P_{BS}^{\max} \lambda_{p1}}\right)\right] \\ &- \sum_{n=1}^{N} \sum_{m=1}^{N} \binom{N}{n} \binom{N}{m} (-1)^{n+m-2} \tfrac{mH\lambda_{1n}}{n\xi\lambda_{p1} + mH\lambda_{1n}} \times \exp\left(-\left(\tfrac{n\xi}{H\lambda_{1n}} + \tfrac{m}{\lambda_{p1}}\right) \tfrac{H}{P_{BS}^{\max}}\right). \end{aligned} \tag{5.66}$$

Proof: See Appendix A

5.3.3.2 The outage probability of D_2

For the second scenario, the outage events D_2 for FD NOMA are described below. One of the events is when can be detected at D_1, but the received of SINR after SIC at D_2 in one slot is less than its target SNR. Another event is that neither D_1 nor D_2 can detect . Therefore, the OP D_2 is expressed as [95]

$$\begin{aligned} OP_2 &= \Pr\left(\max\left(\gamma_{BS-D_2*}^{(x_2)}, \min\left(\gamma_{D_1*}^{(x_2)}, \gamma_{D_1-D_2*}^{(x_2)}\right)\right) < \gamma_2\right) \\ &= \Pr\left(\gamma_{BS-D_2*}^{(x_2)} < \gamma_2, \min\left(\gamma_{D_1*}^{(x_2)}, \gamma_{D_1-D_2*}^{(x_2)}\right) < \gamma_2\right) \\ &= \left[1 - \underbrace{\Pr\left(\gamma_{BS-D_2*}^{(x_2)} < \gamma_2\right)}_{B_1}\right] \underbrace{\Pr\left(\min\left(\gamma_{D_1*}^{(x_2)}, \gamma_{D_1-D_2*}^{(x_2)}\right) < \gamma_2\right)}_{B_2}. \end{aligned} \tag{5.67}$$

Theorem 2. The closed-form expression for the OP of D_2 with direct link is given by

$$
\begin{aligned}
OP_2 = & \left\{ \begin{array}{l} 1 - \sum\limits_{n=1}^{N} \binom{N}{n} (-1)^{n-1} \exp\left(-\frac{n\gamma_2 N_0}{P_{BS}^{\max}(a_2-\gamma_2 a_1)\lambda_{2n}}\right) \\ \times \left[1 - \sum\limits_{n=1}^{N} \binom{N}{n} (-1)^{n-1} \exp\left(-\frac{nH}{P_{BS}^{\max}\lambda_{p1}}\right)\right] \\ - \sum\limits_{n=1}^{N}\sum\limits_{m=1}^{N} \binom{N}{n}\binom{N}{m} (-1)^{n+m-2} \times \frac{mH(a_2-\gamma_2 a_1)\lambda_{2n}}{n\gamma_2 N_0 \lambda_{p1} + mH(a_2-\gamma_2 a_1)\lambda_{2n}} \\ \times \exp\left(-\left(\frac{n\gamma_2 N_0}{H(a_2-\gamma_2 a_1)\lambda_{2n}} + \frac{m}{\lambda_{p1}}\right)\frac{H}{P_{BS}^{\max}}\right) \end{array} \right\} \\
& \times \left\{ \begin{array}{l} 1 - \left\{ \begin{array}{l} \sum\limits_{n=1}^{N} \binom{N}{n} (-1)^{n-1} \exp\left(-\frac{n\gamma_2\omega_0}{P_{BS}^{\max}(a_2-\gamma_2 a_1)\lambda_{1n}}\right) \times \left[\begin{array}{l} 1 - \sum\limits_{n=1}^{N} \binom{N}{n} (-1)^{n-1} \\ \times \exp\left(-\frac{nH}{P_{BS}^{\max}\lambda_{p1}}\right) \end{array} \right] \\ + \sum\limits_{n=1}^{N}\sum\limits_{m=1}^{N} \binom{N}{n}\binom{N}{m} (-1)^{n+m-2} \frac{mH(a_2-\gamma_2 a_1)\lambda_{1n}}{n\gamma_2 N_0 \lambda_{p1} + mH(a_2-\gamma_2 a_1)\lambda_{1n}} \\ \times \exp\left(-\left(\frac{n\gamma_2 N_0}{H(a_2-\gamma_2 a_1)\lambda_{1n}} + \frac{m}{\lambda_{p1}}\right)\frac{H}{P_{BS}^{\max}}\right) \end{array} \right\} \\ \times \frac{H\lambda_3}{N_0\gamma_2\lambda_{p2} + H\lambda_3} \exp\left(-\frac{N_0\gamma_2}{P_{D_1}^{\max}\lambda_3}\right) \times \sqrt{\frac{2N_0\gamma_2(1-\alpha)}{\eta P_B \alpha \lambda_3 \lambda_b}} K_1\left(\sqrt{\frac{2N_0\gamma_2(1-\alpha)}{\eta P_B \alpha \lambda_3 \lambda_b}}\right) \end{array} \right\}.
\end{aligned}
\tag{5.68}
$$

Proof: See Appendix B

5.3.3.3 Asymptotic Outage Probability Analysis

Where $P_{BS}^{\max} \to \infty$ it can be obtained asymptotic performance of D_1 and D_2. We first look at the asymptotic performance of the first user in term of OP as

$$
OP_{1-asym} = 1 - \sum_{n=1}^{N}\sum_{m=1}^{N} \binom{N}{n}\binom{N}{m} (-1)^{n+m-2} \frac{mH\lambda_{1n}}{n\xi\lambda_{p1} + mH\lambda_{1n}}, \tag{5.69}
$$

$$
\begin{aligned}
OP_{2-asym} = & \left\{1 - \sum_{n=1}^{N}\sum_{m=1}^{N} \binom{N}{n}\binom{N}{m} (-1)^{n+m-2} \times \frac{mH(a_2-\gamma_2 a_1)\lambda_{2n}}{n\gamma_2 N_0 \lambda_{p1} + mH(a_2-\gamma_2 a_1)\lambda_{2n}}\right\} \\
& \times \left\{ \begin{array}{c} 1 - \sum\limits_{n=1}^{N}\sum\limits_{m=1}^{N} \binom{N}{n}\binom{N}{m} (-1)^{n+m-2} \frac{mH(a_2-\gamma_2 a_1)\lambda_{1n}}{n\gamma_2 N_0 \lambda_{p1} + mH(a_2-\gamma_2 a_1)\lambda_{1n}} \\ \times \frac{H\lambda_3}{N_0\gamma_2\lambda_{p2} + H\lambda_3} \sqrt{\frac{2N_0\gamma_2(1-\alpha)}{\eta P_B \alpha \lambda_3 \lambda_b}} K_1\left(\sqrt{\frac{2N_0\gamma_2(1-\alpha)}{\eta P_B \alpha \lambda_3 \lambda_b}}\right) \end{array} \right\}.
\end{aligned}
\tag{5.70}
$$

5.3.4 Numerical Results and simulations

In this section, we show the comparisons related to the outage performance of two users using NOMA. These users are grouped in the downlink of the using Rayleigh fading channels under different simulated parameters.

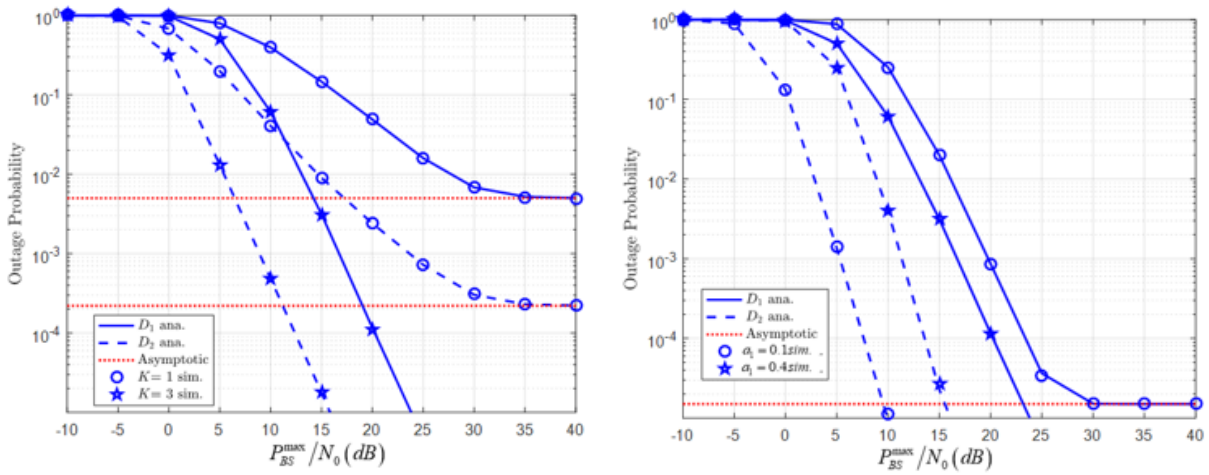

(a) varying N. Fixed $a_1 = 0.2$, $\eta = 0.8$, $\alpha = 0.6$..

(b) varying a_1. Fixed $\eta = 0.8$, $\alpha = 0.6, N = 3$.

Figure 5.9: Outage performance comparison of D_1 and D_2 versus $P_{BS}^{\max}/N_0$ with $R_1 = R_2 = 0.5\,(bps/Hz)$, $\lambda_{1n} = \lambda_{2n} = \lambda_3 = \lambda_b = \lambda_{p1} = \lambda_{p2} = 1$, $P_{D_1}^{\max}/N_0 = 50\,(dB)$, $P_B/N_0 = 30\,(dB)$.

The OP versus the transmit SNR at the BS is illustrated in Figure 5.9a, where we considered two main scenarios. The different power allocation coefficients are assigned to two users, and hence outage performance of the first user is less than that of the second user. It can be easily seen that more antennas result in the lowest outage. When the SNR is greater than 30 (dB), outage probabilities for these cases go to a straight line, which means they meet the saturation situation. In addition, imperfect SIC at the first user has worse outage performance compared with the perfect SIC case.

We considered the outage performance of two users versus transmit SNR with different power allocation factors, as in Figure 5.9b, the users' performance change based on the amount of power allocated. Higher R leads to better outage performance at the first user. These trends of curves related to outage behavior are similar as in Figure 5.10a. While considering how to transmit SNR at power beacon impacts outage probability, it can be seen similar performance as in Figure 5.10b.

5.3.5 Conclusion

In this section, we investigated the CR-NOMA scheme in an underlay CRN by enabling energy harvesting and transmit antenna selection schemes. To this end, exact closed-form expressions and asymptotic expressions for the outage probabilities of the two users were derived with imperfect SIC. Furthermore, the direct link between BS and the far user was utilized to convey information, and one diversity order was obtained for the distant user.
Appendix A: Proof of **Theorem 1**

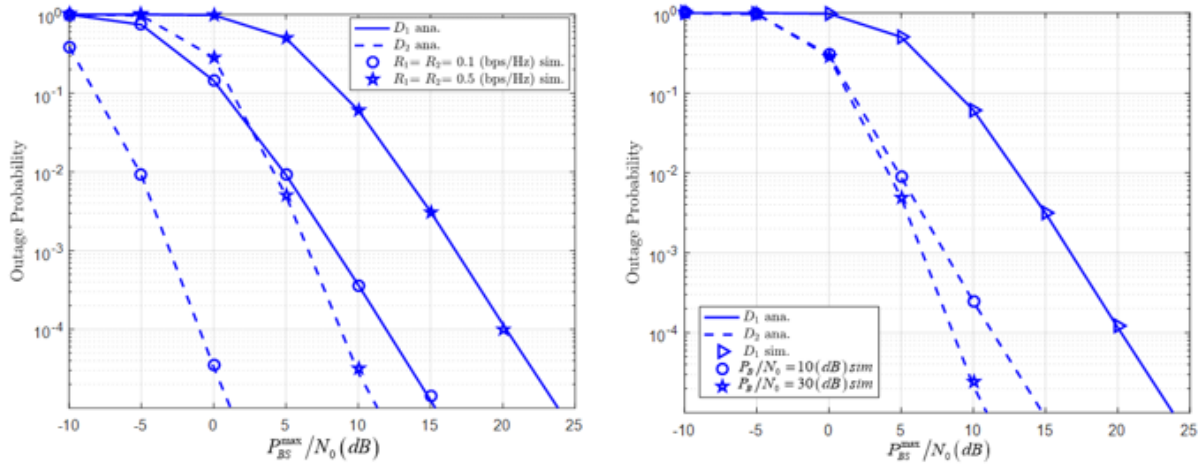

(a) varying $R_1 = R_2$. Fixed $a_1 = 0.2, \eta = 0.8, \alpha = 0.6, N = 3$.

(b) varying P_B/N_0. Fixed $a_1 = 0.2, \eta = 0.8, \alpha = 0.6, N = 3, R_1 = R_2 = 0.5\,(bps/Hz)$.

Figure 5.10: Outage performance comparison of D_1 and D_2 versus $P_{BS}^{\max}/N_0$ with $\lambda_{1n} = \lambda_{2n} = \lambda_3 = \lambda_b = \lambda_{p1} = \lambda_{p2} = 1, P_{D_1}^{\max}/N_0 = 50\,(dB)$.

From (5.65), A can be formulated by

$$\begin{aligned} A &= \Pr\left(|h_{1n*}|^2 > \tfrac{\xi}{P_{BS}^{\max}}, P_{BS}^{\max} < \tfrac{H}{|h_{p1*}|^2}\right) + \Pr\left(|h_{1n*}|^2 > \tfrac{\xi}{\frac{H}{|h_{p1*}|^2}}, P_{BS}^{\max} > \tfrac{H}{|h_{p1*}|^2}\right) \\ &= \underbrace{\Pr\left(|h_{1n*}|^2 > \frac{\xi}{P_{BS}^{\max}}, P_{BS}^{\max} < \frac{H}{|h_{p1*}|^2}\right)}_{A_1} + \underbrace{\Pr\left(|h_{1n*}|^2 > \frac{\xi}{\frac{H}{|h_{p1*}|^2}}, P_{BS}^{\max} > \frac{H}{|h_{p1*}|^2}\right)}_{A_2}. \end{aligned} \tag{5.A.1}$$

Next, A_1 it can be first calculated as

$$\begin{aligned} A_1 &= \Pr\left(|h_{1n*}|^2 > \tfrac{\xi}{P_{BS}^{\max}}, |h_{p1}|^2 < \tfrac{H}{P_{BS}^{\max}}\right) = \Pr\left(|h_{1n*}|^2 > \tfrac{\xi}{P_{BS}^{\max}}\right)\left[1 - \Pr\left(|h_{p1}|^2 \geq \tfrac{H}{P_{BS}^{\max}}\right)\right] \\ &= \sum_{n=1}^{N} \binom{N}{n} (-1)^{n-1} \exp\left(-\tfrac{n\xi}{P_{BS}^{\max}\lambda_{1n}}\right) \times \left[1 - \sum_{n=1}^{N} \binom{N}{n} (-1)^{n-1} \exp\left(-\tfrac{nH}{P_{BS}^{\max}\lambda_{p1}}\right)\right]. \end{aligned} \tag{5.A.2}$$

In a similar way, A_2 it can be first calculated as

$$\begin{aligned} A_2 &= \Pr\left(|h_{1n*}|^2 > \tfrac{|h_{p1*}|^2\xi}{H}, |h_{p1*}|^2 > \tfrac{H}{P_{BS}^{\max}}\right) = \int_{\frac{H}{P_{BS}^{\max}}}^{\infty} \left(1 - F_{|h_{1n*}|^2}\left(\tfrac{\xi x}{H}\right)\right) f_{|h_{p1*}|^2}(x)\, dx \\ &= \sum_{n=1}^{N}\sum_{m=1}^{N} \binom{N}{n}\binom{N}{m} (-1)^{n+m-2} \tfrac{m}{\lambda_{p1}} \int_{\frac{H}{P_{BS}^{\max}}}^{\infty} \exp\left(-\left(\tfrac{n\xi}{H\lambda_{1n}} + \tfrac{m}{\lambda_{p1}}\right)x\right) dx \end{aligned} \tag{5.A.3}$$

From (5.A.2) and (5.A.3), A can write such as

$$\begin{aligned} A = &\sum_{n=1}^{N} \binom{N}{n} (-1)^{n-1} \exp\left(-\tfrac{n\xi}{P_{BS}^{\max}\lambda_{1n}}\right) \times \left[1 - \sum_{n=1}^{N} \binom{N}{n} (-1)^{n-1} \exp\left(-\tfrac{nH}{P_{BS}^{\max}\lambda_{p1}}\right)\right] \\ &+ \sum_{n=1}^{N}\sum_{m=1}^{N} \binom{N}{n}\binom{N}{m} (-1)^{n+m-2} \tfrac{mH\lambda_{1n}}{n\xi\lambda_{p1}+mH\lambda_{1n}} \times \exp\left(-\left(\tfrac{n\xi}{H\lambda_{1n}} + \tfrac{m}{\lambda_{p1}}\right)\tfrac{H}{P_{BS}^{\max}}\right). \end{aligned} \tag{5.A.4}$$

We plug (5.A.4) into (5.65), it can be achieved as the proposition.

This is the end of the proof.

Appendix B: Proof of **Theorem 2**

From (5.67), B_1 can be formulated by

$$\begin{aligned} B_1 &= \Pr\left(\gamma_{BS-D_2*}^{(x_2)} \geq \gamma_2\right) = \Pr\left(|h_{2n*}|^2 \geq \tfrac{\gamma_2 N_0}{P_{BS}^{\max}(a_2 - \gamma_2 a_1)}, P_{BS}^{\max} < \tfrac{H}{|h_{p1*}|^2}\right) \\ &\quad - \Pr\left(|h_{2n*}|^2 \geq \tfrac{\gamma_2 N_0}{\frac{H}{|h_{p1*}|^2}(a_2 - \gamma_2 a_1)}, P_{BS}^{\max} > \tfrac{H}{|h_{p1*}|^2}\right) \\ &= \underbrace{\Pr\left(|h_{2n*}|^2 \geq \frac{\gamma_2 N_0}{P_{BS}^{\max}(a_2 - \gamma_2 a_1)}, P_{BS}^{\max} < \frac{H}{|h_{p1*}|^2}\right)}_{B_{1a}} \\ &\quad \underbrace{- \Pr\left(|h_{2n*}|^2 \geq \frac{\gamma_2 N_0 |h_{p1*}|^2}{H(a_2 - \gamma_2 a_1)}, P_{BS}^{\max} > \frac{H}{|h_{p1*}|^2}\right)}_{B_{1b}}. \end{aligned} \tag{5.B.1}$$

Next, B_{1a} it can be first calculated as

$$\begin{aligned} B_{1a} &= \Pr\left(|h_{2n*}|^2 \geq \tfrac{\gamma_2 N_0}{P_{BS}^{\max}(a_2 - \gamma_2 a_1)}\right) \times \left[1 - \Pr\left(|h_{p1*}|^2 \geq \tfrac{H}{P_{BS}^{\max}}\right)\right] \\ &= \sum_{n=1}^{N} \binom{N}{n} (-1)^{n-1} \exp\left(-\tfrac{n\gamma_2 N_0}{P_{BS}^{\max}(a_2 - \gamma_2 a_1)\lambda_{2n}}\right) \\ &\quad \times \left[1 - \sum_{n=1}^{N} \binom{N}{n} (-1)^{n-1} \exp\left(-\tfrac{nH}{P_{BS}^{\max}\lambda_{p1}}\right)\right]. \end{aligned} \tag{5.B.2}$$

From (5.B.1), B_{1b} it can be first calculated as

$$\begin{aligned}
B_{1b} &= \Pr\left(|h_{2n*}|^2 \geq \tfrac{\gamma_2 N_0 |h_{p1*}|^2}{H(a_2-\gamma_2 a_1)}, |h_{p1*}|^2 > \tfrac{H}{P_{BS}^{\max}}\right) \\
&= \int_{\frac{H}{P_{BS}^{\max}}}^{\infty} \left(1 - F_{|h_{2n*}|^2}\left(\tfrac{\varepsilon_2 \omega_0 x}{H(\beta_2 - \varepsilon_2 \beta_1)}\right)\right) f_{|h_{p1*}|^2}(x)\, dx \\
&= \sum_{n=1}^{N}\sum_{m=1}^{N} \binom{N}{n}\binom{N}{m} (-1)^{n+m-2} \tfrac{m}{\lambda_{p1}} \times \int_{\frac{H}{P_{BS}^{\max}}}^{\infty} \exp\left(-\left(\tfrac{n\gamma_2 N_0}{H(a_2-\gamma_2 a_1)\lambda_{2n}} + \tfrac{m}{\lambda_{p1}}\right) x\right) dx \\
&= \sum_{n=1}^{N}\sum_{m=1}^{N} \binom{N}{n}\binom{N}{m} (-1)^{n+m-2} \tfrac{mH(a_2-\gamma_2 a_1)\lambda_{2n}}{n\gamma_2 N_0 \lambda_{p1} + mH(a_2-\gamma_2 a_1)\lambda_{2n}} \\
&\times \exp\left(-\left(\tfrac{n\gamma_2 N_0}{H(a_2-\gamma_2 a_1)\lambda_{2n}} + \tfrac{m}{\lambda_{p1}}\right) \tfrac{H}{P_{BS}^{\max}}\right).
\end{aligned} \tag{5.B.3}$$

From (5.B.2) and (5.B.3), B_1 can writen such as

$$\begin{aligned}
B_1 &= \sum_{n=1}^{N} \binom{N}{n} (-1)^{n-1} \exp\left(-\tfrac{n\gamma_2 N_0}{P_{BS}^{\max}(a_2-\gamma_2 a_1)\lambda_{2n}}\right) \\
&\times \left[1 - \sum_{n=1}^{N} \binom{N}{n} (-1)^{n-1} \exp\left(-\tfrac{nH}{P_{BS}^{\max}\lambda_{p1}}\right)\right] \\
&+ \sum_{n=1}^{N}\sum_{m=1}^{N} \binom{N}{n}\binom{N}{m} (-1)^{n+m-2} \tfrac{mH(a_2-\gamma_2 a_1)\lambda_{2n}}{n\gamma_2 N_0 \lambda_{p1} + mH(a_2-\gamma_2 a_1)\lambda_{2n}} \\
&\times \exp\left(-\left(\tfrac{n\gamma_2 N_0}{H(a_2-\gamma_2 a_1)\lambda_{2n}} + \tfrac{m}{\lambda_{p1}}\right) \tfrac{H}{P_{BS}^{\max}}\right).
\end{aligned} \tag{5.B.4}$$

From (5.67), B_2 can be formulated by

$$B_2 = \Pr\left(\min\left(\gamma_{D_1*}^{(x_2)}, \gamma_{D_1-D_2*}^{(x_2)}\right) < \gamma_2\right) = 1 - \underbrace{\Pr\left(\gamma_{D_1*}^{(x_2)} \geq \gamma_2\right)}_{B_{2a}} \underbrace{\Pr\left(\gamma_{D_1-D_2*}^{(x_2)} \geq \gamma_2\right)}_{B_{2b}}. \tag{5.B.5}$$

B_{2a} can be formulated such as B_1, we have

$$\begin{aligned}
B_{2a} &= \sum_{n=1}^{N} \binom{N}{n} (-1)^{n-1} \exp\left(-\tfrac{n\gamma_2 N_0}{P_{BS}^{\max}(a_2-\gamma_2 a_1)\lambda_{1n}}\right) \\
&\times \left[1 - \sum_{n=1}^{N} \binom{N}{n} (-1)^{n-1} \exp\left(-\tfrac{nH}{P_{BS}^{\max}\lambda_{p1}}\right)\right] \\
&+ \sum_{n=1}^{N}\sum_{m=1}^{N} \binom{N}{n}\binom{N}{m} (-1)^{n+m-2} \tfrac{mH(a_2-\gamma_2 a_1)\lambda_{1n}}{n\gamma_2 N_0 \lambda_{p1} + mH(a_2-\gamma_2 a_1)\lambda_{1n}} \\
&\times \exp\left(-\left(\tfrac{n\gamma_2 N_0}{H(a_2-\gamma_2 a_1)\lambda_{1n}} + \tfrac{m}{\lambda_{p1}}\right) \tfrac{H}{P_{BS}^{\max}}\right).
\end{aligned} \tag{5.B.6}$$

From (5.B.5), B_{2b} it can be first calculated as

$$\begin{aligned} B_{2b} &= \Pr\left(\gamma_{D_1-D_2}^{(x_2)} \geq \gamma_2\right) = \Pr\left(\min\left\{P_{D_1}^{EH}, P_{D_1}^{\max}, H/|h_{p2}|^2\right\} \geq N_0\gamma_2\right) \\ &= \Pr\left(P_{D_1}^{EH} \geq \tfrac{N_0\gamma_2}{|h_3|^2}\right) \Pr\left(P_{D_1}^{\max} \geq \tfrac{N_0\gamma_2}{|h_3|^2}\right) \Pr\left(\tfrac{H}{|h_{p2}|^2} \geq \tfrac{N_0\lambda_2}{|h_3|^2}\right) \\ &= \exp\left(-\tfrac{N_0\gamma_2}{P_{D_1}^{\max}\lambda_3}\right) \underbrace{\Pr\left(|h_3|^2 \geq \frac{N_0\gamma_2\left(1-\alpha\right)}{2\eta P_B\alpha|h_b|^2}\right)}_{B_{2b}^{(1)}} \times \underbrace{\Pr\left(|h_3|^2 \geq \frac{N_0\gamma_2|h_{p2}|^2}{H}\right)}_{B_{2b}^{(2)}}. \end{aligned} \tag{5.B.7}$$

From (5.B.7), $B_{2b}^{(1)}$ it can be first calculated as

$$\begin{aligned} B_{2b}^{(1)} &= \Pr\left(|h_3|^2 \geq \tfrac{N_0\gamma_2(1-\chi)}{2\eta P_B\chi|h_b|^2}\right) = \int_0^\infty \exp\left(-\tfrac{N_0\gamma_2(1-\alpha)}{2\eta P_B\alpha\lambda_3 x}\right) \tfrac{1}{\lambda_b} \exp\left(-\tfrac{x}{\lambda_b}\right) dx \\ &= \sqrt{\tfrac{2N_0\gamma_2(1-\alpha)}{\eta P_B\alpha\lambda_3\lambda_b}} K_1\left(\sqrt{\tfrac{2N_0\gamma_2(1-\alpha)}{\eta P_B\alpha\lambda_3\lambda_b}}\right). \end{aligned} \tag{5.B.8}$$

It is worth noting that the last equation follows from the fact that
$\int_0^\infty \exp\left(-\frac{\delta}{4x} - \varphi x\right) dx = \sqrt{\frac{\delta}{\varphi}} K_1\left(\sqrt{\delta\varphi}\right)$ in [[76], eq. (3.324)].
From (5.B.7), $B_{2b}^{(2)}$ it can be first calculated as

$$B_{2b}^{(2)} = \Pr\left(|h_3|^2 \geq \frac{N_0\gamma_2|h_{p2}|^2}{H}\right) = \frac{1}{\lambda_{p2}} \int_0^\infty \exp\left(-\left(\frac{N_0\gamma_2}{H\lambda_3} + \frac{1}{\lambda_{p2}}\right) x\right) dx = \frac{H\lambda_3}{N_0\gamma_2\lambda_{p2} + H\lambda_3}. \tag{5.B.9}$$

From (5.B.6), (5.B.7), (5.B.8), (5.B.9), B_2 can writen such as

$$\begin{aligned} B_2 = 1 - \Bigg\{ & \left\{ \begin{array}{l} \sum_{n=1}^{N} \binom{N}{n} (-1)^{n-1} \exp\left(-\frac{n\gamma_2 N_0}{P_{BS}^{\max}(a_2-\gamma_2 a_1)\lambda_{1n}}\right) \\ \times \left[1 - \sum_{n=1}^{N} \binom{N}{n} (-1)^{n-1} \exp\left(-\frac{nH}{P_{BS}^{\max}\lambda_{p1}}\right)\right] \end{array} \right. \\ & \left. \begin{array}{l} + \sum_{n=1}^{N}\sum_{m=1}^{N} \binom{N}{n}\binom{N}{m} (-1)^{n+m-2} \frac{mH(a_2-\gamma_2 a_1)\lambda_{1n}}{n\gamma_2 N_0\lambda_{p1} + mH(a_2-\gamma_2 a_1)\lambda_{1n}} \\ \times \exp\left(-\left(\frac{n\gamma_2 N_0}{H(a_2-\gamma_2 a_1)\lambda_{1n}} + \frac{m}{\lambda_{p1}}\right)\frac{H}{P_{BS}^{\max}}\right) \end{array} \right\} \\ & \times \tfrac{H\lambda_3}{N_0\gamma_2\lambda_{p2}+H\lambda_3} \exp\left(-\tfrac{N_0\gamma_2}{P_{D_1}^{\max}\lambda_3}\right) \times \sqrt{\tfrac{2N_0\gamma_2(1-\alpha)}{\eta P_B\alpha\lambda_3\lambda_b}} K_1\left(\sqrt{\tfrac{2N_0\gamma_2(1-\alpha)}{\eta P_B\alpha\lambda_3\lambda_b}}\right). \end{aligned} \tag{5.B.10}$$

We plug (5.B.4), (5.B.10) into (5.67), it can be achieved OP_2 as the proposition. This is the end of the proof.

6 Performance Analysis of Cooperative Relaying Network Using CR-NOMA and Calculating to Enhance Power Spectrum Distribution Efficiency of Users in Wireless Communication

In this chapter, the second aim of the dissertation, we proposed two system models of efficiency power spectrum allocation and fairness to the end-users. In the first model, we proposed a model of cooperative relaying network cognitive radio-assisted NOMA to improved the performance of far NOMA end users. In the second model, we designed a new system model integrated networks satellite-terrestrial. Finally, we presented a study on the performance analysis of NOMA underlay cognitive hybrid satellite-terrestrial relaying network (CSTRN) and highlight the performance gaps between multiple the end-users. **[NHN02]**, **[NHN03]**, **[NHN05]**, **[NHN07]**, **[NHN11]**, **[NHN12]**, **[NHN14]** **[NHN16]**

6.1 Cognitive radio assisted Non-Orthogonal Multiple Access: Outage performance

In this section, the performance of overlay CR in secondary networks utilizing NOMA is examined. We considered transmission quality from the relay to the far NOMA users who expect multiple access to the core network. In this system model, weak users with a weak signal and weak channel conditions are focused on. Our proposal analysis contributes to improving the outage performance of far NOMA the end-users. We first identify SNR to discover separated signals for each user, and exact expressions of OP are examined, assuming that the receiver can completely delete the interference with successive interference elimination. Then, we determined outage and throughput performance based on the SNR achieved. **[NHN11]**

6.1.1 Introduction

CR has been noticed remarkably thanks to its ability to improve spectrum utilization [8]. In the context as CR is proposed to the 5G mobile networks, both the PUs (including BS and mobile users served by the BS) and the SUs (mobile users non-served by the BS) can coexist together in the same licensed band [96]. In this scenario, the intervention from SUs is detrimental to the PU, and accordingly, the intervention must be limited to a certain level [97]. The first solution is CR technology that can automatically select channels without user interference (overlay CR) or under certain intervention temperatures (underlay CR). The other solution, NOMA, is more promising than OMA, which allows various users to transfer signals using the same time slot and carrier. However, both technologies mentioned above to improve spectral efficiency based on spectrum sharing may lead to a secure problem during communications [98]. For example, wiretapping legitimate signals of SUs may occur due to a lack of adequate spectrum management policies even though they have access rights to a spectrum of a PU in CRNs. Accordingly, there have been many models inspections to assure the optimal secure transmission quality of primary

systems in CRNs [99–101]. The authors in [15, 38, 48, 70, 102, 103] have proved that relaying network displays prolonged coverage with sufficient outage performance. This relay scheme has been combined with NOMA technology to create collaborative NOMA [10, 104]. Therefore, the user transmission quality is ensured with poor channels [94] and more users can access a spectrum resource block at the same time.

6.1.2 System Model

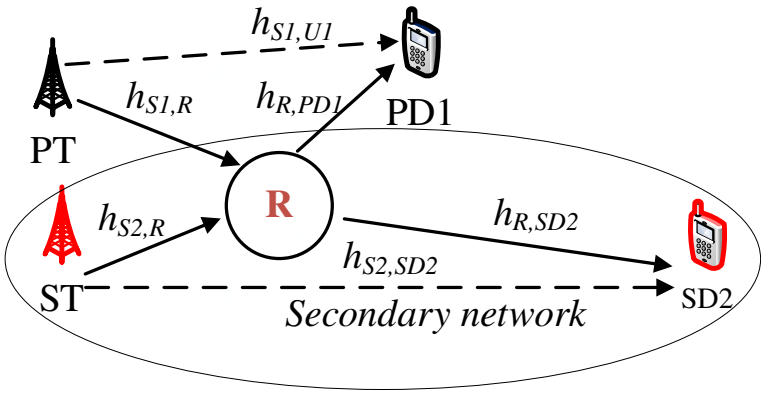

Figure 6.1: System model of CR based NOMA.

This section examines a CR communication together with NOMA as displayed in Figure 6.1. This model is called as CR- NOMA including a base station (PT) in primary network and source ST in secondary network, a relay R and a pair of NOMA users (near user PD1 and far user SD2). A single antenna is equipped for all components in the network which gives performance in such model using the NOMA transmission regulations. In our assumption, both the relay and two NOMA users can inspect their SNR because they can identify the channel state information (CSI) of all the channels entirely. Additionally, it is assumed that all channels are quasi- static Rayleigh fading, where the channel coefficients are fixed for each transmission block but alter separately between different blocks. The first antenna and the second antenna in such model transmit x_1, x_2 respectively to both relay and far NOMA users simultaneously. a_1, a_1 are power distribution factors for two NOMA user PD1, SD2 respectively. We call P_{S_1}, P_{S_2} are transmit power at PT, ST respectively. We call $d_{a,b}$ is distance between node a and node b.

In this case, the SN is focused on for the first phase, relay R may receive the synthetic message from the ST.

$$y_R = \sqrt{a_1 P_{S1}} x_1 h_{S1,R} + \sqrt{a_2 P_{S2}} x_2 h_{S2,R} + n_R \tag{6.1}$$

The received signal at destination SD2 in relay link is shown by

$$y_{R,SD2} = (\sqrt{a_1 P_R} x_1 + \sqrt{a_2 P_R} x_2) h_{R,SD2} + n_{R,SD2} \tag{6.2}$$

The received signal at destination SD2 in direct link is given by

$$y_{S2,SD2} = \sqrt{P_{S2}} x_2 h_{S2,SD2} + n_{S2,SD2} \tag{6.3}$$

In this case, we assume equality variances of these noise terms $n_{(.)}$ as σ^2, $\rho = \frac{P_{S1}}{\sigma^2} = \frac{P_{S2}}{\sigma^2} = \frac{P_R}{\sigma^2}$. It can be computed various SNRs as below. SNR at relay to detect x_2 is given by

$$\gamma_{R,x2} = \frac{a_2 \rho |h_{S2,R}|^2}{a_1 p |h_{S1,R}|^2 + 1}. \tag{6.4}$$

SNR at relay to detect x_1 is given by

$$\gamma_{R,x1} = a_1 \rho |h_{S1,R}|^2 \tag{6.5}$$

.

It is noted that relay follows decode-and-forward scheme. We compute SNR at SD2 to detect x_2

$$\gamma_{RSD2,x2} = \frac{a_2 \rho |h_{R,SD2}|^2}{a_1 \rho |h_{R,SD2}|^2 + 1}. \tag{6.6}$$

In direct link, SNR is given by

$$\gamma_{S2SD2,x2} = \rho |h_{S2,SD2}|^2 \tag{6.7}$$

6.1.3 Outage Probability and Throughput Analysis

In this section, we investigated the OP for the CR NOMA downlink cooperative network with excellent CSI. The Maximal Ratio Combining (MRC) is employed to further process signal at SD2 as representatives of direct link and relay link between the ST and NOMA end-users.

Firstly, SNR at user SD2 can be formulated as

$$\gamma_{SD2}^{MRC} = \gamma_{S2,SD2} + \gamma_{RSD2,x2} = \rho |h_{S2,SD2}|^2 + \frac{a_2 \rho |h_{R,SD2}|^2}{a_1 \rho |h_{R,SD2}|^2 + 1} \tag{6.8}$$

An outage event occurs at the far NOMA user, such outage probability at user SD2 can be computed by

$$P_{SD2} = \underbrace{\Pr\left(\gamma_{SD2}^{MRC} < \gamma_2\right)}_{B_1} \underbrace{\Pr\left(\gamma_{R,x2} > \gamma_2\right)}_{B_2} + \underbrace{\Pr\left(\gamma_{R,x2} < \gamma_2, \gamma_{S2SD2,x2} < \gamma_2\right)}_{B_3} \tag{6.9}$$

To look performance of SU,

Proposition 1:

The closed-form expression of OP at user SD2 can be expressed by

$$P_{SD2} = \left[1 - e^{\frac{\tau}{d_{RU2}^{-m}}} - \frac{e^{\xi}}{\Psi_2} \sum_{n=0}^{\infty} \frac{(-1)^n}{n!\left(d_{RSD2}^{-m} a_1 \rho\right)^n} \Xi_2\right] \frac{d_{S2R}^{-m}}{d_{S2R}^{-m} + \gamma_2 d_{S1R}^{-m}} e^{\frac{-\gamma_2}{d_{sRR}^{-m}\rho}} 1 - e^{-\frac{\gamma_2}{d_{S2SD2}^{-m}\rho_2\rho}} - \frac{d_{S2R}^{-m}}{d_{S2R}^{-m} + d_{S1R}^{-m}\gamma_2} \left(e^{\frac{\gamma_2}{d_{S2R}^{m}\rho}} - e^{-\gamma_2\left(\frac{1}{d_{S2SD2}^{-m}\rho} + \frac{1}{d_{S2R}^{-m}\rho}\right)}\right). \tag{6.10}$$

where $\Xi_2 = \frac{(-1)^{2n+1}\Psi_1^{n+1}}{(n+1)!}(Ei(\xi) - Ei(\Psi_1)) + \sum_{k=0}^{n} \frac{e^{\xi}(1+a_1\rho\tau.)^{n.+1}\xi^k - e^{\Psi_1}\Psi_1^k}{(n+1)n.(n+1-k)}$,

and $\xi = \frac{1}{a_1\rho d_{RU2}^{-m}} - \frac{\gamma_2}{\rho d_{S2U2}^{-m}} - \Psi_1, \Psi_1 = -\frac{a_2}{a_1\rho d_{S2U2}^{-m}}, \Psi_2 = a_1 p d_{RU2}^{-m}$.

Proof: See in Appendix C

After that, we further examine optimal throughput in case of fixed data rate R_2 is prior known. Such system throughput can be calculated by

$$\tau = (1 - P_{SD2})R_2 \tag{6.11}$$

6.1.4 Numerial Results

In this section, a two-user CR NOMA system is considered. We conduct some computer simulations to validate the accuracy of the analytical results. The SNR at the ST is determined as previous section. The analytical result is presented in many figures where the parameters are set as wherein.

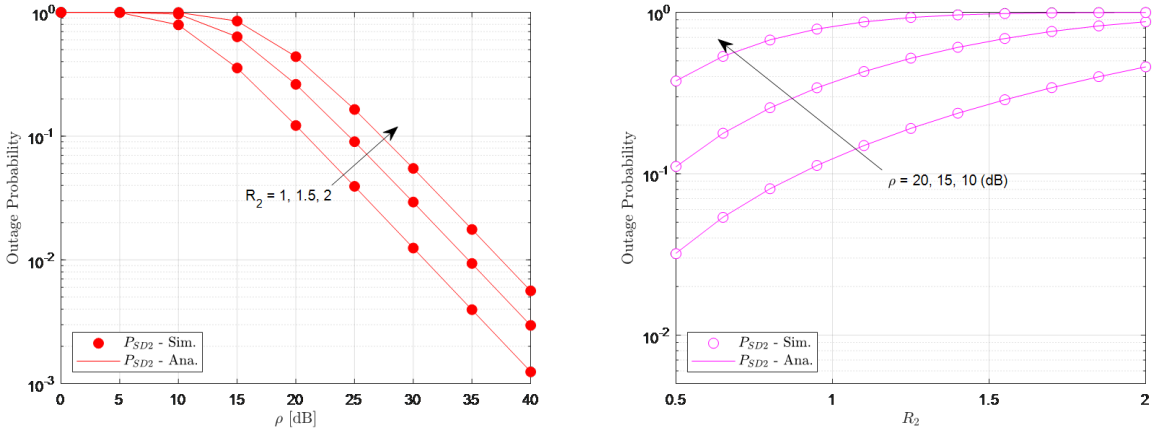

(a) OP versus transmit SNR at ST.

(b) OP versus target rate at SD2.

Figure 6.2: Outage probability versus transmit SNR at ST and versus target rate at SD2.

We can observe the OP performance in Figure 6.2a. For this target rate setup, it is obvious that OP decreases when SNR increases and the performance gaps among three cases of NOMA users in different rates exist in range of SNR. By observing such figures, it can be confirmed that the lower target rate demonstrates better performance, which means that $R_1 = 1\,(bps/Hz)$ is the best one among these cases. This result can be explained as such target rate make different outage levels. Both analytical and simulation results are matched well.

Figure 6.2b demonstrates that OP displays worse performance at higher target rates. In another observation, the higher SNR at the source ST contributes to improve outage performance of the considered system. In three cases, the performance gaps of such CR NOMA scheme still remain in range of acceptable target rate regime.

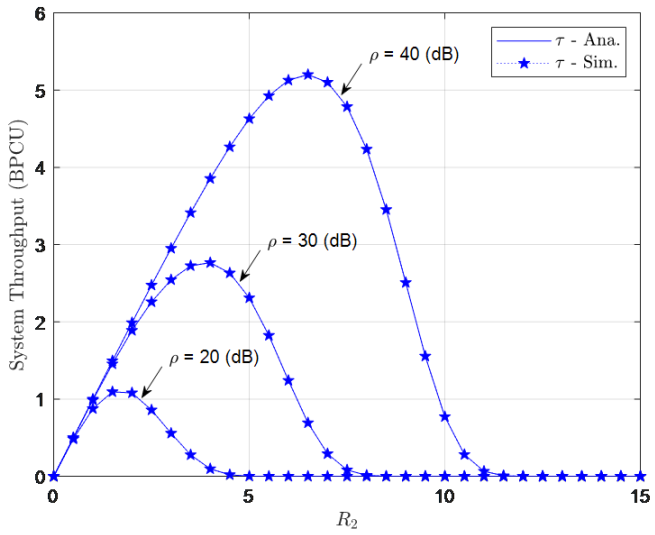

Figure 6.3: Throughput versus target rates.

In Figure 6.3, we can observe throughput performance where the throughput is optimal when we change target rates and transmit SNR at the ST. In this situation, the optimal throughout can be achieved at $\rho = 40\,(dB)$, $R_2 = 7\,(bps/Hz)$.

6.1.5 Conclusion

In this section, the outage and throughput performance in CR-based NOMA systems have been examined. The signal is transmitted to the relay thanks to the relaying model in the SN, and then the superimposed signal can be attained at the NOMA end users. This scheme was applied to provide multiple access in downlink (DL). The simulation results show that with the proposed fixed power distribution scheme, the considered CR-NOMA system can ensure fairness in NOMA remarkably. Therefore, the highest throughput can be achieved at a specific data rate.

Appendix C

It can be calculated each component in such outage of SD2 as [94]

$$\begin{aligned} B_1 &= \Pr\left(\gamma_{SD2}^{MRC} < \gamma_2\right) = \Pr\left(\rho|h_{S2,SD2}|^2 + \frac{a_2\rho\left|h_{R,SD2}\right|^2}{a_1\rho\left|h_{R,SD2}\right|^2+1} < \gamma_2\right) \\ &= \Pr\left(|h_{S2,SD2}|^2 < \frac{\gamma_2}{\rho} - \frac{a_2\left|h_{R,SD2}\right|^2}{a_1\rho\left|h_{R,SD2}\right|^2+1}, |h_{R,SD2}|^2 < \tau\right) \\ &= \int_0^{\tau} F_{\left|h_{S2,SD2}\right|^2}\left(\frac{\gamma_2}{\rho} - \frac{a_2 x}{a_1\rho x+1}\right) f_{\left|h_{R,SD2}\right|^2}(x)\, dx. \end{aligned} \tag{C.1}$$

New variable is set as $y = a_1\rho x + 1$ then it can be rewritten as

$$\begin{aligned} \Xi_1 &= \frac{1}{d_{RSD2}^{-m}} e^{-\frac{\gamma_2}{\rho d_{S2SD2}^{-m}}} \int_1^{\tau a_1\rho+1} e^{-\frac{y-1}{\rho a_1 d_{RSD2}^{-m}}} e^{\frac{a_2(y-1)}{\rho d_{S2SD2}^{-m} a_1 y}} dy \\ &= \frac{e^{\xi}}{\Psi_2} \sum_{n=0}^{\infty} \frac{(-1)^n}{n!\left(d_{RSD2}^{-m} a_1\rho\right)^n} \underbrace{\int_1^{\tau a_1\rho+1} y^n e^{-\frac{y}{\rho d_{S2SD2}^{-m} a_1 y}} dy}_{\Xi_2}, \end{aligned} \tag{C.2}$$

where $\xi = \frac{1}{a_1\rho d_{RSD2}^{-m}} - \frac{\gamma_2}{\rho d_{S2SD2}^{-m}} - \Psi_1$, $\Psi_1 = -\frac{a_2}{a_1\rho d_{S2SD2}^{-m}}$ and $\Psi_2 = a_1\rho d_{RU2}^{-m}$. Note that it can be further calculated new equation by using Binomial theorem.

We set $z = \frac{1}{y}$ and it can be achieved that

$$\begin{aligned} \Xi_2 &= \int_{\frac{1}{\tau a_1\rho+1}}^{1} \frac{1}{z^{n+2}} e^{-\frac{a_2 z}{\rho d_{S2SD2}^{-m} a_1}} dz \\ &= \frac{(-1)^{2n+1}\Psi_1^{n+1}}{(n+1)!}\left(\mathrm{Ei}(\xi) - \mathrm{Ei}(\Psi_1)\right) + \sum_{k=0}^{n} \frac{e^{\xi}(1+a_1\rho\tau)^{n+1}\xi^k - e^{\Psi_1}\Psi_1^k}{(n+1)n\ldots(n+1-k)}. \end{aligned} \tag{C.3}$$

It then can be rewritten as follow

$$\begin{aligned} B_1 = 1 &- e^{-\frac{\tau}{d_{RU2}^{-m}}} - e^{\xi} \sum_{n=0}^{\infty} \frac{(-1)^n}{n!\Psi_2^{n+1}} \\ &\times \left[\frac{(-1)^{2n+1}\Psi_1^{n+1}}{(n+1)!}\left(\mathrm{Ei}(\xi) - \mathrm{Ei}(\Psi_1)\right) + \sum_{k=0}^{n} \frac{e^{\xi}(1+a_1\rho\tau)^{n+1}\xi^k - e^{\Psi_1}\Psi_1^k}{(n+1)n\ldots(n+1-k)}\right]. \end{aligned} \tag{C.4}$$

Next, we continue to compute the other components as below

$$\begin{aligned} B_2 &= \Pr\left(\gamma_{R,x2} > \gamma_2\right) \\ &= \Pr\left(|h_{S2,R}|^2 > \frac{\gamma_2}{\rho}\left(\rho|h_{S1,R}|^2 + 1\right)\right) = \int_0^{\infty} \int_{\frac{\gamma_2}{\rho}(\rho x+1)}^{\infty} f_{\left|h_{S1,R}\right|^2}(x)\, f_{\left|h_{S2,R}\right|^2}(y)\, dxdy \\ &= \frac{d_{S2R}^{-m}}{d_{S2R}^{-m} + \gamma_2 d_{S1R}^{-m}} e^{-\frac{\gamma_2}{d_{S2R}^{-m}\rho}}, \end{aligned} \tag{C.5}$$

$$
\begin{aligned}
B_3 &= \Pr\left(\gamma_{R,x2} < \gamma_2, \gamma_{S2SD2,x2} < \gamma_2\right) = \Pr\left(\frac{\rho\left|h_{S2,R}\right|^2}{\rho\left|h_{S1,R}\right|^2+1} < \gamma_2, \rho\left|h_{S2,SD2}\right|^2 < \gamma_2\right) \\
&= \Pr\left(\left|h_{S2,R}\right|^2 < \tfrac{\gamma_2}{\rho}\left(\rho\left|h_{S1,R}\right|^2+1\right), \left|h_{S2,SD2}\right|^2 < \tfrac{\gamma_2}{\rho}\right) \\
&= \int_0^{\frac{\gamma_2}{\rho}} f_{\left|h_{S2,SD2}\right|^2}(x)\,dx \int_0^{\infty} \int_0^{\frac{\gamma_2}{\rho}(\rho y+1)} f_{\left|h_{S1,R}\right|^2}(y)\, f_{\left|h_{S2,R}\right|^2}(z)\,dydz \\
&= \left(1 - e^{-\frac{\gamma_2}{d_{S2U2}^{-m}\rho}}\right)\left(1 - \frac{d_{S2R}^{-m}}{d_{S2R}^{-m}+d_{S1R}^{-m}\gamma_2} e^{-\frac{\gamma_2}{d_{S2R}^{-m}\rho}}\right) \\
&= 1 - e^{-\frac{\gamma_2}{d_{S2SD2}^{-m}\rho}} - \frac{d_{S2R}^{-m}}{d_{S2R}^{-m}+d_{S1R}^{-m}\gamma_2}\left(e^{-\frac{\gamma_2}{d_{S2R}^{-m}\rho}} - e^{-\gamma_2\left(\frac{1}{d_{S2SD2}^{-m}\rho}+\frac{1}{d_{S2R}^{-m}\rho}\right)}\right).
\end{aligned}
\tag{C.6}
$$

It can be replaced above results to achieve final equation.

This is the end of the proof.

6.2 Enhancing Spectrum Efficiency for Multiple Users in Hybrid Satellite-Terrestrial Networks to the fairness of users

This section presents a study on the performance analysis of a NOMA underlay cognitive hybrid satellite-terrestrial relaying network (CSTRN) and highlights the performance gaps between multiple the end-users. The satellite source communicates with users by enabling the CR scheme to forward signals to secondary destinations on the ground which belong to dedicated groups following the principle of NOMA. In this scenario, the secondary source acts as a relay and employs AF mode to serve distant NOMA users under a given interference constraint. The shadowed-Rician fading and Nakagami-m fading models are widely adopted to the relevant hybrid channels to characterize the transmission environment. To provided a detailed examination of the system performance metrics, we aim to derived closed-form formulas for the OP of the secondary destination in the presence of the primary interference power constraint imposed by the adjacent primary satellite network. Finally, our simulation results showed that more antennas, better quality of wireless channels, and power allocation factors exhibit the main effects on system performance. **[NHN03]**

6.2.1 Introduction

Regarded as an attractive method for achieving high throughput with a broad coverage area, hybrid satellite systems, and terrestrial networks can be integrated to form hybrid satellite-terrestrial networks (HSTNs) [59]. In an HSTN, a wide range of applications can be offered for the purposes of navigation, broadcasting, and disaster relief [105]. Improve area coverage, system performance can be achieved in the system models by employing cooperative relaying techniques, which are reported in [106, 107]. In addition, both relaying network and CR technology can major applications of HSTNs by enhancing the efficiency of spectrum utilization. The promising

architecture is studied as cognitive HSTN (CHSTN) [108–113]. In such a CHSTN, a secondary terrestrial network operates in the same spectrum resource as the primary satellite network. The two main factors in CHSTNs, i.e., SU transmit power constraints and inefficient use of available spectrum resources, may degrade the performance of the SN.

There are other challenges since current communication systems possess limited power and spectrum resources. Existing systems can potentially overcome these challenges by enabling the recently proposed NOMA. Unlike conventional OMA, NOMA-aided BSs employ the power domain to assist multiplexing before sending to mobile users. The NOMA technique, superposition coding (SC), and SIC performed at the corresponding transmitters, and receivers allow users to achieve higher spectrum efficiency [114]. In the principle of NOMA, more power levels are allocated to users with poorer channels. As such, weak users can decode signals directly by considering other signals, such as noise. Before detecting the main signal, the user who experiences a better channel decodes the strong signals and eliminates them. The NOMA technique has three main benefits: low latency, massive connectivity, and high spectral efficiency [115]. The authors in [116] investigated a downlink NOMA scenario with randomly deployed users to demonstrate its superior performance, i.e., ergodic capacity. The authors in [117] studied a real scenario with a transmitter that only achieved statistical channel state information (CSI) associated with each user. They proposed this model to implement a NOMA system by employing the Nakagami-m fading channels as a practical downlink. The authors in [118] presented the capability of unmanned aerial vehicle (UAV) communications using full-duplex NOMA (FD-NOMA) to enhance spectrum utilization. They described closed-form outage probability formulas for several scenarios such as FD-NOMA, half-duplex NOMA (HD-NOMA), and half-duplex OMA (HD-OMA) schemes over Rician shadowed fading channels. The authors in [119] studied an exciting alternative to conventional power domain-NOMA, known as NOMA-2000, in which multiple access was implemented by applying two sets of orthogonal waveforms. The simulation results in [120] for a fair-NOMA approach reported that each user's capacity was greater than or equal to the capacity of a system relying on OMA. Recent studies such as [121, 122] have also developed the application of device-to-device (D2D) communication in the context of NOMA. A cooperative NOMA scheme was studied in [19, 123, 124] to increase reliability and coverage. Users experiencing better channels were treated as relays to forward the messages of distant users experiencing poorer channels. The authors in [125, 126] proposed a UAV-NOMA network architecture. The authors in [126] indicated that D2D can be used to increase file dispatching efficiency. In a D2D-enhanced UAV-NOMA network, ground users (GUEs) may reuse the time-frequency resources assigned to NOMA links to share with other GUEs. The study in [127] presented two practical schemes of downlink UAV-NOMA. The first method minimized the transmit power of the UAV, satisfying the minimum achievable rate requirements.

To further improve the efficiency of spectrum utilization, NOMA can gain more benefit from cognitive radio (CR) and forming CR-inspired NOMA scenarios [65, 128–130]. The work in [65] investigated the integration of NOMA with CR to introduce more intelligent spectrum sharing

paradigms. Besides, to evaluate the performance of secondary NOMA users, end-to-end outage probability is considered the main performance metric. The recent work in [28] studied error rate performance in a scenario of relay-assisted NOMA with partial relay selection applied in an underlay CR network. Based on this system model, K relays were used to support transmission between secondary NOMA users and a secondary base station (SBS). In such a system, the relay which experiences the strongest link with the SBS is selected to forward the received signals to secondary receivers.

Related Work

The authors in [63] considered the performance of an overlay cognitive hybrid satellite-terrestrial relaying network (CSTRN). This system contains a primary satellite transmitter set up to send signals to multiple terrestrial receivers and a secondary transmitter-receiver pair located on the ground—the primary satellite transmitter employing NOMA architecture to serve all users simultaneously. Furthermore, the secondary transmitter assisted primary communication through a cooperative relaying method to deal with spectrum access. The authors in [62] studied the widely adopted shadowed-Rician fading and Nakagami-m fading models for relevant hybrid channels. Their main results were deriving a closed-form formula for the OP of an SN by considering the conditions on primary interference power constraints associated with the adjacent primary satellite network. The system reported in [20] introduced two main performance metrics: closed-form OP and approximate ergodic capacity expressions for the PU and SU. In this system, generalized Shadowed-Rician fading and a Nakagami-m fading were applied to satellite and terrestrial links. The simulation results verified the superiority of NOMA compared to conventional OMA schemes by varying specific key parameters. The authors in [131] presented the critical effect of HIs at user devices in an overlay cognitive hybrid terrestrial network which included a primary satellite source-receiver pair and a secondary transmitter-receiver pair on the ground. To mitigate the effect of HIs, the authors studied an adaptive relaying (AR) protocol for both AF and DF modes and compared its performance to competitor fixed relaying schemes.

However, the most benefit of NOMA in the CSTRN system is enabler of multiple served users in dedicated group of group. This paper motivated by recent studies [20, 62, 63, 131] to highlight how we benefit from enabling CR and NOMA in the CSTRN system.

The keys findings of this section can be summarized as follows:

- This study aims to proposed a framework of multiple NOMA user in the CSTRN system by exploiting set of analytical expressions to indicate the system performance metrics. In particular, we considered the OP and throughput of a complicated system which is designed with enablers of NOMA, CR, multiple secondary users and multiple-antenna satellite.

- Although reference [63] quantified the performance of a NOMA-assisted the CSTRN of the primary and secondary networks in terms of outage probability by considering the

pertinent heterogeneous fading models, our study mentions on complicated scenario of multiple antennas at the satellite and multiple users in a considered group. It is beneficial to improvement performance of NOMA-assisted the CSTRN. Due to complicated results computed in studies related to CSTRN system [20, 62, 63, 131], we also investigate the approximation performance of such outage behavior to look insights of such system. This important finding should be guidelines to design NOMA-CSTRN in practice. Table 6.1 should emphasize our key findings compared with recent studies

- Our numerical simulations are expected to provided main parameters which are used to improve specific performance metrics for the NOMA-CSTRN. These parameters are power allocation factors, the number of transmit antennas, channel fading gains, and transmit signal-to-noise ratio at the satellite.

Table 6.1: Comparision of proposed system with related works.

Context	**Cooperative Relay Network**	**Multiple Antenna**	**NOMA**	**Multiple Users**	**Asymptotic**
Our Work	Yes	Yes	Yes	Yes	Yes
[63]	Yes	No	Yes	Yes	Yes
[62]	No	No	Yes	No	No
[20]	Yes	No	Yes	No	No
[131]	Yes	No	No	No	No

6.2.2 System Model

In the present study, we examined satellite (S) equipped N_S antennas, a single antenna secondary relay (R), K secondary terrestrial destinations $D_k(1 \leqslant k \leqslant K)$ and a single primary terrestrial destination (PD) in Figure 6.4. The key parameters and denotations can be seen in Table 6.2

Two phases are required to process overall communication of the secondary network in such CSTRN. In the first phase, the superposition signal $s = \sum_{i=1}^{K} \sqrt{P_S a_i} x_i$ is sent from the S to the R using a weight vector $\mathbf{w}_{SR}$. The received signal at R is given by

$$y_R = \mathbf{h}_{SR}^{\dagger} \mathbf{w}_{SR} \sum_{i=1}^{K} \sqrt{P_S a_i} x_i + n_R, \tag{6.12}$$

where $\mathbf{h}_{SR} = \left[h_{SR}^1 \cdots h_{SR}^{N_S}\right]^T$ and n_R the additive white Gaussian noise (AWGN) with $n_R \sim \mathcal{CN}(0, N_0)$. By employing a MRT scheme [132], the transmit BF vector is formulated by $\mathbf{w}_{SR} = \frac{\mathbf{h}_{SR}}{\|\mathbf{h}_{SR}\|_F}$.

After signal processing at the first phase, the R first amplifies the received signal y_R with a gain factor G. This variable gain is defined $G = \sqrt{\frac{1}{P_S Z_R + N_0}}$, $Z_R = \|\mathbf{h}_{SR}\|_F^2$. Then, R forwards processed signal to all distant users. In particular, the received signal at the k-th user is given

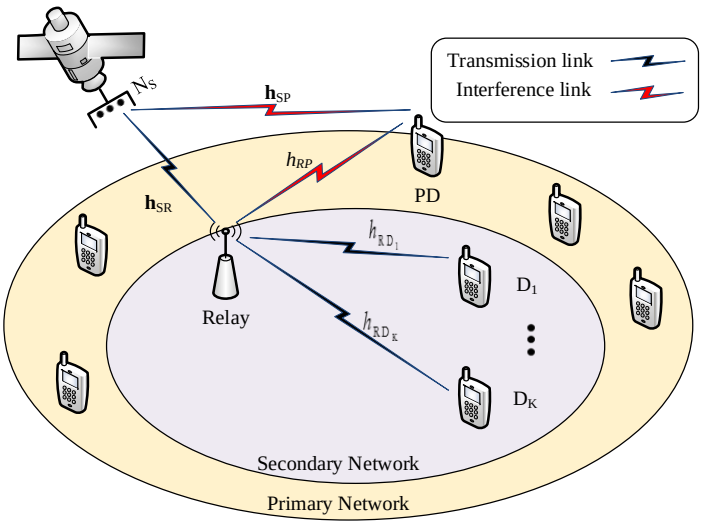

Figure 6.4: The system model of NOMA-CSTRN.

Table 6.2: The Description of Symbols.

Symbol	**Description**
N_S	number of antennas at satellite
K	number of terrestrial destination
P_S	The transmit power at S
P_R	The transmit power at S
x_i	The information required by destination i
a_i	The power allocation coefficient
h_{Sv}	The $N_S \times 1$ channel vector between satellite and relay with $v \in (R, P)$
h_{RD_k}	The channel coefficient between relay and terrestrial destination
h_{RD}	The channel coefficient between relay and primary user
$\|\bullet\|_F$	The Frobenius norm
$(\bullet)^\dagger$	The Conjugate transpose
$\beta(.,.)$	The Beta function
$\Gamma(.)$	The Gamma function
$\gamma(.,.)$	The lower incomplete Gamma function
${}_1F_1(.;.;.)$	The confluent hypergeometric function of the first kind
$G_{1,1}^{1,1}[.]$	The Meifer's G-function

by

$$y_{D_k} = \sqrt{P_R} h_{RD_k} G y_R + n_{D_k} = G h_{RD_k} \mathbf{h}_{SR}^\dagger \mathbf{w}_{SR} \sum_{i=1}^{K} \sqrt{P_S P_R a_i} x_i + G\sqrt{P_R} h_{RD_k} n_R + n_{D_k}, \quad (6.13)$$

Without loss of generality, the channel gains from R to D_k are ordered $h_{RD_1} \leqslant h_{RD_2} \leqslant \cdots \leqslant$

h_{RD_K}. This ordering procedure is associated with NOMA requirements. $n_{D_k} \sim \mathcal{CN}(0, N_0)$ is the AWGN.

To prevent interference at the PU beyond an acceptable level Q, the transmit power at S and R are given by [133] $P_S = \frac{Q}{Z_P}$ and $P_R = \frac{Q}{|h_{RP}|^2}$, respectively, where $Z_v = \|\mathbf{h}_{Sv}\|_F^2, v \in \{R, P\}$.

Considering how the system precisely detects the required signal at each user, we mention SIC in the context of NOMA. Since the desired signal encounters interference from the other users' signals, SIC is required at each user to eliminate the adverse effect of the inter-user interference. Therefore, at the k-th user, the m-th user's signal, $k < m$, must be detected. The system then deletes it from the received signal of the k-th user in a successive manner. In this situation, the m-th user's signal is treated as noise at the k-th user. We can therefore compute the signal-to-interference-and-noise ratio (SINR) for the k-th user to decode the m-th user's signal, $k \leq m$, as follows

$$\gamma_{m \to k} = \frac{G^2 P_R P_S Z_R |h_{RD_k}|^2 \phi_m}{G^2 P_R P_S Z_R |h_{RD_k}|^2 \sum\limits_{i=m+1}^{K} a_i + G^2 \sqrt{P_R} |h_{RD_k}|^2 N_0 + N_0} = \frac{\gamma_R \gamma_k \phi_m}{\gamma_R \gamma_{Y_k} \sum\limits_{i=p+1}^{K} a_i + \gamma_k + \gamma_R + 1}, \tag{6.14}$$

where $\rho = \frac{Q}{N_0}$, $\gamma_R = \rho Z_R / Z_P$ and $\gamma_k = \rho |h_{RD_k}|^2 / |h_{RP}|^2$. If x_m can be detected successfully, signal x_m can be deleted before the signal for user D_k is detected. The SINR of D_k to decode its own signal is given by

$$\gamma_k = \frac{\gamma_R \gamma_k \phi_k}{\gamma_R \gamma_{Y_k} \sum\limits_{i=k+1}^{K} a_i + \gamma_k + \gamma_R + 1}. \tag{6.15}$$

For successive processing of many users, the standard SIC component is operated until all other users' signals are detected. For the final user, the SINR of D_K to decode its own signal can be computed according to

$$\gamma_K = \frac{\gamma_R \gamma_K \phi_K}{\gamma_K + \gamma_R + 1}. \tag{6.16}$$

In term of the characteristic of wireless channels, the channel vector $\mathbf{h}_{Sv}$ is associated with i.i.d. Shadowed-Rician fading entries. By denoting $\delta_v = \Omega_{Sv} / (2b_{Sv}) (2b_{Sv} m_{Sv} + \Omega_{Sv})$ in which m_{Sv} represent as the fading severity parameter, Ω_{Sv} and b_{Sv} are the average power of Line-of-Sight (LoS) and multipath components, respectively, and ${}_1F_1(.;.;.)$ is the confluent hypergeometric function of the first kind [76, Eq. 9.210.1], the probability density function (PDF) of the squared amplitude of the channel coefficient $\left|h_{Sv}^{(i)}\right|^2$ is given by [107, 132]

$$f_{\left|h_{Sv}^{(i)}\right|^2}(x) = \alpha_v e_1^{-\beta_v x} {}_1F_1(m_{Sv}; 1; \delta_v x), x > 0, \tag{6.17}$$

where $\alpha_v = \left(2b_{Sv}m_{Sv}/\left(2b_{Sv}m_{Sv}+\Omega_{Sv}\right)\right)^{m_{Sv}}/2b_{Sv}$,$\beta_v = 0.5b_{Sv}$. For Shadowed-Rician fading with integer-valued severity parameters, we can rewrite (6.17) as

$$f_{\left|h_{Sv}^{(i)}\right|^2}(x) = \alpha_v \sum_{\kappa=0}^{m_{Sv}-1} \zeta_v(\kappa) x^{\kappa} e^{-\Psi_v x}, \tag{6.18}$$

where $\zeta_v(\kappa) = (-1)^{\kappa}\left(1-m_{Sv}\right)_{\kappa}\delta_v^{\kappa}/\left(\kappa!\right)^2$, $\Psi_v = \beta_v - \delta_v$ and $(.)_{\kappa}$ is the Pochhammer symbol [76, p. xliii], the PDF of Z_v under i.i.d. Shadowed Rician fading is given as

$$f_{Z_v}(x) = \sum_{i_1=0}^{m_{Sv}-1} \cdots \sum_{i_{N_S}=0}^{m_{Sv}-1} \Theta(v, N_S) x^{\Delta_v - 1} e^{-\Psi_v x}, \tag{6.19}$$

where

$$\Theta(v, N_S) = \alpha_v^{N_S} \prod_{\ell=1}^{N_S} \zeta_v(i_\ell) \prod_{j=1}^{N_S-1} ß\left(\sum_{l=1}^{j} i_l + j, i_{j+1}+1\right), \tag{6.20a}$$

$$\Delta_v = \sum_{q=1}^{N_S} i_q + N_S. \tag{6.20b}$$

and ß(.; ,) is the Beta function [76, Eq. 8.384.1].

The cumulative distribution functions (CDF) of Z_v can be obtained as [76, Eq. 3.351.2], the CDF of Z_v

$$F_{Z_v}(x) = 1 - \sum_{i_1=0}^{m_{Sv}-1} \cdots \sum_{i_{N_S}=0}^{m_{Sv}-1} \Theta(v, N_S) \times \sum_{p=0}^{\Delta_v - 1} \frac{\Gamma(\Delta_v)\Psi_v^{-\Delta_v+p}}{p!} x^p e^{-\Psi_v x}. \tag{6.21}$$

Considering the characterization of Nakagami-m fading, the PDF and CDF of channel gain $\left|\tilde{h}_{RD_k}\right|^2$ are given, respectively by [134]

$$f_{\left|\tilde{h}_{RD_k}\right|^2}(x) = \frac{x^{m_D-1}}{\Gamma(m_D)\lambda_D^{m_D}} e^{-\frac{x}{\lambda_D}}, \tag{6.22}$$

and

$$F_{\left|\tilde{h}_{RD_k}\right|^2}(x) = \frac{\gamma(m_D, x/\lambda_D)}{\Gamma(m_D)} = 1 - e^{-\frac{x}{\lambda_D}} \sum_{n_D=0}^{m_D-1} \frac{x^{n_D}}{\lambda_D^{n_D} n_D!}, \tag{6.23}$$

where $\lambda_D = \frac{\Omega_D}{m_D}$, m_D and $\Omega_D = \Omega_1 = \Omega_2 = \cdots = \Omega_K$ in this case is denoted as the fading severity and average power, respectively, and $\gamma(.,.)$ is the lower incomplete gamma function [76, Eq.

8.350.1]. Using order statistics, the PDF of $|h_{RD_k}|^2$ can be represented as

$$\begin{aligned} f_{|h_{RD_k}|^2}(x) &= \Upsilon f_{|\tilde{h}_{RD_k}|^2}(x) \left[F_{|\tilde{h}_{RD_k}|^2}(x)\right]^{k-1} \times \left[1 - F_{|\tilde{h}_{RD_k}|^2}(x)\right]^{K-k} \\ &= \Upsilon \sum_{m=0}^{K-k} (-1)^m \begin{pmatrix} K-k \\ m \end{pmatrix} \times f_{|\tilde{h}_{RD_k}|^2}(x) \left[F_{|\tilde{h}_{RD_k}|^2}(x)\right]^{k+m-1}, \end{aligned} \tag{6.24}$$

where $\Upsilon = \frac{K!}{(K-k)!(k-1)!}$. Furthermore, the CDF of $|h_{RD_k}|^2$ is expressed as

$$F_{|h_{RD_k}|^2}(x) = \Upsilon \sum_{m=0}^{K-k} \binom{K-k}{m} \frac{(-1)^m}{k+m} \left[F_{|\tilde{h}_{RD_k}|^2}(x)\right]^{k+m}. \tag{6.25}$$

The PDF and CDF of $|h_{RP}|^2$ are computed, respectively, according to

$$f_{|h_{RP}|^2}(x) = \frac{x^{m_{RP}-1}}{\Gamma(m_{RP})\lambda_{RP}^{m_{RP}}} e^{-\frac{x}{\lambda_{RP}}}, \tag{6.26}$$

and

$$F_{|h_{RP}|^2}(x) = \frac{\gamma(m_{RP}, x/\lambda_D)}{\Gamma(m_{RP})} = 1 - e^{-\frac{x}{\lambda_{RP}}} \sum_{n_{RP}=0}^{m_{RP}-1} \frac{x^{n_{RP}}}{\lambda_{RP}^{n_{RP}} n_{RP}!}, \tag{6.27}$$

where $\lambda_{RP} = \frac{\Omega_{RP}}{m_{RP}}$, m_{RP} is the fading severity and Ω_{RP} represent the average power.

6.2.3 System Performance Analysis

6.2.3.1 Outage Propbability

The main performance metric, i.e. OP, requires studied. In this case, the SIC is applied to many users. In particular, SIC is performed at the k-th user in two steps. The first and second steps correspond to detecting and canceling the m-th user's signal ($m \leqslant k$). The intended users are then able to decode its own signal. In an unwanted scenario, the k-th user cannot detect the k-th user's signal and outage occurs. It is denoted by $E_{k,m}$. In particular, the OP of k-th is computed by

$$\mathcal{OP}_k^{out} = 1 - \Pr\left(E_{k,1}^c \cap \ldots \cap E_{k,k}^c\right), \tag{6.28}$$

where $E_{k,m}^c$ is the complement event of $E_{k,m}$. It can be written as

$$E_{k,m}^c = \left[\frac{\gamma_R \gamma_k \phi_m}{\gamma_R \gamma_k \sum_{i=p+1}^{K} a_i + \gamma_k + \gamma_R + 1} > \gamma_m\right] \overset{(a)}{=} \left[\gamma_k > \delta_m, \gamma_R > \frac{\delta_m(\gamma_k + 1)}{\gamma_k - \delta_m}\right], \tag{6.29}$$

where $\gamma_m = 2^{R_m} - 1$, R_m is the target rate at the m-th user, $\delta_m = \frac{\gamma_m}{\phi_m - \gamma_m \sum_{i=p+1}^{K} \phi_i}$ and step (a) follows as $\phi_m > \gamma_m \sum_{i=p+1}^{K} a_i$.

We can then rewrite:

$$OP_k^{out} = 1 - \Pr\left(\gamma_k > \delta_k^*, \gamma_R > \frac{\delta_k^* (\gamma_k + 1)}{\gamma_k - \delta_k^*}\right), \tag{6.30}$$

where $\delta_k^* = \underbrace{\max}_{1 \leqslant m \leqslant k} \delta_m$.

Proposition 1: The CDF of γ_R is obtained as

$$F_{\gamma_R}(x) = 1 - \sum\nolimits^{\sim}(R,P) \times \sum_{p=0}^{\Delta_R - 1} \frac{\Gamma(\Delta_R)\Gamma(\Delta_P + p)\Psi_R^{-\Delta_R + p}\rho^{\Delta_P} x^p}{p!(\Psi_R x + \rho\Psi_P)^{\Delta_P + p}}. \tag{6.31}$$

where

$$\sum\nolimits^{\sim}(R,P) = \sum_{i_1=0}^{m_{SR}-1} \cdots \sum_{i_{N_S}=0}^{m_{SR}-1} \Theta(R, N_S) \times \sum_{i_1=0}^{m_{SR}-1} \cdots \sum_{i_{N_S}=0}^{m_{SR}-1} \Theta(P, N_S). \tag{6.32}$$

Proof: See Appendix D

Since $\gamma_k = \rho|h_{RD_k}|^2 / |h_{RP}|^2$ as the ratio of two Gamma random variables, one can derive the PDF of γ_k with $x > 0$ as

$$\begin{aligned} F_{\gamma_k}(x) = 1 - \sum_{m=0}^{K-k} \sum_{a=0}^{k+m} \sum_{b=0}^{a(m_D-1)} \binom{K-k}{m} \binom{k+m}{a} \\ \times \frac{\Upsilon\Gamma(m_{RP}+b)(-1)^{m+a}\vartheta_b(a)}{(k+m)\Gamma(m_{RP})} \times \frac{x^b \rho^{m_{RP}} \lambda_{RP}^b (\lambda_D)^{m_{RP}+b}}{(a\lambda_{RP}x + \rho\lambda_D)^{m_{RP}+b}}. \end{aligned} \tag{6.33}$$

By taking the first derivative of (6.30), the corresponding PDF can be obtained as

$$\begin{aligned} f_{\gamma_k}(x) = \Upsilon \sum_{m=0}^{K-k} \sum_{a=0}^{k+m-1} \sum_{b=0}^{a(m_D-1)} \binom{K-k}{m} \binom{k+m-1}{a} \\ \times \frac{\vartheta_b(a)(-1)^{m+a}\Gamma(m_{RP}+m_D+b)}{\Gamma(m_D)\Gamma(m_{RP})} \times \frac{\rho^{m_{RP}} \lambda_{RP}^{m_D+b} \lambda_D^{m_{RP}+b} x^{m_D+b-1}}{(\lambda_D\rho + \lambda_{RP}(a+1)x)^{m_{RP}+m_D+b}}. \end{aligned} \tag{6.34}$$

Proposition 2: The closed-form formula of $\mathcal{OP}_{out}$ of the k-th user is given by

$$
\begin{aligned}
OP_k^{out} &= 1 - \widetilde{\sum}\,(R,P) \\
&\times \sum_{p=0}^{\Delta_R-1}\sum_{m=0}^{K-k}\sum_{a=0}^{k+m-1}\sum_{b=0}^{a(m_D-1)}\sum_{l_1=0}^{p}\sum_{l_2=0}^{m_D+b+l_1-1}\binom{k+m-1}{a}\binom{K-k}{m}\binom{p}{l_1}\binom{m_D+b+l_1-1}{l_2} \\
&\quad\times \frac{\tilde{\Gamma}\Upsilon\vartheta_b(a)(-1)^{m+a}\left(\delta_k^*\right)^{p+m_D+b+l_1-l_2-1}\partial_3^{\Delta_P-m_{RP}-m_D-b+l_2+1}}{\Psi_R^{\Delta_R-p}\rho^{-\Delta_P-m_{RP}}\lambda_{RP}^{m_{RP}}\lambda_D^{-m_{RP}-b}\partial_1^{\Delta_P+p}(1+a)^{m_{RP}+m_D+b}} \\
&\quad\times G_{2,2}^{2,2}\left[\partial_2\partial_3\,\middle|\,\begin{matrix}-\Delta_P-l_2, 1-\Delta_P-p \\ m_{RP}+m_D+b-\Delta_P-l_2-1, 0\end{matrix}\right]
\end{aligned}
\tag{6.35}
$$

Proof: See Appendix E

6.2.3.2 Asymptotic Outage Probability and Diversity Order Analysis

To gain more insight into CSTRN performance, the asymptotic OP should be considered in the high SNR region ($\rho \to \infty$). Interestingly, when $\rho \to \infty$ we can apply the Maclaurin series expansion of the exponential function in (6.18) to approximate. Then the PDF of ρZ_R is given as

$$
f_{\rho Z_R}(x) \simeq \frac{\alpha^{N_S}}{(N_S-1)!\rho^{N_S}}x^{N_S-1}, \tag{6.36}
$$

and the corresponding CDF follows asymptotic behavior according to

$$
F_{\rho Z_R}(x) \simeq \frac{\alpha^{N_S}}{(N_S)!\rho^{N_S}}x^{N_S}. \tag{6.37}
$$

Hence, substilizing (6.37) and (6.19) into (6.43) and along with [76, Eq. 3.351.3], the asymptotic CDF of γ_R is obtain as

$$
F_{\gamma_R}(x) \simeq \sum_{i_1=0}^{m_{SP}-1}\cdots\sum_{i_{N_S}=0}^{m_{SP}-1}\Theta(P,N_S)\times\frac{\alpha^{N_S}x^{N_S}(N_S+\Delta_P-1)!}{(N_S)!\rho^{N_S}(\Psi_P)^{N_S+\Delta_P}}. \tag{6.38}
$$

Similarly, by applying the Maclaurin series representation of exponential function the CDF of ρY can be obtained as

$$
F_{\rho|h_{RD_k}|^2}(x) \simeq \frac{1}{[\Gamma(m_D+1)]^K}\left(\frac{x}{\lambda_D\rho}\right)^{m_DK}. \tag{6.39}
$$

Assisted by (6.41) and (6.26), the asymptotic behavior of γ_Y is write as

$$
F_{\gamma_k}(x) \simeq \frac{\Gamma(m_DK+m_{RP})}{[\Gamma(m_D+1)]^K\Gamma(m_{RP})}\left(\frac{x\lambda_{RP}}{\lambda_D\rho}\right)^{m_DK} \tag{6.40}
$$

With a large SNR, we can rewrite $\Gamma_{RD} \simeq \frac{\gamma_R \gamma_Y}{\gamma_R + \gamma_Y}$ and hence, system performance is dominated by the weakest link.

We can thus represent the asymptotic OP as

$$\begin{aligned} OP_k^{out,\rho\to\infty} \simeq & \sum_{i_1=0}^{m_{SP}-1} \cdots \sum_{i_{N_S}=0}^{m_{SP}-1} \Theta\left(P, N_S\right) \\ & \times \frac{\alpha^{N_S}\left(\delta_k^*\right)^{N_S}\Gamma(N_S+\Delta_P)}{(N_S)!\rho^{N_S}(\Psi_P)^{N_S+\Delta_P}} + \frac{\Gamma(N_D m_D K + m_{RP})}{[\Gamma(m_D+1)]^K \Gamma(m_{RP})}\left(\frac{\delta_k^* \lambda_{RP}}{\lambda_D \rho}\right)^{m_D K}. \end{aligned} \tag{6.41}$$

It is straightforward to indicate that when $\rho \to \infty$, the diversity order is $\min\left(N_S, m_D K\right)$.

Table 6.3: Comparison of proposed system with related works.

Parameter	m_{Sv}	b_{Sv}	Ω_{Sv}
The heavy shadowing	1	0.063	0.007
The average shadowing	5	0.251	0.279

6.2.3.3 Throughput

Based on outage probability, we can further evaluate throughput in delay-limited transmission mode. For a fixed target rate R_k, we can compute the overall throughput as follows [135]

$$\mathrm{T} = \frac{1}{2}\sum_{k=1}^{K} R_k \left(1 - OP_k^{out}\right). \tag{6.42}$$

6.2.3.4 Numerical Results

This section provides and discusses the numerical results. To verified the accuracy of the expressions, we compared the analytical results with Monte Carlo simulation results. Unless mentioned otherwise, we set $K = 3$, $a_1 = 0.5$, $a_2 = 0.4$, $a_3 = 0.1$, the target rate $R_1 = 0.1$, $R_2 = 0.5$ and $R_3 = 1$, main parameters before simulation as $m_D = m_{RP} = m$ and $\Omega_D = \Omega_{RP} = 1$. The Shadowed-Rician fading parameters for the satellite links are described in the Table 6.3.

Figure 6.5a demonstrates the comparison of OP performance of three users by changing the number of satellite's antenna N_S . It can be intuitively seen that, by increasing NS the considered system obviously improves the outage performance of three users. The first user D_1 shows its superiority in term of outage performance in case of single antenna at the satellite $N_S = 1$, then the worst performance occurs in user D_3 which is allocated less percentage of transmit power. The system based on OMA scheme shows its performance, but such outage behavior just better than user D_3. The main reason is that OMA-based system need more time slots to process the same number of users compared with NOMA-based system. It is valuable finding since Monte-Carlo based simulation and analytical result are matched very well. If we increase the number of antennas at the satellite, such performance metrics show its improvement which demonstrating the benefits of introducing multiple antennas in the NOMA-CSTRN. Furthermore, asymptotic

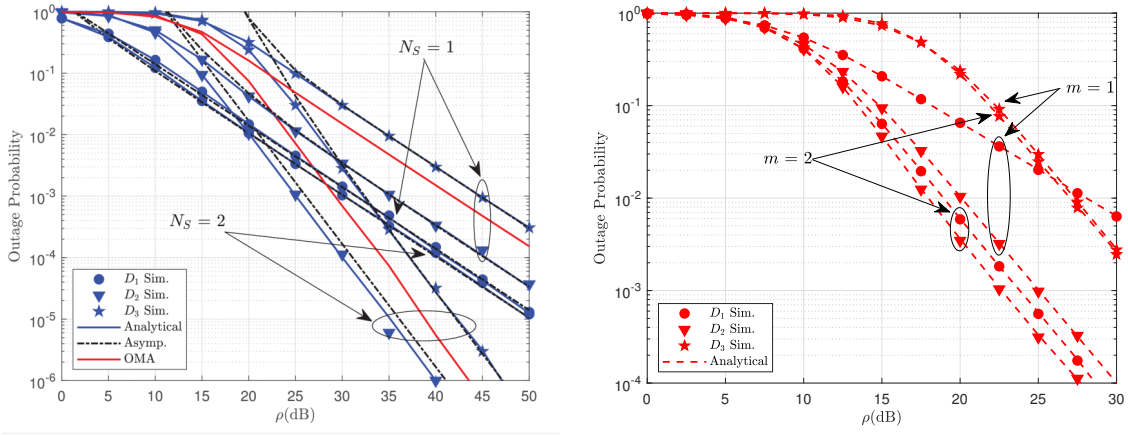

(a) varying N_S at satellite with $m = 1$.

(b) varying m with $N_S = 2$.

Figure 6.5: Outage probability versus transmit ρ with satellite link in the HS scenario.

lines of OP match exact curves at high SNR regime which indicates the exactness of our derived expressions in term of OP.

Figure 6.5b depicts the outage performance of the secondary users against two crucial parameters i.e., Nakagami channel parameter m with the number of transmit antennas set as $N_S = 2$. Similarly with previous figure, we can see significant improvement in term of outage behavior once SNR is greater than 25 dB. It can be explained that since the OP is a function of ρ, we can see that the OP decreases since ρ increases, shown in (6.15), (6.16), and (6.17). However, outage performance improves significantly for case of $m = 2$. Consequently, by improving quality of channels at ground, an increasing m will improve the outage performance of all users.

Figure 6.6 illustrates the effect of different channel conditions about satellite link from S to R, the outage performance of these users can be improved when either the terrestrial link quality gets better, i.e. AS case is better case among two considered cases. In particular, comparing those analytical and asymptotic OP curves in Figure 6.5a and Figure 6.5b, we can see that asymptotic results agree with analytical results across the entire average SNR range.

As can be seen in Figures 6.7a and 6.7b the throughput performance of such NOMA-CSTRN system can be improved by changing configurations of transmit antennas at the satellite and links from the satellite to base station at ground. From (6.42), it can be explained that further metric, throughput depends on the outage probability achieved in previous steps. Therefore, quality of channels results in the curves of the throughput of system. The higher value of NS contributes to improve SINRs, then the higher throughput performance can be benefited. These observations become important guidelines to design such NOMA-CSTRN system.

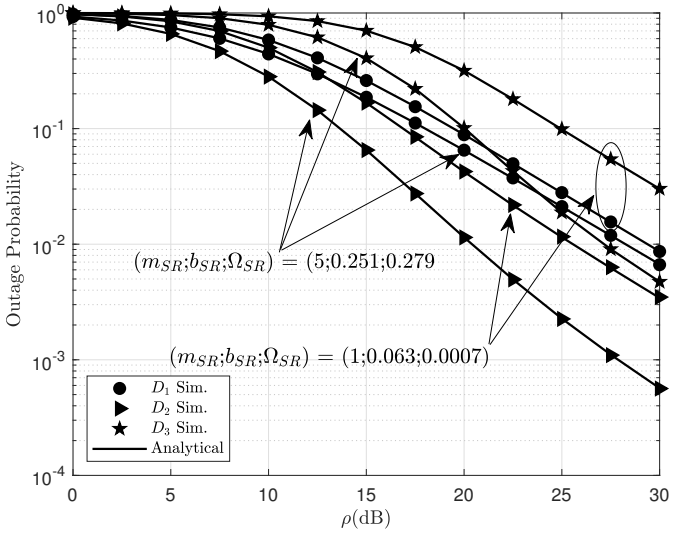

Figure 6.6: Outage probability versus transmit ρ and varying satellite link form S to R with $N_S = m = 1$ and satellite link form S to PD in HS scenario.

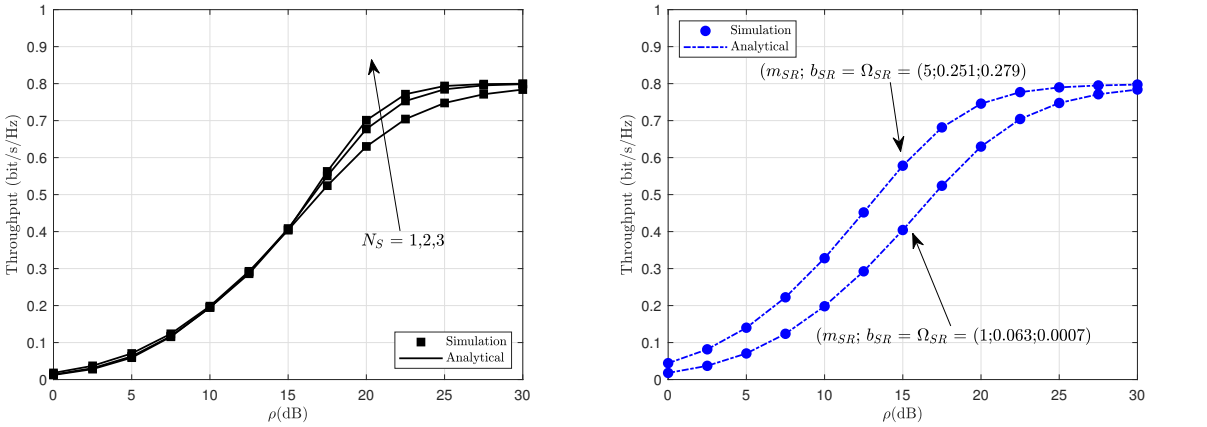

(a) varying N_S at satellite, $m = 1$ (HS).

(b) two kinds of link from S to R (AS and HS), N_S =m= 1.

Figure 6.7: System throughput versus transmit ρ with antenna configurations satellite and links from the satellite to base station at ground.

6.2.4 Conslusion

This section has investigated the performance of a NOMA-CSTRN system wherein multiple secondary terrestrial users enjoy access to spectrum with a primary satellite network to achieve higher spectrum efficiency further. Different from the current studies, we have considered multiple antennas designed at the satellite and NOMA to indicate the performance of several users, which are groups in the context of the NOMA scheme. Furthermore, we also consider through-

put performance with different channels associated with transmission links and key parameters necessary to improve performance metrics, i.e., outage probability and throughput. Above all, a comparison with many scenarios revealed that the proposed NOMA-CSTRN system provides different performance for many users while efficiently utilizing the spectrum resource.

Appendix D

The CDF of γ_R can be rewritten as

$$F_{\gamma_R}(x) = \Pr\left(Z_R < \frac{xZ_P}{\rho}\right) = \int_0^\infty f_{Z_P}(z) F_{Z_R}\left(\frac{xZ_P}{\rho}\right) dz = 1 - \int_0^\infty f_{Z_P}(z)\left(1 - F_{Z_R}\left(\frac{xz}{\rho}\right)\right) dz. \tag{6.43}$$

With assistance from (6.19) and (6.21), we can express (6.43) as

$$F_{\gamma_R}(x) = 1 - \widetilde{\sum}(R,P) \times \sum_{p=0}^{\Delta_R - 1} \frac{\Gamma(\Delta_R)\Psi_R^{-\Delta_R+p}}{p!}\left(\frac{x}{\rho}\right)^p \times \int_0^\infty z^{\Delta_P+p-1} e^{-\left(\frac{\Psi_R x}{\rho}+\Psi_P\right)z} dz. \tag{6.44}$$

Based on [76, Eq. 3.351], we obtain

$$F_{\gamma_R}(x) = 1 - \widetilde{\sum}(R,P) \times \sum_{p=0}^{\Delta_R - 1} \frac{\Gamma(\Delta_R)\Gamma(\Delta_P+p)\Psi_R^{-\Delta_R+p}\rho^{\Delta_P}x^p}{p!\left(\Psi_R x + \rho\Psi_P\right)^{\Delta_P+p}}. \tag{6.45}$$

This is the end of the proof.

Appendix E

Then, we can calculate (6.30) as

$$\begin{aligned}\mathcal{OP}_k^{out} = 1 - \widetilde{\sum}(R,P) & \sum_{p=0}^{\Delta_R-1}\sum_{m=0}^{K-k}\sum_{a=0}^{k+m-1}\sum_{b=0}^{a(m_D-1)} \\ \times \binom{k+m-1}{a}\binom{K-k}{m} & \frac{\tilde{\Gamma}\Upsilon(-1)^{m+a}\vartheta_b(a)}{\Psi_R^{\Delta_R-p}} \times \frac{\Gamma(\Delta_P+p)\Gamma(m_{RP}+m_D+b)(\delta_k^*)^p}{\rho^{-\Delta_P-m_{RP}}\lambda_{RP}^{-m_D-b}\lambda_D^{-m_{RP}-b}} \\ \times \int_{\delta_k}^\infty \frac{(x-\delta_k^*)^{\Delta_P}}{\left(\lambda_D\rho + \lambda_{RP}(a+1)x\right)^{m_{RP}+m_D+b}} & \times \frac{x^{m_D+b-1}(x+1)^p}{\left(\Psi_R\delta_k^*(x+1) + \rho\Psi_P(x-\delta_k^*)\right)^{\Delta_P+p}},\end{aligned} \tag{6.46}$$

where $\tilde{\Gamma} = \frac{\Gamma(\Delta_R)}{p!\Gamma(m_D)\Gamma(m_{RP})}$. Here, we apply the identity [136, Eq. 10]

$$(1+ax)^{-b} = \frac{1}{\Gamma(b)} G_{1,1}^{1,1}\left[ax \,\middle|\, \begin{matrix} 1-b \\ 0 \end{matrix}\right]. \tag{6.47}$$

where $G_{1,1}^{1,1}[.]$ denotes Meijer's G-function [76, Eq. 8.2.1.1]. Then, we represent (6.46) as

$$\begin{aligned}\mathcal{OP}_k^{out} &= 1-\widetilde{\sum}\left(R,P\right)\sum_{p=0}^{\Delta_R-1}\sum_{m=0}^{K-k}\sum_{a=0}^{k+m-1}\sum_{b=0}^{a(m_D-1)}\sum_{l_1=0}^{p}\sum_{l_2=0}^{m_D+b+l_1-1}\\ &\times\left(\begin{array}{c}k+m-1\\ a\end{array}\right)\left(\begin{array}{c}K-k\\ m\end{array}\right)\left(\begin{array}{c}p\\ l_1\end{array}\right)\left(\begin{array}{c}m_D+b+l_1-1\\ l_2\end{array}\right)\\ &\times\frac{\Upsilon\tilde{\Gamma}\Gamma\left(m_{RP}+m_D+b\right)\left(-1\right)^{m+a}\vartheta_b\left(a\right)\left(\delta_k^*\right)^{p+m_D+b+l_1-l_2-1}}{\Psi_R^{\Delta_R-p}\rho^{-\Delta_P-m_{RP}}\lambda_{RP}^{m_{RP}}\lambda_D^{-m_{RP}-b}\partial_1^{\Delta_P+p}\left(1+a\right)^{m_{RP}+m_D+b}}\\ &\times\int_0^{\infty}\frac{t^{\Delta_P+l_2}}{\left(\partial_3+t\right)^{m_{RP}+m_D+b}}G_{1,1}^{1,1}\left[\partial_2 t\left|\begin{array}{c}1-\Delta_P-p\\ 0\end{array}\right.\right]dt,\end{aligned}\tag{6.48}$$

where $\partial_1=\Psi_R\delta_k^*\left(\delta_k^*+1\right)$,$\partial_2=\frac{\left(\Psi_R\delta_k^*+\rho\Psi_P\right)}{\partial_1}$ and $\partial_3=\frac{\lambda_D\rho+\lambda_{RP}(a+1)\delta_k^*}{\lambda_{RP}(a+1)}$. Based on [76, Eq. 7.811.5] and after some algebraic manipulation, we obtain (6.33). This is the end of the proof.

7 Design of reliable and secure transmission in multiple antennas hybrid satellite-terrestrial cognitive networks relying on NOMA to further strengthen power distribution efficiency of integrated network

In this chapter, the dissertation's third aim was to proposed a model hybrid satellite-terrestrial cognitive network (HSTCN) relying on NOMA interconnecting a satellite and multiple terrestrial nodes. We applied DF and BF techniques to reliable and secure transmission in the network system. The OP, IP, average throughput, and hardware impairments are calculated to highlight essential performance metrics to minimize the total transmit power. [**NHN01**], [**NHN15**]

We studied a hybrid satellite-terrestrial cognitive network (HSTCN) relying on NOMA interconnecting a satellite and multiple terrestrial nodes. In this scenario, long-distance communication is achieved by the satellite equipped with multiple antennas to send information to multi-antenna destinations through the base station acting as a relay. The secure performance is necessary to study by exploiting the appearance of an eavesdropper attempting to intercept the transmissions from relay to destinations. We explore the hardware imperfections in the secondary network and the design of multiple antennas in terms of physical-layer security by adopting the DF relay strategy. Specifically, we guarantee coverage area by enabling relaying scheme and keep OP performance satisfying required data rates. Moreover, suppose that only the main channels' state information is known while the wiretap channels' state information is unavailable due to the passive eavesdropper [**NHN01**]:

- The outage behaviors of NOMA-based HSTCN network does not depend on transmit SNR at source at high SNR,
- Numerical results show that the such system using higher number of transceiver antennas generally outperform the system with less antennas in terms of OP and IP and reasonable selection of parameters is necessary to remain the secrecy performance of such systems,
- By allocating different power levels to tow users, the second user has better secure behavior compared with the first user regardless of other set of satellite links or the number of antennas, which means that the superiority of the second user compared with user the first user in terms of OP and IP are same.

7.1 Introduction

To provide advances such as navigation assistance, ubiquitous large coverage and fast services in disaster areas, land mobile satellite (LMS) communication systems benefit to deployment of future wireless networks [20]. Besides these advantages, LMS systems meet the major challenges such as the masking effect due to nonexistence of a direct line-of-sight (LoS) link between the satellite and terrestrial user equipments (UEs) related to heavy rain, fog attenuation and/or poor angles [110]. In particular, the low-power and low-cost terrestrial UEs located in a tunnel or a building meet difficulties to send information to the satellite due to limited transmit power. A hybrid terrestrial-satellite relaying communications have has been recommended in [132, 137, 138] to overcome the effect of masking. Since then, such system has attracted a significant amount of works. For instance, in [137], the authors studied the impact of co-channel interference (CCI) from the terrestrial network for the context of AF protocol deployed at the terrestrial

relay. More importantly, they derived the approximate statistical distributions SINR and hence exhibited some asymptotical computations of bit-error rate (BER) as main evaluation for the system performance. To obtain more insights into the system performance. Later, a hybrid satellite-terrestrial relay system employing multiple amplify-and-forward relays was explored by further exploiting a multi-antenna satellite to communicate with multiple users [132]. A max-max user-relay selection approach is provided to minimize the outage probability of the considered system [132]. The authors in [138] presented the average symbol error rate (SER) and obtained expression of the diversity order in the considered network in which technique for channel estimation and detection of transmitted signal are adopted related transmission between the terrestrial UE and the satellites. Moreover, the authors in [105] examined performance of AF hybrid terrestrial-satellite relaying networks with opportunistic Scheduling by deriving expressions in term of the ergodic capacity.

Raised issues need to be studied due to the challenges of low spectrum resource utilization, and high cost in implementation of mobile satellite users [139]. As a model of cognitive radio (CR), spectrum sharing among satellite and terrestrial networks is known as a promising candidate to design HSTCNs [23, 60, 140]. By looking at the requirements of both spectrum efficiency and reliability, HSTCN can provide comprehensive wireless coverage and improve spectrum resource usage. The authors in [23] provided the closed-form formula of the OP for the considered system in the presence of interference power constraints imposed by multiple adjacent terrestrial primary users (PUs). The authors in [141] studied the interweave architecture for HSTCN to allow the satellite to share idle spectrum with terrestrial networks. They indicated that cognitive satellite systems could improve spectrum utilization and benefit their operational revenues. However, finding out the real-time idle spectrum is a difficult task for the terrestrial networks. To this end, the underlay paradigm recommended in HSTCNs as [142, 143], which, however, would cause unavoidable CCI among SUs and PUs. Therefore, as a further difficult task due to the unknown channel state information (CSI) exchange, a key issue regarding reliable coordination between satellite and terrestrial networks has become a necessary open problem. Reference [110] addressed its achievable rate maximization. They first converted the CCI threshold into transmit power constraints and then formulated the achievable rate maximization as an optimization problem. The authors in [21] explored the security problem for energy harvesting assisted cognitive satellite-terrestrial network containing a BS, some mobile users (MUs), and energy receivers (ERs), in which a multi-beam satellite sub-network shares the portion of millimeter-wave bands with multiple cellular networks. The work in [144] considered the system model to allow the secondary network selection to achieve optimal outage probability of the primary satellite system and then provide spectrum sharing opportunities.

In principle, NOMA employs non-orthogonal transmission at the transmitter and users' superposed information achieved in the power domain for higher spectrum efficiency. NOMA can serve multiple users over the same resource block, which is different from traditional OMA [145], [38], and hence it can effectively improve sum rate. At the receiver, SIC is implemented to decode the users' information. Specifically, by considering other users as interference, the user with the best channel condition can be decoded firstly In [145], the authors studied the relaying scheme employed in the secondary network of the proposed CR-NOMA, and the relay can be harvest energy from the secondary transmitter to serve signal forwarding to distant secondary users. They considered the complex model of wireless powered CR-NOMA in terms of outage behavior and throughput performance as awareness on imperfect SIC at the receiver. The authors [38] examined the SUs in the CR-NOMA network opportunistically access the licensed spectrum resources to foster the number of accessible SUs sharing the limited and dynamic spectrum resources. Moreover, partial relay selection architecture is exploited at full-duplex (FD) and

half-duplex (HD) relays to enhance the performance of far users. Reference [46,146–148] introduced lots of scenarios of CR-NOMA systems along with the system performance analysis. For example, [146] designed a CR-NOMA model and a spectrum efficiency optimization problem which was solved by optimizing the sensing sub-slot. Since CR-NOMA combines the advantages of energy harvesting and device-to-device transmission mode, it is considered as a promising approach for the coming 5G communication system [147, 148].

The authors in [60], [62,63] investigated benefits of NOMA in HSTCN. For example, [62] explored the performance of an underlay cognitive hybrid satellite-terrestrial network comprising a primary satellite source with its terrestrial receiver and the secondary transmitter (ST) with its pre-paired users on the ground. Particularly, the ST uses a cooperative NOMA scheme to permit a nearby NOMA user operating as a relay and detects and forwards signals to the distant NOMA user during the cooperation phase. Reference [8] investigated the OP performance of amplify-and-forward (AF) HSTCN with the NOMA scheme. In such, half-duplexing terrestrial SNs cooperate with a primary satellite network to provide dynamic spectrum access. By adopting pertinent heterogeneous fading models the authors in [63] obtained the closed-form expressions for the OP of primary satellite network and secondary terrestrial network. Further, we derived the asymptotic outage behavior at high SNR for the primary and secondary networks, and thereby calculated the achievable diversity orders.

Table 7.1: Comparison of Proposed System With Related Works.

Context	**Cooperative Relay Network**	**Relay Protocol**	**NOMA**	**CR**	**IP**	**Diversity order**	**Hardware Impairments**
Our Work	Yes	DF	Yes	Yes	Yes	Yes	Yes
[149]	Yes	DF	No	No	No	No	Yes
[150]	Yes	AF	No	No	No	No	Yes
[151]	Yes	AF	Yes	No	No	Yes	No
[152]	Yes	DF	Yes	No	No	Yes	No
[151]	Yes	DF	No	No	No	Yes	No

Related Work and Motivation

The authors in [29] proposed BF schemes to utilize the interference from the terrestrial network as a green source to improve the PLS for the HSTRN network, provided that the two networks share the portion of millimeter-wave frequencies. In [30], HSTRN system is studied in the situation that the satellite sends information to a destination through multiple relays at the existence of an eavesdropper attempting to intercept the transmissions from both the satellite and relays. They explored the context of the single-relay selection and multi-relay selection as well as round-robin scheduling schemes to address the physical-layer security of this considered HSTRN by adopting the DF relay scheme. Reference [61] investigated the secure transmission for HSTRN where the terrestrial base station serving as a green interference resource to enhance the security of the satellite link. The authors adopted a stochastic model for the channel state information uncertainty and proposed a secure and robust BF framework to minimize the transmit power, while satisfying a range of outage (probabilistic) constraints at the satellite user and the terrestrial user.

The detailed contributions of this section are outlined as follows:

- This framework is different from the system models of [58, 59, 61]. In particular, we experienced the practical situation that the eavesdropper is able to intercept from only the terrestrial network.

More specifically, we proposed a practical framework of PLS in a NOMA-HSTCN containing nodes with hardware impairments. In such, we designed one satellite to communicate to two terrestrial destination through terrestrial relay at the existence of one terrestrial eavesdropper.

- We presented analytical expressions to indicate two important performance metrics such as the OP and IP of the such system, which is applicable to evaluated reliable and secure transmission of such NOMA-HSTCN which benefits from design of multiple-antenna.
- To provided further insight, we show trends of for OP and IP at high SNR region. This is interesting guidelines to configure such system in practice. Then, we indicated which parameters are used to improved performance of specific user to satisfy specific demands in the context of NOMA.
- To provided details of our contribution, we summarize main advances in Table 7.2 which indicates some achieved improvements compared with other recent studies.

7.2 System Model

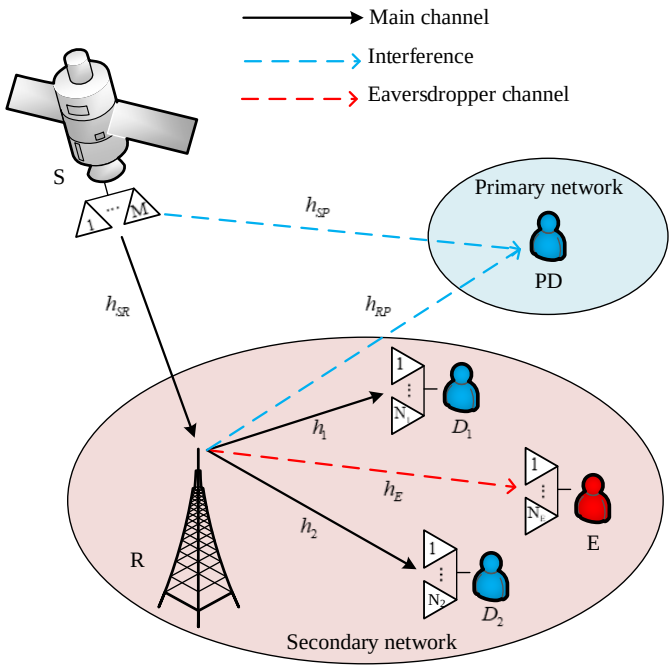

Figure 7.1: System model of NOMA-HSTCN networks.

As depicted in Figure 7.1, we consider the secondary network of the NOMA-HSTCN which consists a BS (S) facilitated M antenna, a relay (R) adopted half-duplex along with DF protocol. It is noted that relay equipped single antenna due to low-cost and limited power, two destinations D_i with N_i antennas, a eavesdropper (E) with N_E antennas. In primary network, we assumed the primary destination (PD)

Table 7.2: The symbols in considered systems.

Symbol	Description
x_S	The signal of BS
x_R	The signal of relay
$x_i (i \in \{1,2\})$	The signal of D_i
P_S	The transmit power at base station
P_R	The transmit power at relay
P_P	The transmit power at primary destination
$\bar{P}_S$	The maximum available transmit power at base station
$\bar{P}_R$	The maximum available transmit power at relay
a_i and b_i	The power allocation coefficients with $a_1 + a_2 = 1$, $b_1 + b_2 = 1$, $a_2 > a_1$ and $b_2 > b_1$
η_{SR}, η_{RD_i} and η_E	The distortion noise caused by hardware impairments (HIs) with $\mathcal{CN}\left(0, P_R k_{SR}^2\right)$, $\mathcal{CN}\left(0, P_R k_{RD_i}^2\right)$ and $\mathcal{CN}\left(0, P_R k_E^2\right)$ respectively
n_R, $\mathbf{n}_i$ and $\mathbf{n}_E$	The additive white Gaussian noise (AWGN) with $\mathcal{CN}\left(0, \sigma_R^2\right)$, $\mathcal{CN}\left(0, \sigma_i^2\right)$ and $\mathcal{CN}\left(0, \sigma_E^2\right)$ respectively
k_u^2	The level of hardware impairments related to link u [153]
$\mathbf{w}_{SR}$	The transmit beamforming vector
$\mathbf{w}_{RD_i}$ and $\mathbf{w}_E$	The received beamforming vector
$\mathbf{h}_{SR}$	The channel vector from base station to relay
$\mathbf{h}_{SP}$	The channel vector from base station to primary destination
$\mathbf{h}_{RD_i}$	The channel vector from relay to D_i
$\mathbf{h}_E$	The channel vector from relay to E
h_{RP}	The channel from relay to primary destination

equipped single antenna has significant impacts from secondary network. Furthermore, we assume no direct link between S and D_i [154] due to obstructions. Then, the transmit signal of (S) is given as

$$x_S = \sqrt{P_S}\left(\sqrt{a_1}x_1 + \sqrt{a_2}x_2\right). \tag{7.1}$$

In the first phase, S transmits the signal x_S to relay R. Thus, the received signal at R is given as

$$y_R = \mathbf{h}_{SR}^{\dagger}\mathbf{w}_{SR}\left[x_S + \eta_{SR}\right] + n_R = \mathbf{h}_{SR}^{\dagger}\mathbf{w}_{SR}\left[\sqrt{P_S}\left(\sqrt{a_1}x_1 + \sqrt{a_2}x_2\right) + \eta_{SR}\right] + n_R. \tag{7.2}$$

According to the principle of maximum ratio transmission (MRT), $\mathbf{w}_{SR} = \frac{\mathbf{h}_{SR}}{\|\mathbf{h}_{SR}\|_F}$.The signal to interference plus D_i and E. Then, the received signal at D_i and E are given respectively by

$$\gamma_{R,x_2} = \frac{P_S a_2 \mathcal{H}_{SR}}{P_S a_1 \mathcal{H}_{SR} + P_S k_{SR}^2 \mathcal{H}_{SR} + \sigma_R^2}, \tag{7.3}$$

where $\mathcal{H}_j = \|\mathbf{h}_j\|_F^2$ with $j \in \{SR, SP\}$. Further, the SINR to detect x_1 at R is given by

$$\gamma_{R,x_1} = \frac{P_S a_1 \mathcal{H}_{SR}}{P_S k_{SR}^2 \mathcal{H}_{SR} + \sigma_R^2}. \tag{7.4}$$

Due interference constraint, it is necessary to limit interference of the PD being beyond an acceptable level P_P, the transmit power at S and R are given as respectively [133]

$$P_S = \min\left(\bar{P}_S, \frac{P_P}{\mathcal{H}_{SP}}\right), \tag{7.5}$$

and

$$P_R = \min\left(\bar{P}_R, \frac{P_P}{|h_{RP}|^2}\right). \tag{7.6}$$

In the second phase, the relay employs DF protocol and transmits the information $x_R = \sqrt{P_R}(\sqrt{b_1}x_1 + \sqrt{b_2}x_2)$ to D_i and E. Then, the received signal at D_i and E are given respectively by

$$\begin{aligned} y_{D_i} &= \mathbf{h}_{RD_i}\mathbf{w}_{RD_i}^{\dagger}\left[x_R + \eta_{RD_1}\right] + \mathbf{w}_{RD_i}^{\dagger}\mathbf{n}_i \\ &= \mathbf{h}_{RD_i}\mathbf{w}_{RD_i}^{\dagger} \times \left[\sqrt{P_R}\left(\sqrt{b_1}x_1 + \sqrt{b_2}x_2\right) + \eta_{RD_1}\right] + \mathbf{w}_{RD_i}^{\dagger}\mathbf{n}_i, \end{aligned} \tag{7.7}$$

and

$$y_E = \mathbf{h}_E\mathbf{w}_E^{\dagger}\left[x_R + \eta_E\right] + \mathbf{w}_E^{\dagger}\mathbf{n}_E = \mathbf{h}_E\mathbf{w}_E^{\dagger}\left[\sqrt{P_R}\left(\sqrt{b_1}x_1 + \sqrt{b_2}x_2\right) + \eta_E\right] + \mathbf{w}_E^{\dagger}\mathbf{n}_E. \tag{7.8}$$

Based on the maximal-ratio combining (MRC) scheme [155], we have $\mathbf{w}_{RD_i} = \frac{\mathbf{h}_{RD_i}}{\|\mathbf{h}_{RD_i}\|_F}$. Then, the SINR to detect x_2 at D_2 is given as

$$\gamma_{D_2,x_2} = \frac{P_R b_2 \mathcal{H}_{RD_2}}{P_R b_1 \mathcal{H}_{RD_2} + P_R k_{RD_2}^2 \mathcal{H}_{RD_2} + \sigma_2^2}, \tag{7.9}$$

where $\mathcal{H}_i = \|\mathbf{h}_{RD_i}\|_F^2$. Moreover, the SINR to detect the signal x_2 at D_1 is given as

$$\gamma_{D_1,x_2} = \frac{P_R b_2 \mathcal{H}_{RD_1}}{P_R b_1 \mathcal{H}_{RD_1} + P_R k_{RD_1}^2 \mathcal{H}_{RD_1} + \sigma_1^2} \tag{7.10}$$

Applying SIC, the SINR at D_1 to detected the own signal x_1 is given as

$$\gamma_{D_1,x_1} = \frac{P_R b_1 \mathcal{H}_{RD_1}}{P_R k_{RD_1}^2 \mathcal{H}_{RD_1} + \sigma_1^2} \tag{7.11}$$

According to the NOMA principle, E successfully eliminates the signal x_2 and treats the signal x_1 as noise. Then, we can obtain as

$$\gamma_{E,x_2} = \frac{P_R b_2 \mathcal{H}_E}{P_R b_1 \mathcal{H}_E + P_R k_E^2 \mathcal{H}_E + \sigma_E^2} \tag{7.12}$$

where $\mathcal{H}_E = \|\mathbf{h}_E\|_F^2$. Moreover, E successfully eliminates the signal x_1 of D_1 with SIC. Thus, we can obtain as

$$\gamma_{E,x_1} = \frac{P_R b_1 \mathcal{H}_E}{P_R k_E^2 \mathcal{H}_E + \sigma_E^2} \tag{7.13}$$

7.3 Performance Analysis

As most of research on physical layer security, a couple of common criterion to characterize the secrecy performance are secure outage probability (SOP) and intercept probability (IP). In this section, we want to evaluate reliable characteristic with outage probability rather than considering SOP, which is reported

a lot in the literature, for example in [156]. Therefore, we measure the OP and IP performance, which provide important guidelines to deploy such NOMA-HSTCN systems.

7.3.1 Channel Model

First, we assume the channel vector h_j independent and identically distributed (i.i.d.) Shadowed-Rician fading. Moreover, the probability density function (PDF) of $h_j^{(k)}$ with satellites' k-th antenna is computed by [132]

$$f_{\left|h_j^{(k)}\right|^2}(x) = \alpha_j e_1^{-\beta_j x} F_1\left(m_j; 1; \delta_j x\right), x > 0, \tag{7.14}$$

where m_j are the fading severity parameter, Ω_j and $2b_j$ are the average power of LoS and multi-path components, respectively, $\alpha_j = (2b_j m_j/(2b_j m_j + \Omega_j)^{m_j}/2b_j$, $\beta_j = 0.5b_j$, $\delta_j = \Omega_j/(2b_j)(2b_j m_j + \Omega_j)$ and ${}_1F_1(\cdot;\cdot;\cdot)$ is the confluent hypergeometric function of the first kind [76, Eq. 9.210.1].

Moreover, with m_j is an integer number (7.14) is rewritten as

$$f_{\left|h_j^{(k)}\right|^2}(x) = \alpha_j \sum_{k_j=0}^{m_j-1} \zeta_j(k_j) x^{k_j} e^{-(\beta_j-\delta_j)x} \tag{7.15}$$

where $\zeta_j(\ell) = (-1)^\ell (1-m_j)_\ell \delta_j^\ell/(\ell!)^2$, $(.)_\ell$ is the Pochhammer symbol [76, p.xliii]. Thus, the PDF of $\mathcal{H}_j$ is given as

$$f_{\mathcal{H}_j}(x) = \sum_{i_1=0}^{m_j-1} \cdots \sum_{i_M=0}^{m_j-1} \Theta(j,M) x^{\Delta_j - 1} e^{-(\beta_j-\delta_j)x}, \tag{7.16}$$

where $\Theta(j,M) = \alpha_j^M \prod_{\ell=1}^{M} \zeta_j(i_\ell) \prod_{j=1}^{M-1} ß(\sum_{l=1}^{j} i_l + j, i_{j+1} + 1)$, $\Delta_j = \sum_{q=1}^{M} i_q + M$ and $ß(.,.)$ is the Beta function.

Regarding channels in ground, the PDF of $|h_{RP}|^2$ is given as

$$f_{|h_{RP}|^2}(x) = \frac{x^{m_{RP}-1}}{\Gamma(m_{RP})\Lambda_{RP}^{m_{RP}}} e^{-\frac{x}{\Lambda_{RP}}}, \tag{7.17}$$

where $\Lambda = \frac{\lambda}{m}$, m and Ω are present the fading severity factor and mean, respectively.

Moreover, the PDF of $\mathcal{H}_v$ in which $v \in \{1, 2, E\}$ are given as respectively [134]

$$f_{\mathcal{H}_v}(x) = \frac{x^{N_v m_v - 1}}{\Gamma(N_v m_v)\Lambda^{N_v m_v}} e^{-\frac{x}{\Lambda_v}}. \tag{7.18}$$

7.3.2 Outage Probability

7.3.2.1 Outage Probability of D_1

The OP is evaluated as ability to a user detect its signal at related nodes . In this manner, signal x_1 of user of D_1 is processed at relay and destination D_1. Such outage probability at D_1 is expressed as

$$P_{D_1}^{out} = \Pr\left(\min\left(\gamma_{R,x_1}, \gamma_{D_1,x_1}\right) < \gamma_{th_1}\right) = 1 - \underbrace{\Pr\left(\gamma_{R,x_1} > \gamma_{th_1}\right)}_{A_1} \underbrace{\Pr\left(\gamma_{D_1,x_1} > \gamma_{th_1}\right)}_{A_2}, \tag{7.19}$$

where $\gamma_{th_1} = 2^{2R_1} - 1$ and R_i is the target rates for user D_i.

Proposition 1: The component of overall OP, A_1 can be obtained as (7.20)

$$\begin{aligned} A_1 = &\sum\nolimits^{\sim} (m_{SR}, m_{SP}) \frac{(\beta_{SP}-\delta_{SP})^{-\Delta_{SP}}}{(\beta_{SR}-\delta_{SR})^{\Delta_{SR}}} \gamma\left(\Delta_{SP}, \frac{\rho_D(\beta_{SP}-\delta_{SP})}{\bar{\rho}_S}\right) \Gamma\left(\Delta_{SR}, \frac{\phi_1(\beta_{SR}-\delta_{SR})}{\bar{\rho}_S}\right) \\ &+ \sum\nolimits^{\sim} (m_{SR}, m_{SP}) \sum_{p_1=0}^{\Delta_{SR}-1} \frac{\Gamma(\Delta_{SR}) \phi_1^{p_1} \rho_D^{\Delta_{SP}} \Gamma\left(\Delta_{SP}+p_1, \frac{(\beta_{SP}-\delta_{SP})\rho_D + (\beta_{SR}-\delta_{SR})\phi_1}{\bar{\rho}_S}\right)}{p_1! (\beta_{SR}-\delta_{SR})^{\Delta_{SR}-p_1} ((\beta_{SP}-\delta_{SP})\rho_D + (\beta_{SR}-\delta_{SR})\phi_1)^{\Delta_{SP}+p_1}}. \end{aligned} \tag{7.20}$$

Proof: See Appendix F

Proposition 2: The second term of (7.19) an be calculated as

$$\begin{aligned} A_2 = &\frac{\gamma\left(m_{RP}, \frac{\rho_D}{\Lambda_{RP}\bar{\rho}_R}\right) \Gamma\left(N_1 m_1, \frac{\bar{\phi}_1}{\bar{\rho}_R \Lambda_1}\right)}{\Gamma(m_{RP})\Gamma(N_1 m_1)} \\ &+ \sum_{p_2=0}^{N_1 m_1 - 1} \frac{(\Lambda_1 \rho_D)^{m_{RP}} \left(\bar{\phi}_1 \Lambda_{RP}\right)^{p_2}}{p_2! \Gamma(m_{RP}) \left(\bar{\phi}_1 \Lambda_{RP} + \Lambda_1 \rho_D\right)^{m_{RP}+p_2}} \times \Gamma\left(m_{RP}+p_2, \frac{\bar{\phi}_1 \Lambda_{RP} + \Lambda_1 \rho_D}{\Lambda_1 \bar{\rho}_R \Lambda_{RP}}\right). \end{aligned} \tag{7.21}$$

Proof: See Appendix G

Finally, the closed-form expression for the OP of user D_1 is given by

$$P_{D_1}^{out} = 1 - A_1 \times A_2. \tag{7.22}$$

7.3.2.2 Outage Probability of D_2

It is worth noting that signal x_2 is detected at user D_1, and hence OP of user D_2 can be characterized by evaluating related SINRs compared with the thresholds. Therefore, the OP of user D_2 can be formulated by

$$\begin{aligned} P_{D_2}^{out} &= \Pr\left(\min\left(\gamma_{R,x_2}, \gamma_{D_2,x_2}, \gamma_{D_1,x_2}\right) < \gamma_{th_2}\right) \\ &= 1 - \underbrace{\Pr\left(\gamma_{R,x_2} > \gamma_{th_2}\right)}_{B_1} \underbrace{\Pr\left(\gamma_{D_2,x_2} < \gamma_{th_2}\right)}_{B_2} \times \underbrace{\Pr\left(\gamma_{D_1,x_2} < \gamma_{th_2}\right)}_{B_3}. \end{aligned} \tag{7.23}$$

Proposition 3: The closed-form expression of B_1 is given as (7.24)

$$\begin{aligned} B_1 = &\sum\nolimits^{\sim} (m_{SR}, m_{SP}) \frac{(\beta_{SP}-\delta_{SP})^{-\Delta_{SP}}}{(\beta_{SR}-\delta_{SR})^{\Delta_{SR}}} \gamma\left(\Delta_{SP}, \frac{\rho_D(\beta_{SP}-\delta_{SP})}{\bar{\rho}_S}\right) \Gamma\left(\Delta_{SR}, \frac{(\beta_{SR}-\delta_{SR})\varphi_2}{\bar{\rho}_S}\right) \\ &+ \sum\nolimits^{\sim} (m_{SR}, m_{SP}) \sum_{p_3=0}^{\Delta_{SR}-1} \frac{\Gamma(\Delta_{SR}) \varphi_2^{p_3} \rho_D^{\Delta_{SP}} \Gamma\left(\Delta_{SP}+p_3, \frac{(\beta_{SP}-\delta_{SP})\rho_D + (\beta_{SR}-\delta_{SR})\varphi_2}{\bar{\rho}_S}\right)}{p_3! (\beta_{SR}-\delta_{SR})^{\Delta_{SR}-p_3} ((\beta_{SP}-\delta_{SP})\rho_D + (\beta_{SR}-\delta_{SR})\varphi_2)^{\Delta_{SP}+p_3}}. \end{aligned} \tag{7.24}$$

Proof: With the help of (7.3), B_1 is written as

$$B_1 = \Pr\left(\mathcal{H}_{SP} < \frac{\rho_D}{\bar{\rho}_S}, \mathcal{H}_{SR} > \frac{\varphi_2}{\bar{\rho}_S}\right) + \Pr\left(\mathcal{H}_{SP} > \frac{\rho_D}{\bar{\rho}_S}, \mathcal{H}_{SR} > \frac{\varphi_2 \mathcal{H}_{SP}}{\rho_D}\right), \tag{7.25}$$

where $\varphi_2 = \frac{\gamma_{th_2}}{\left(a_2 - a_1\gamma_{th_2} - k_{SR}^2\gamma_{th_2}\right)}$. It then can be rewritten by

$$B_1 = \int_0^{\frac{\rho_D}{\bar{\rho}_S}} f_{\mathcal{H}_{SP}}(x) \int_{\frac{\varphi_2}{\bar{\rho}_S}}^{\infty} f_{\mathcal{H}_{SR}}(y)dydx + \int_{\frac{\rho_D}{\bar{\rho}_S}}^{\infty} f_{\mathcal{H}_{SP}}(x) \int_{\frac{\varphi_2 x}{\rho_D}}^{\infty} f_{\mathcal{H}_{SR}}(y)dydx. \tag{7.26}$$

Similar in Appendix F, (7.24) is obtained. The proof is completed.

Then, putting (7.9) into (7.23) we can write B_2 as

$$\begin{aligned} B_2 &= \Pr\left(|h_{RP}|^2 < \frac{\rho_D}{\bar{\rho}_S}, \mathcal{H}_{RD_2} > \frac{\bar{\varphi}_2}{\bar{\rho}_S}\right) + \Pr\left(|h_{RP}|^2 > \frac{\rho_D}{\bar{\rho}_S}, \mathcal{H}_{RD_2} > \frac{\bar{\varphi}_2 |h_{RP}|^2}{\rho_D}\right) \\ &= \int_0^{\frac{\rho_D}{\bar{\rho}_S}} f_{|h_{RP}|^2}(x) \int_{\frac{\bar{\varphi}_2}{\bar{\rho}_S}}^{\infty} f_{\mathcal{H}_{RD_2}}(y)dydx \quad + \int_{\frac{\rho_D}{\bar{\rho}_S}}^{\infty} f_{|h_{RP}|^2}(x) \int_{\frac{\bar{\varphi}_2 x}{\rho_D}}^{\infty} f_{\mathcal{H}_{RD_2}}(y)dydx, \end{aligned} \tag{7.27}$$

where $\bar{\varphi}_2 = \frac{\gamma_{th_2}}{b_2 - \gamma_{th_2}b_1 - \gamma_{th_2}k_{RD_2}^2}$.

By performing similar computation, B_2, B_3 can be expressed respectively by

$$\begin{aligned} B_2 = &\frac{\gamma\left(m_{RP}, \frac{\rho_D}{\Lambda_{RP}\bar{\rho}_R}\right)\Gamma\left(N_2 m_2, \frac{\bar{\varphi}_2}{\bar{\rho}_R\Lambda_2}\right)}{\Gamma(m_{RP})\Gamma(N_2 m_2)} \\ &+ \sum_{p_3=0}^{N_2 m_2 - 1} \frac{(\Lambda_2\rho_D)^{m_{RP}}(\bar{\varphi}_2\Lambda_{RP})^{p_3}}{p_3!\Gamma(m_{RP})(\bar{\varphi}_2\Lambda_{RP} + \Lambda_2\rho_D)^{m_{RP}+p_3}} \times \Gamma\left(m_{RP} + p_3, \frac{\bar{\varphi}_2\Lambda_{RP} + \Lambda_2\rho_D}{\Lambda_2\bar{\rho}_R\Lambda_{RP}}\right), \end{aligned} \tag{7.28}$$

$$\begin{aligned} B_3 = &\frac{\gamma\left(m_{RP}, \frac{\rho_D}{\Lambda_{RP}\bar{\rho}_R}\right)\Gamma\left(N_1 m_1, \frac{\bar{\varphi}_2}{\bar{\rho}_R\Lambda_1}\right)}{\Gamma(m_{RP})\Gamma(N_1 m_1)} \\ &+ \sum_{p_4=0}^{N_1 m_1 - 1} \frac{(\Lambda_1\rho_D)^{m_{RP}}(\bar{\varphi}_2\Lambda_{RP})^{p_4}}{p_4!\Gamma(m_{RP})(\bar{\varphi}_2\Lambda_{RP} + \Lambda_1\rho_D)^{m_{RP}+p_4}} \times \Gamma\left(m_{RP} + p_4, \frac{\bar{\varphi}_2\Lambda_{RP} + \Lambda_1\rho_D}{\Lambda_1\bar{\rho}_R\Lambda_{RP}}\right). \end{aligned} \tag{7.29}$$

Then, we can compute OP for user D_2 as below

$$P_{D_2}^{out} = \begin{cases} 1 - B_1 \times B_2 \times B_3, \text{if}: & \gamma_{th_2} < \frac{b_2}{b_1 + k_{RD_2}^2} \\ & \gamma_{th_2} < \frac{a_2}{a_1 + k_{RD_2}^2} \\ 1 \quad , \text{otherwise} & \end{cases} \tag{7.30}$$

7.3.2.3 Diversity Order Analysis

In this section, we consider asymptotic at high SNR. It is worth noting that the diversity order for D_1, D_2 are defined by

$$d = -\lim_{\bar{\rho}\to\infty} \frac{\log\left(P_{D_i}^{out,\infty}(\bar{\rho})\right)}{\log\bar{\rho}}. \tag{7.31}$$

When $\bar{\rho} \to \infty$, we apply a series representation of the incomplete Gamma function [76, Eq. 8.354.1] we have

$$\gamma\left(m,x\right) \overset{x\to 0}{\approx} \frac{x^m}{m}. \tag{7.32}$$

Then, we can write $P_{D_1}^{out,\infty}$ as

$$\begin{aligned} P_{D_1}^{out,\infty} = 1 - & \left(\begin{array}{l} \widetilde{\sum}\left(m_{SR},m_{SP}\right) \frac{\left(\beta_{SP}-\delta_{SP}\right)^{-\Delta_{SP}}}{\left(\beta_{SR}-\delta_{SR}\right)^{\Delta_{SR}}\Delta_{SP}\Delta_{SR}} \left(\frac{\rho_D(\beta_{SP}-\delta_{SP})}{\bar{\rho}_S}\right)^{\Delta_{SP}} \\ \times \left(\Gamma\left(\Delta_{SR}+1\right) - \left(\frac{\phi_1(\beta_{SR}-\delta_{SR})}{\bar{\rho}_S}\right)^{\Delta_{SR}}\right) \end{array} \right. \\ & \left. + \widetilde{\sum}\left(m_{SR},m_{SP}\right) \sum_{p_1=0}^{\Delta_{SR}-1} \frac{\Gamma(\Delta_{SR})\phi_1^{p_1}\rho_D^{\Delta_{SP}} \left(\Gamma(\Delta_{SP}+p_1+1) - \left(\frac{(\beta_{SP}-\delta_{SP})\rho_D+(\beta_{SR}-\delta_{SR})\phi_1}{\bar{\rho}_S}\right)^{\Delta_{SP}+p_1}\right)}{p_1!(\beta_{SR}-\delta_{SR})^{\Delta_{SR}-p_1}(\Delta_{SP}+p_1)((\beta_{SP}-\delta_{SP})\rho_D+(\beta_{SR}-\delta_{SR})\phi_1)^{\Delta_{SP}+p_1}} \right) \\ \times & \left(\begin{array}{l} \frac{\left(\frac{\rho_D}{\Lambda_{RP}\bar{\rho}_R}\right)^{m_{RP}}\left(1-\frac{(\bar{\phi}_1/\bar{\rho}_R\Lambda_1)^{N_1m_1}}{\Gamma(N_1m_1+1)}\right)}{\Gamma(m_{RP}+1)} \\ + \sum_{p_2=0}^{N_1m_1-1} \frac{(\Lambda_1\rho_D)^{m_{RP}}\left(\bar{\phi}_1\Lambda_{RP}\right)^{p_2}\left(\Gamma(m_{RP}+p_2+1) - \left(\frac{\bar{\phi}_1\Lambda_{RP}+\Lambda_1\rho_D}{\Lambda_1\bar{\rho}_R\Lambda_{RP}}\right)^{m_{RP}+p_2}\right)}{p_2!\Gamma(m_{RP})(m_{RP}+p_2)\left(\bar{\phi}_1\Lambda_{RP}+\Lambda_1\rho_D\right)^{m_{RP}+p_2}} \end{array} \right). \end{aligned} \tag{7.33}$$

Next, $P_{D_2}^{out,\infty}$ is write as

$$P_{D_2}^{out} = 1 - B_1^{\infty} \times B_2^{\infty} \times B_3^{\infty}, \tag{7.34}$$

where B_1^{∞} is expressed as

$$\begin{aligned} B_1^{\infty} = & \widetilde{\sum}\left(m_{SR},m_{SP}\right) \frac{\left(\beta_{SP}-\delta_{SP}\right)^{-\Delta_{SP}}}{\left(\beta_{SR}-\delta_{SR}\right)^{\Delta_{SR}}\Delta_{SP}\Delta_{SR}} \left(\frac{\rho_D(\beta_{SP}-\delta_{SP})}{\bar{\rho}_S}\right)^{\Delta_{SP}} \\ & \times \left(\Gamma\left(\Delta_{SR}+1\right) - \left(\frac{(\beta_{SR}-\delta_{SR})\varphi_2}{\bar{\rho}_S}\right)^{\Delta_{SR}}\right) \\ & + \widetilde{\sum}\left(m_{SR},m_{SP}\right) \sum_{p_3=0}^{\Delta_{SR}-1} \frac{\Gamma(\Delta_{SR})\varphi_2^{p_3}\rho_D^{\Delta_{SP}} \left(\Gamma(\Delta_{SP}+p_3+1) - \left(\frac{(\beta_{SP}-\delta_{SP})\rho_D+(\beta_{SR}-\delta_{SR})\varphi_2}{\bar{\rho}_S}\right)^{\Delta_{SP}+p_3}\right)}{p_3!(\beta_{SR}-\delta_{SR})^{\Delta_{SR}-p_3}(\Delta_{SP}+p_3)((\beta_{SP}-\delta_{SP})\rho_D+(\beta_{SR}-\delta_{SR})\varphi_2)^{\Delta_{SP}+p_3}}. \end{aligned} \tag{7.35}$$

Hence, B_2^{∞} and B_3^{∞} are given as, respectively.

$$\begin{aligned} B_2^{\infty} = & \left(\frac{\rho_D}{\Lambda_{RP}\bar{\rho}_R}\right)^{m_{RP}} \frac{\left(1-\frac{(\bar{\varphi}_2/\bar{\rho}_R\Lambda_2)^{N_1m_1}}{\Gamma(N_2m_2+1)}\right)}{\Gamma(m_{RP}+1)} + \sum_{p_3=0}^{N_2m_2-1} \frac{(\Lambda_2\rho_D)^{m_{RP}}(\bar{\varphi}_2\Lambda_{RP})^{p_3}}{p_3!\Gamma(m_{RP})(m_{RP}+p_3)(\bar{\varphi}_2\Lambda_{RP}+\Lambda_2\rho_D)^{m_{RP}+p_3}} \\ & \times \left(\Gamma\left(m_{RP}+p_3+1\right) - \left(\frac{\bar{\varphi}_2\Lambda_{RP}+\Lambda_2\rho_D}{\Lambda_2\bar{\rho}_R\Lambda_{RP}}\right)^{m_{RP}+p_3}\right). \end{aligned} \tag{7.36}$$

$$\begin{aligned} B_3^{\infty} = & \left(\frac{\rho_D}{\Lambda_{RP}\bar{\rho}_R}\right)^{m_{RP}} \frac{\left(1-\frac{(\bar{\varphi}_2/\bar{\rho}_R\Lambda_1)^{N_1m_1}}{\Gamma(N_1m_1+1)}\right)}{\Gamma(m_{RP}+1)} + \sum_{p_4=0}^{N_1m_1-1} \frac{(\Lambda_1\rho_D)^{m_{RP}}(\bar{\varphi}_2\Lambda_{RP})^{p_4}}{p_4!\Gamma(m_{RP})(m_{RP}+p_4)(\bar{\varphi}_2\Lambda_{RP}+\Lambda_1\rho_D)^{m_{RP}+p_4}} \\ & \times \left(\Gamma\left(m_{RP}+p_4+1\right) - \Gamma\left(\frac{\bar{\varphi}_2\Lambda_{RP}+\Lambda_1\rho_D}{\Lambda_1\bar{\rho}_R\Lambda_{RP}}\right)^{m_{RP}+p_4}\right). \end{aligned} \tag{7.37}$$

Therefore, the diversity orders of D_1 and D_2 are equal zero.

7.3.2.4 Intercept Probability Analysis

Intercept Probability D_1

The intercept probability of D_1 is expressed as [156]

$$IP_{D_1}^{out} = \Pr\left(\gamma_{R,x_1} > \gamma_{th_1}, \gamma_{R,x_2} > \gamma_{th_2}, \gamma_{E,x_1} > \gamma_{E_1}\right) \tag{7.38}$$

where γ_{E_i} is the secrecy SNR threshold of D_i.

Proposition 4: The closed-form expression for IP of D_1 is given as

$$\begin{aligned} IP_{D_1}^{out} &= \left(\widetilde{\sum}\left(m_{SR}, m_{SP}\right) \frac{\left(\beta_{SP}-\delta_{SP}\right)^{-\Lambda_{SP}}}{\left(\beta_{SR}-\delta_{SR}\right)^{\Lambda_{SR}}} \gamma\left(\Lambda_{SP}, \frac{\rho_D\left(\beta_{SP}-\delta_{SP}\right)}{\bar{\rho}_S}\right) \Gamma\left(\Lambda_{SR}, \frac{\left(\beta_{SR}-\delta_{SR}\right)\eta}{\bar{\rho}_S}\right)\right. \\ &\left. + \widetilde{\sum}\left(m_{SR}, m_{SP}\right) \sum_{p=0}^{\Lambda_{SR}-1} \frac{\Gamma(\Lambda_{SR})\eta^p \rho_D^{\Lambda_{SP}} \Gamma\left(\Lambda_{SP}+p, \frac{\left(\beta_{SP}-\delta_{SP}\right)\rho_D+\left(\beta_{SR}-\delta_{SR}\right)\eta}{\bar{\rho}_S}\right)}{p!\left(\beta_{SR}-\delta_{SR}\right)^{\Lambda_{SR}-p}\left(\left(\beta_{SP}-\delta_{SP}\right)\rho_D+\left(\beta_{SR}-\delta_{SR}\right)\eta\right)^{\Lambda_{SP}+p}}\right) \\ &\times \left(\frac{\gamma\left(m_{RP}, \frac{\rho_D}{\Lambda_{RP}\bar{\rho}_R}\right)\Gamma\left(N_E m_E, \frac{\bar{\phi}_3}{\bar{\rho}_R \Lambda_E}\right)}{\Gamma(m_{RP})\Gamma(N_E m_E)} + \sum_{p=0}^{N_E m_E - 1} \frac{\left(\Lambda_E \rho_D\right)^{m_{RP}}\left(\bar{\phi}_3 \Lambda_{RP}\right)^p \Gamma\left(m_{RP}+p, \frac{\bar{\phi}_3 \Lambda_{RP}+\Lambda_E \rho_D}{\Lambda_E \bar{\rho}_R \Lambda_{RP}}\right)}{p!\Gamma(m_{RP})\left(\bar{\phi}_3 \Lambda_{RP}+\Lambda_E \rho_D\right)^{m_{RP}+p}}\right). \end{aligned} \tag{7.39}$$

Proof: Putting (7.3), (7.4) and (7.5) into (7.39), we get (7.40)

$$\begin{aligned} IP_{D_1}^{out} = &\left[\underbrace{\Pr\left(\mathcal{H}_{SP} < \frac{\rho_D}{\bar{\rho}_S}, \mathcal{H}_{SR} > \frac{\eta}{\bar{\rho}_S}\right)}_{C_1} + \underbrace{\Pr\left(\mathcal{H}_{SP} > \frac{\rho_D}{\bar{\rho}_S}, \mathcal{H}_{SR} > \frac{\eta \mathcal{H}_{SP}}{\rho_D}\right)}_{C_2}\right] \\ &\times \left[\underbrace{\Pr\left(\left|h_{RP}\right|^2 < \frac{\rho_D}{\bar{\rho}_R}, \mathcal{H}_E > \frac{\bar{\phi}_3}{\bar{\rho}_R}\right)}_{C_3} + \underbrace{\Pr\left(\left|h_{RP}\right|^2 > \frac{\rho_D}{\bar{\rho}_R}, \mathcal{H}_E > \frac{\bar{\phi}_3\left|h_{RP}\right|^2}{\rho_D}\right)}_{C_4}\right], \end{aligned} \tag{7.40}$$

where $\eta = \max\left(\phi_1, \phi_2\right)$ and $\bar{\phi}_3 = \frac{\gamma_{E_1}}{\left(b_1 - \gamma_{E_1} k_E^2\right)}$. After some variable substitutions and manipulations C_1 is expressed as

$$\begin{aligned} C_1 &= \int_0^{\frac{\rho_D}{\bar{\rho}_S}} f_{\mathcal{H}_{SP}}(x) \int_{\frac{\eta}{\bar{\rho}_S}}^{\infty} f_{\mathcal{H}_{SR}}(y) dy dx \\ &= \widetilde{\sum}\left(m_{SR}, m_{SP}\right) \frac{\left(\beta_{SP}-\delta_{SP}\right)^{-\Lambda_{SP}}}{\left(\beta_{SR}-\delta_{SR}\right)^{\Lambda_{SR}}} \\ &\times \gamma\left(\Lambda_{SP}, \frac{\rho_D\left(\beta_{SP}-\delta_{SP}\right)}{\bar{\rho}_S}\right) \Gamma\left(\Lambda_{SR}, \frac{\left(\beta_{SR}-\delta_{SR}\right)\eta}{\bar{\rho}_S}\right). \end{aligned} \tag{7.41}$$

Next, C_2 can be further calculated as follow

$$\begin{aligned} C_2 &= \int_{\frac{\rho_D}{\bar{\rho}_S}}^{\infty} f_{\mathcal{H}_{SP}}(x) \int_{\frac{\eta x}{\rho_D}}^{\infty} f_{\mathcal{H}_{SR}}(y) dy dx \\ &= \sum\nolimits^{\sim} (m_{SR}, m_{SP}) \sum_{p=0}^{\Lambda_{SR}-1} \frac{\Gamma(\Lambda_{SR}) \eta^p \rho_D^{\Lambda_{SP}}}{p! (\beta_{SR} - \delta_{SR})^{\Lambda_{SR}-p}} \times \frac{\Gamma\left(\Lambda_{SP}+p, \frac{(\beta_{SP}-\delta_{SP})\rho_D + (\beta_{SR}-\delta_{SR})\eta}{\bar{\rho}_S}\right)}{((\beta_{SP}-\delta_{SP})\rho_D + (\beta_{SR}-\delta_{SR})\eta)^{\Lambda_{SP}+p}}. \end{aligned} \tag{7.42}$$

Similarly, C_3 is expressed as

$$C_3 = \int_0^{\frac{\rho_D}{\bar{\rho}_R}} f_{|h_{RP}|^2}(x) \int_{\frac{\bar{\varphi}_3}{\bar{\rho}_R}}^{\infty} f_{\mathcal{H}_E}(y) dy dx = \frac{\gamma\left(m_{RP}, \frac{\rho_D}{\Lambda_{RP}\bar{\rho}_R}\right) \Gamma\left(N_E m_E, \frac{\bar{\phi}_3}{\bar{\rho}_R \Lambda_E}\right)}{\Gamma(m_{RP}) \Gamma(N_E m_E)}. \tag{7.43}$$

Furthermore, C_4 can be easily calculated by

$$\begin{aligned} C_4 &= \int_{\frac{\rho_D}{\bar{\rho}_R}}^{\infty} f_{|h_{RP}|^2}(x) \int_{\frac{\bar{\phi}_3 x}{\rho_D}}^{\infty} f_{\mathcal{H}_E}(y) dy dx \\ &= \sum_{p=0}^{N_E m_E - 1} \frac{(\Lambda_E \rho_D)^{m_{RP}} \left(\bar{\phi}_3 \Lambda_{RP}\right)^p}{p! \Gamma(m_{RP}) (\bar{\varphi}_3 \Lambda_{RP} + \Lambda_E \rho_D)^{m_{RP}+p}} \times \Gamma\left(m_{RP}+p, \frac{\bar{\phi}_3 \Lambda_{RP} + \Lambda_E \rho_D}{\Lambda_E \bar{\rho}_R \Lambda_{RP}}\right) \end{aligned} \tag{7.44}$$

Finally, our expected result can be achieved by combining (7.41), (7.42), (7.43) and (7.44). The proof is completed.

Intercept Probability D_2

The intercept probability of D_2 is given as [156]

$$IP_{D_2}^{out} = \Pr\left(\gamma_{R,x_1} > \gamma_{th_1}, \gamma_{R,x_2} > \gamma_{th_2}, \gamma_{E,x_2} > \gamma_{E_2}\right) \tag{7.45}$$

According to the above explanations, with $\bar{\phi}_4 = \frac{\gamma_{E_2}}{\left(b_2 - b_1\gamma_{E_2} - k_E^2 \gamma_{E_2}\right)}$ the closed-form expression of user D_2, i.e. $IP_{D_2}^{out}$ is obtained as

$$\begin{aligned} IP_{D_2}^{out} = &\left(\sum\nolimits^{\sim} (m_{SR}, m_{SP}) \frac{(\beta_{SP}-\delta_{SP})^{-\Lambda_{SP}}}{(\beta_{SR}-\delta_{SR})^{\Lambda_{SR}}} \gamma\left(\Lambda_{SP}, \frac{\rho_D(\beta_{SP}-\delta_{SP})}{\bar{\rho}_S}\right) \Gamma\left(\Lambda_{SR}, \frac{(\beta_{SR}-\delta_{SR})\eta}{\bar{\rho}_S}\right) \right. \\ &\left. + \sum\nolimits^{\sim} (m_{SR}, m_{SP}) \sum_{p=0}^{\Lambda_{SR}-1} \frac{\Gamma(\Lambda_{SR}) \eta^p \rho_D^{\Lambda_{SP}} \Gamma\left(\Lambda_{SP}+p, \frac{(\beta_{SP}-\delta_{SP})\rho_D + (\beta_{SR}-\delta_{SR})\eta}{\bar{\rho}_S}\right)}{p! (\beta_{SR}-\delta_{SR})^{\Lambda_{SR}-p} ((\beta_{SP}-\delta_{SP})\rho_D + (\beta_{SR}-\delta_{SR})\eta)^{\Lambda_{SP}+p}} \right) \\ &\times \left(\begin{array}{l} \frac{\gamma\left(m_{RP}, \frac{\rho_D}{\Lambda_{RP}\bar{\rho}_R}\right) \Gamma\left(N_E m_E, \frac{\bar{\phi}_4}{\bar{\rho}_R \Lambda_E}\right)}{\Gamma(m_{RP}) \Gamma(N_E m_E)} \\ + \sum_{p=0}^{N_E m_E - 1} \frac{(\Lambda_E \rho_D)^{m_{RP}} \left(\bar{\phi}_4 \Lambda_{RP}\right)^p}{p! \Gamma(m_{RP}) \left(\bar{\phi}_4 \Lambda_{RP} + \Lambda_E \rho_D\right)^{m_{RP}+p}} \Gamma\left(m_{RP}+p, \frac{\bar{\phi}_4 \Lambda_{RP} + \Lambda_E \rho_D}{\Lambda_E \bar{\rho}_R \Lambda_{RP}}\right) \end{array} \right). \end{aligned} \tag{7.46}$$

7.3.3 Throughput Performance

It can be further evaluated other metric, i.e. the overall throughput can be achieved based on obtained outage probabilities. In delay-limited mode, at fixed target rates R_1, R_2 the throughput can be achieved. As a result, the overall throughput can be formulated as [157]

$$\mathcal{T}_{total} = \left(1 - P_{D_1}^{out}\right) R_1 + \left(1 - P_{D_2}^{out}\right) R_2. \tag{7.47}$$

7.4 Numerical Results

In this section, to verified mathematical analysis, it is necessary to simulate and illustrate for proposed assisted CR-NOMA scheme. Here, the shadowing scenarios of the satellite links $\mathcal{H}_j$, including the heavy shadowing (HS) with $b_j, m_j, \Omega_j = (1, 0.063, 0.0007)$ and average shadowing (AS) with $b_j, m_j, \Omega_j = (5, 0.251, 0.279)$ as [153].

Next, we set power allocation factors $a_1 = b_1 = 0.2$, $a_2 = b_2 = 0.8$, $\bar{\rho} = \bar{\rho}_S = \bar{\rho}_R$, $k = k_{RD_i} = k_{SR} = k_E$, $N = N_1 = N_2 = N_E$, the target rates $R_1 = R_2 = 0.5$ bit per channel use (BPCU) except for specific cases, the channel gains $\lambda_1 = 1$, $\lambda_2 = 2$, λ_{RP} and $m = m_1 = m_2 = m_{RP} = m_E$. Moreover, case of $m = 1$ is equivalent with the Rayleigh fading channel model. In these following figures, Monte-Carlo simulations are performed to validate the analytical results.

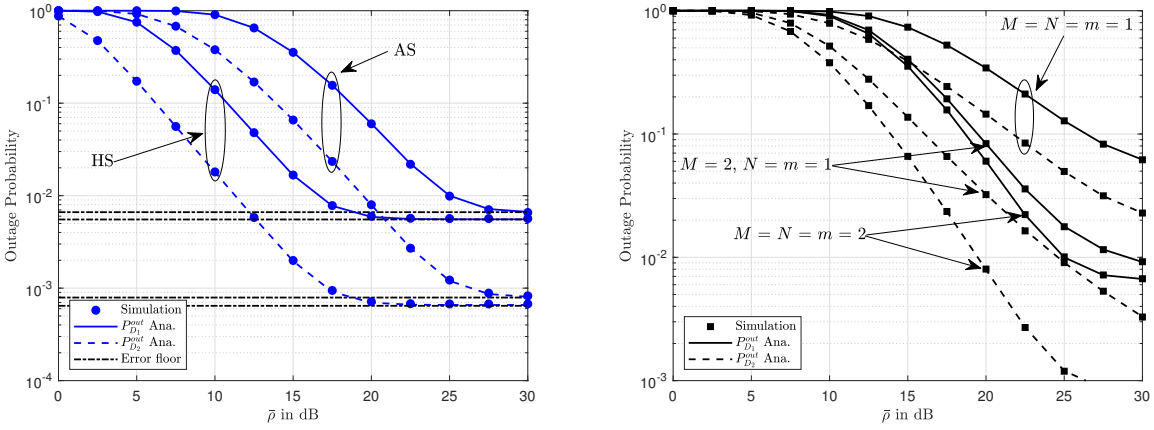

(a) $M = N = m = 2$, $\rho_D = 20$dB and $k = 0.1$ (AS and HS). (b) different values of M, N, m, $\rho_D = 20$dB, $k = 0.1$ (HS case).

Figure 7.2: The OP versus $\bar{\rho}$ with the satellite link is set AS and HS case.

Figure 7.2a shows the comparison of OP performance with HS and AS schemes for two users. By increasing average SNR at the source, OP decreases significantly, especially in the high region of SNR, i.e., $\bar{\rho}$. As can be observed, analytical results agree well with the Monte Carlo simulations, which confirm the corrections of derived expressions. Moreover, an increase of $\bar{\rho}$ obviously improves the SINR, then the corresponding OP performance of two users can be improved. However, such OP depends on on-target rates, and then these curves become saturated. It is worth noting that when adjusting the power allocation coefficient reasonably, we can reduce the OP performance gap among two users. The reason is that the OP depends on SINR, while SINR contains power allocation factors. This phenomenon implies

that a reliable transmission can be achieved by introducing the higher SNR at the source and a reasonable selection of power allocation factors.

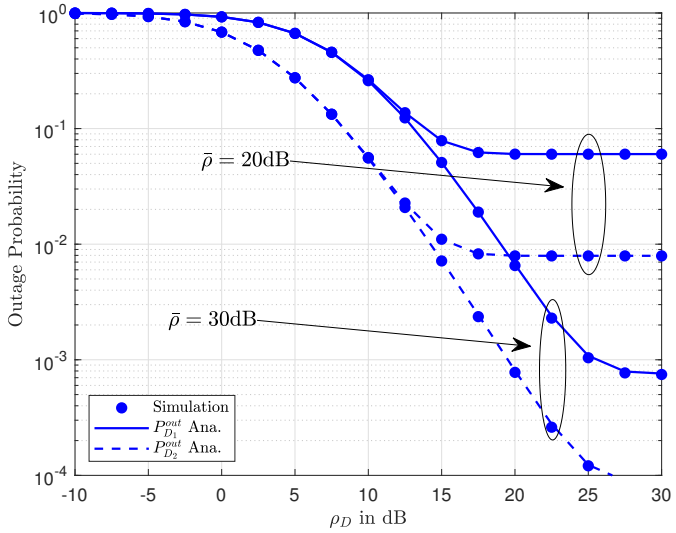

Figure 7.3: The OP versus ρ_D, with different values of ρ, where $M = N = m = 2$, $k = 0.1$ and the satellite link is set HS case.

Figure 7.2b demonstrates the OP performance of the considered NOMA-HSTCN for different antenna configurations, where the satellite-relay link undergoes HS case. As expected, the OP improves with an increase in the number of antennas, demonstrating the advantages of employing multiple antennas and BF in such systems. For example, the antenna configuration with $M = N = 2$ can achieve a significant enhancement compared with systems with case of $M = N = 1$. Similarly, the power constraint with primary network contributes to vary OP of two users as shown in Figure 7.3. In this observation, $\bar{\rho} = 30$ is reported as better OP for two users under evaluation trends of OP by adjusting ρ_D from -10 to 30 dB.

Under impact of hardware imperfection, OP changes once we vary value of k, shown in Figure 7.4. It can be concluded that user D_2 has little impact by hardware imperfection. In contrast, there are gaps among three cases of $k = 0, 0.2; 0.4$ as considering OP performance of user D_1. The reason is that SINRs depend on k.

The impacts of power allocation factors a_1, b_1 on OP performance can be seen clearly as Figure 7.5. As seen from (7.9), (7.10), and (7.11), OP can be decided by varying SINRs while such SINRs depend on power allocation factors. The opposite trends of OP for two users once we increase a_1, b_1 from 0 to 0.5. Of course, systems relying on OMA do not depend on such power factors, it is indicated as straight lines regardless of varying of a_1, b_1.

Figure 7.6a, we can see trends of the IP for two users under various configurations of satellite link modes (AS and HS) as well as antennas. It can be confirmed that user D_2 more secure compared with D_1 regardless of other set of satellite links or the number of antennas, which means that the superiority of user D_2 compared with user D_1 in term of OP and IP are same. In addition, in Figure 7.6b there are similar performance gap regarding IP of two users when we vary value of k which is reported impact of hardware noise to IP performance. Of course, ideal hardware exhibits the best IP performance. Therefore,

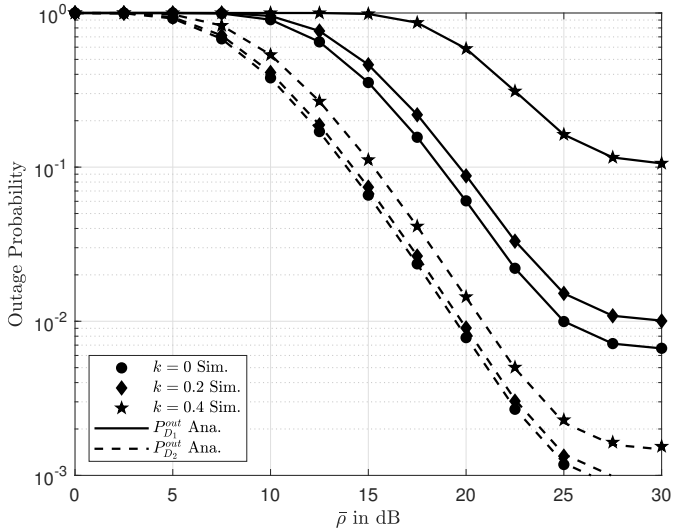

Figure 7.4: The OP versus $\bar{\rho}$, with different values of k, where $M = N = m = 2$, $\rho_D = 20$dB, and the satellite link is set HS case.

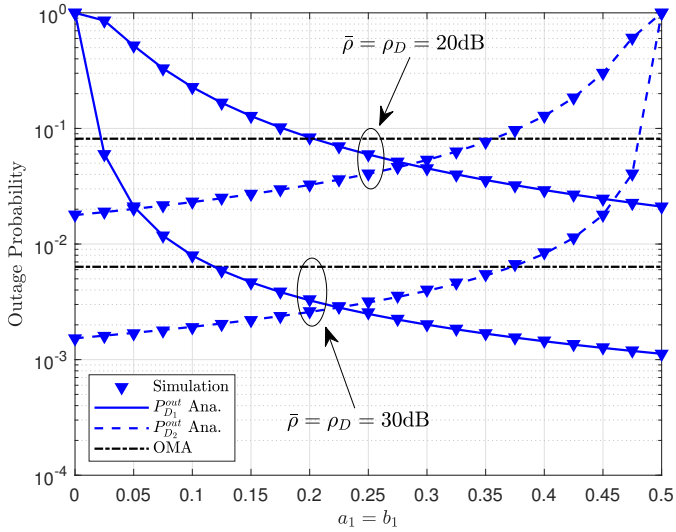

Figure 7.5: The OP versus $a_1 = b_1$, with different values of $\bar{\rho} = \rho_D$, where $M = N = m = 2$, $k = 0.1$ and the satellite link is set HS case.

it can help when designing NOMA-HSTCN communication systems to combat undesired effects related hardware.

In Figure 7.7, we can see how transmit SNR at source contributes to change of the throughput for two users under various configurations of satellite links as well as the number of antennas. It can be reported from (7.20) and (7.24) to confirm that the trend of throughput for two users can be predicted, i.e. it is very high at high SNR region.

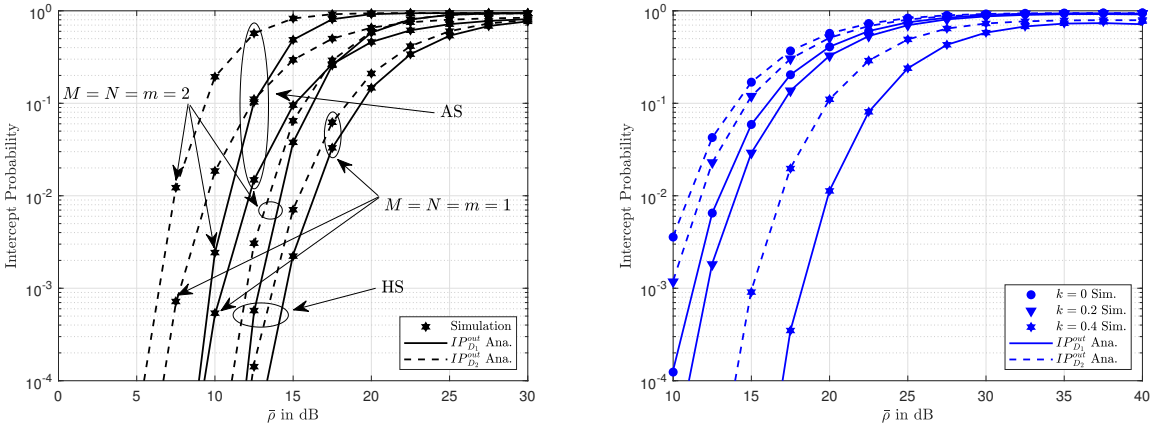

(a) with different values of $M = N = m$, $R_1 = R_2 = 1$ and channel parameter of satellite link.

(b) with different values of k, where $M = N = m = 2$, $R_1 = R_2 = 0.5$ (HS case).

Figure 7.6: The Intercept Probability versus $\bar{\rho}$, where $\rho_D = 20$dB, $\lambda_E = 0.1$, $\gamma_{E_1} = \gamma_{E_2} = 1$.

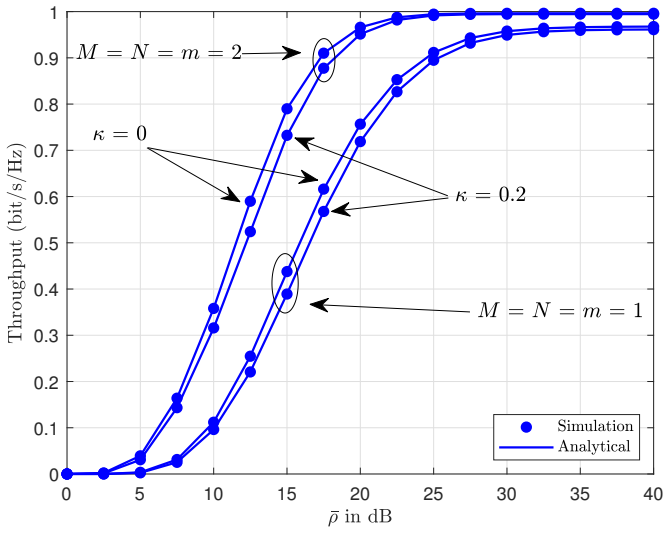

Figure 7.7: Throughput of system with $\rho_D = 20$dB, $R_1 = R_2 = 0.5$ and the satellite link is set HS case.

7.5 Conclusion

This section investigated the effects of hardware impairments on the reliability and security of NOMA-HSTCN systems by enabling multiple antennas design. The practical factor of hardware impairments is studied insightfully. Specifically, we derived the closed-form analytical expressions of the OP and IP from highlighting as essential performance metrics and analyze the limitation of OP in the high SNR region. The Monte Carlo simulation has verified the results obtained. These results show that as the level of hardware impairment increases, the user's OP reduces significantly, and the IP decreases. The power

allocation parameters cause the different trends of curves in terms of OP. It can be concluded that the severity of the performance degradation depends on several factors, including the power allocation ratio, the transmit SNR at the source, and the quality of channels.

Appendix F

With the help (7.4) and (7.5), the term A_1 can be written as

$$\begin{aligned} A_1 &= \Pr\left(\frac{P_S a_1 \mathcal{H}_{SR}}{P_S k_{SR}^2 \mathcal{H}_{SR} + \sigma_R^2} > \gamma_{th_1}\right) \\ &= \Pr\left(\bar{\rho}_S < \frac{\rho_D}{\mathcal{H}_{SP}}, \frac{\bar{\rho}_S a_1 \mathcal{H}_{SR}}{\bar{\rho}_S k_{SR}^2 \mathcal{H}_{SR} + 1} > \gamma_{th_1}\right) + \Pr\left(\bar{\rho}_S > \frac{\rho_D}{\mathcal{H}_{SP}}, \frac{\rho_D a_1 \mathcal{H}_{SR}}{\rho_D k_{SR}^2 \mathcal{H}_{SR} + \mathcal{H}_{SP}} > \gamma_{th_1}\right), \end{aligned} \tag{7.48}$$

where $\sigma^2 = \sigma_R^2 = \sigma_i^2 = \sigma_E^2$, $\bar{\rho}_S = \frac{\bar{P}_S}{\sigma^2}$ and $\rho_D = \frac{\bar{P}_P}{\sigma^2}$. First, we denote the first term of (7.48) is A_{1_1} and it can be computed by

$$A_{1\_1} = \Pr\left(\mathcal{H}_{SP} < \frac{\rho_D}{\bar{\rho}_S}, \mathcal{H}_{SR} > \frac{\phi_1}{\bar{\rho}_S}\right) = \int_0^{\frac{\rho_D}{\bar{\rho}_S}} f_{\mathcal{H}_{SP}}(x) \int_{\frac{\phi_1}{\bar{\rho}_S}}^{\infty} f_{\mathcal{H}_{SR}}(y) dy dx, \tag{7.49}$$

where $\phi_1 = \frac{\gamma_{th_1}}{\left(a_1 - k_{SR}^2 \gamma_{th_1}\right)}$.

Moreover, substituting (7.16) into (7.49) we can be calculate A_{1_1} as

$$A_{1\_1} = \sum\nolimits^{\sim} (m_{SR}, m_{SP}) \int_0^{\frac{\rho_D}{\bar{\rho}_S}} x^{\Delta_{SP}-1} e^{-(\beta_{SP}-\delta_{SP})x} \times \int_{\frac{\phi_1}{\bar{\rho}_S}}^{\infty} y^{\Delta_{SR}-1} e^{-(\beta_{SR}-\delta_{SR})y} dx dy, \tag{7.50}$$

where

$$\sum\nolimits^{\sim} (m_{SR}, m_{SP}) = \sum_{i_1=0}^{m_{SR}-1} \dots \sum_{i_M=0}^{m_{SR}-1} \Theta(SR, M) \times \sum_{i_1=0}^{m_{SP}-1} \dots \sum_{i_M=0}^{m_{SP}-1} \Theta(SP, M). \tag{7.51}$$

Based on [76, Eq. 3.351.1, Eq. 3.351.2], A_{1_1} is obtained as

$$\begin{aligned} A_{1\_1} &= \sum\nolimits^{\sim} (m_{SR}, m_{SP}) \frac{(\beta_{SP} - \delta_{SP})^{-\Delta_{SP}}}{(\beta_{SR} - \delta_{SR})^{\Delta_{SR}}} \\ &\times \gamma\left(\Delta_{SP}, \frac{\rho_D (\beta_{SP} - \delta_{SP})}{\bar{\rho}_S}\right) \Gamma\left(\Delta_{SR}, \frac{\phi_1 (\beta_{SR} - \delta_{SR})}{\bar{\rho}_S}\right). \end{aligned} \tag{7.52}$$

Second, the second term of (7.48) is A_{1_2} and it can be expressed as

$$A_{1\_2} = \Pr\left(\mathcal{H}_{SP} > \frac{\rho_D}{\bar{\rho}_S}, \mathcal{H}_{SR} > \frac{\phi_1 \mathcal{H}_{SP}}{\rho_D}\right) = \int_{\frac{\rho_D}{\bar{\rho}_S}}^{\infty} f_{\mathcal{H}_{SP}}(x) \int_{\frac{\phi_1 x}{\rho_D}}^{\infty} f_{\mathcal{H}_{SR}}(y) dy dx. \tag{7.53}$$

Furthermore, it can be calculated as

$$A_{1\_2} = \sum\nolimits^{\sim} (m_{SR}, m_{SP}) \int_{\frac{\rho_D}{\bar{\rho}_S}}^{\infty} x^{\Delta_{SP}-1} e^{-(\beta_{SP}-\delta_{SP})x} \times \int_{\frac{\varphi_1 x}{\rho_D}}^{\infty} y^{\Delta_{SR}-1} e^{-(\beta_{SR}-\delta_{SR})y} dy dx. \tag{7.54}$$

After some algebraic manipulations, A_{1_2} can be obtain as

$$\begin{aligned} A_{1\_2} = &\sum\nolimits^{\sim} (m_{SR}, m_{SP}) \sum_{p_1=0}^{\Delta_{SR}-1} \frac{\Gamma(\Delta_{SR})\,\phi_1^{p_1}\rho_D^{\Delta_{SP}}}{p_1!\,(\beta_{SR}-\delta_{SR})^{\Delta_{SR}-p_1}} \\ &\times \frac{\Gamma\left(\Delta_{SP}+p_1, \frac{(\beta_{SP}-\delta_{SP})\rho_D+(\beta_{SR}-\delta_{SR})\phi_1}{\bar{\rho}_S}\right)}{\left((\beta_{SP}-\delta_{SP})\,\rho_D+(\beta_{SR}-\delta_{SR})\,\phi_1\right)^{\Delta_{SP}+p_1}} \end{aligned} \tag{7.55}$$

Finally, by substituting (7.52) and (7.55) into (7.48) we obtain (7.20) and the proof is completed.

Appendix G

By substituting (7.5) and (7.11) into (7.19), A_2 is rewritten as

$$\begin{aligned} A_2 &= \Pr\left(\frac{P_R b_1 \mathcal{H}_{RD_1}}{P_R k_{RD_1}^2 \mathcal{H}_{RD_1}+\sigma_1^2} > \gamma_{th_1}\right) \\ &= \Pr\left(\bar{\rho}_R < \frac{\rho_D}{|h_{RP}|^2}, \frac{\bar{\rho}_R b_1 \mathcal{H}_{RD_1}}{\bar{\rho}_R k_{RD_1}^2 \mathcal{H}_{RD_1}+1} > \gamma_{th_1}\right) \\ &+ \Pr\left(\bar{\rho}_R > \frac{\rho_D}{|h_{RP}|^2}, \frac{\rho_D b_1 \mathcal{H}_{RD_1}}{\rho_D k_{RD_1}^2 \mathcal{H}_{RD_1}+|h_{RP}|^2} > \gamma_{th_1}\right) \end{aligned} \tag{7.56}$$

Similarly, we denote the first and second term of (7.56) are A_{2_1} and A_{2_2} respectively. Then, A_{2_1} is express as

$$A_{2\_1} = \Pr\left(|h_{RP}|^2 < \frac{\rho_D}{\bar{\rho}_R}, \mathcal{H}_{RD_1} > \frac{\bar{\phi}_1}{\bar{\rho}_R}\right) = \int_0^{\frac{\rho_D}{\bar{\rho}_R}} f_{|h_{RP}|^2}(x) \int_{\frac{\bar{\phi}_1}{\bar{\rho}_R}}^{\infty} f_{\mathcal{H}_{RD_1}}(y) dy dx \tag{7.57}$$

where $\bar{\phi}_1 = \frac{\gamma_{th_1}}{\left(b_1-\gamma_{th_1}k_{RD_1}^2\right)}$. With the help of (7.17), (7.18) and after some variable substitutions and manipulations, we can obtain A_{2_1} as

$$\begin{aligned} A_{2\_1} &= \int_0^{\frac{\rho_D}{\bar{\rho}_R}} \frac{x^{m_{RP}-1}}{\Gamma(m_{RP})\,\Lambda_{RP}^{m_{RP}}} e^{-\frac{x}{\Lambda_{RP}}} \times \int_{\frac{\bar{\phi}_1}{\bar{\rho}_R}}^{\infty} \frac{y^{N_1 m_1-1}}{\Gamma(N_1 m_1)\,\Lambda_1^{N_1 m_1}} e^{-\frac{y}{\Lambda_1}} dy dx \\ &= \frac{\gamma\left(m_{RP}, \frac{\rho_D}{\Lambda_{RP}\bar{\rho}_R}\right)\Gamma\left(N_1 m_1, \frac{\bar{\phi}_1}{\bar{\rho}_R \Lambda_v}\right)}{\Gamma(m_{RP})\,\Gamma(N_1 m_1)}. \end{aligned} \tag{7.58}$$

Furthermore, the term A_{2_2} is expressed as

$$A_{2\_2} = \Pr\left(|h_{RP}|^2 > \frac{\rho_D}{\bar{\rho}_R}, \mathcal{H}_{RD_1} > \frac{\bar{\phi}_1 |h_{RP}|^2}{\rho_D}\right) = \int_0^{\infty} f_{|h_{RP}|^2}(x) \int_{\frac{\bar{\phi}_1 x}{\rho_D}}^{\infty} f_{\mathcal{H}_{RD_1}}(y) dy dx \tag{7.59}$$

Similar in (7.55), A_{2_2} is given by

$$A_{2\_2} = \sum_{p_2=0}^{N_1 m_1-1} \frac{(\Lambda_1\rho_D)^{m_{RP}}\left(\bar{\phi}_1\Lambda_{RP}\right)^{p_2}}{p_2!\Gamma(m_{RP})\left(\bar{\phi}_1\Lambda_{RP}+\Lambda_1\rho_D\right)^{m_{RP}+p_2}} \times \Gamma\left(m_{RP}+p_2, \frac{\bar{\phi}_1\Lambda_{RP}+\Lambda_1\rho_D}{\Lambda_1\bar{\rho}_R\Lambda_{RP}}\right). \tag{7.60}$$

Now, using (7.58) and (7.60), the expected result can be attained.
This completes the proof.

8 Conclusion and future work

8.1 Summary of results and insights

This dissertation thesis explored and extended the EH concept and applied it to wireless relay networks, in which relay nodes harvest energy from the source and use this energy to forward the data from the source nodes to the destination nodes. In the in-studied integrated satellite-terrestrial networks, during the relaying process, the relay nodes utilize the power domain for the fair and efficient power allocation to the end users and minimize the total transmit power. We have performed the design, analysis, and simulation of the proposed system model following the aforementioned framework and have fulfilled the three aims as presented below.

The most contribution of my dissertation is the proposal of two integrated models between satellite and terrestrial networks with reliable and secure transmission in hybrid satellite-terrestrial cognitive networks relying on NOMA and the fairness for power distribution efficiency to the end-users.

- With regard to the first aim, the closed-form expression and simulation for OP and average throughput have been derived for each EH-based relay network model proposed in this dissertation thesis. Furthermore, apart from the basic relaying models for energy harvesting and information transmission, we have proposed some relaying models for D2D communication and calculated the effect of the network parameters on the OP and throughput to improve the energy consumption and prolong the lifetime of the wireless communication [**NHN04**], [**NHN08**], [**NHN10**], [**NHN15**].
- Secondly, the outage and throughput performance in CR-based NOMA systems have been examined. In these systems, the superimposed signal is transmitted from the base station to the relay and then forwarded to the end users in the SN. The NOMA scheme is applied to provide multiple access in the downlink. We used a fixed power distribution scheme so that the CR-NOMA system can ensure the fairness in power allocation to the end users. Therefore, the highest throughput can be achieved at a specific data rate. We provided the mathematical analysis and simulation results to evaluate the performance of the CR-NOMA-based integrated network [**NHN02**], [**NHN03**], [**NHN11**].
- Finally, to fulfill the third aim, we provided the mathematical analysis and simulation results to evaluate the effect of network parameters on the performance of HSTCNs relaying network on the NOMA scheme. We applied beamforming (BF) methods in HSTCNs where a relay (R) is used as base station (BS) to transmit signal from the satellite to multiple secondary users (SUs) in the SN. Meanwhile, the interference constraint was applied to limit the negative effect of SN on the PN. As a result, the total transmit power was minimized and the QoS of all the end users was guaranteed. Finally, computer simulations were provided to verify the effectiveness of the BF methods as well as the advantages of HSTCNs relaying network using the NOMA scheme [**NHN01**], [**NHN15**].

To conclude, a thorough analysis of the EH solution was conducted. Besides, factor selection studies for fair power allocation and interference minimization to the PN, to guarantee the QoS for all the end users, were carried out from multiple perspectives, i.e., the theoretical framework, the practical consideration, the variety of the strategies serving different applications, and the variety of the channel conditions.

8.2 Future work

In this dissertation, we proposed two novel schemes of energy harvesting and power spectrum distribution technology with system models integrated into wireless communication to provide seamless connectivity and extend the network coverage. However, there are still many issues to be investigated regarding green networking, aiming at further reducing unnecessary energy consumption and power spectrum efficiency usage of wireless communication. These issues should be considered to make the herein idea full-grown and applicable for further studies.

Multi-user connection has always been of great interest in wireless communication. In our research, we considered more than a pair of secondary users in the proposed system models and applied the half-duplex relay model. This scenario may be extended to the full-duplex case. Moreover, as possible future works, switching policies to other channels and analyzing network performance under such conditions for a multi-channel platform and multi-utility are suggested.

Additionally, our research can also be extended to other integrated network models, bringing efficiency to research and application. Besides, advanced techniques can be used to improve the spectrum efficiency, energy savings and utility. Finally, further studies into the hardware implementation of the proposed algorithm, and antenna parameters for the secondary BS, such as the gain, the optimum inclination, and azimuth angles, could be considered. These are important research topics that could be investigated in the future.

References

[1] I.F.Akyildiz, W.Y.Lee, M.C.Vuran, and S.Mohanty, "Next generation/dynamic spectrum access/cognitive radio wireless networks: A survey," *Computer networks*, vol. 50, no. 13, pp. 2127–2159, 2006.

[2] H.Yang, A.Alphones, Z.Xiong, D.Niyato, J.Zhao, and K.Wu, "Artificial-intelligence-enabled intelligent 6g networks," *IEEE Network*, vol. 34, no. 6, pp. 272–280, 2020.

[3] D.Liu, Y.Chen, K.K.Chai, T.Zhang, and M.Elkashlan, "Opportunistic user association for multi-service hetnets using nash bargaining solution," *IEEE Communications Letters*, vol. 18, no. 3, pp. 463–466, 2014.

[4] R.Madan, J.Borran, A.Sampath, N.Bhushan, A.Khandekar, and T.Ji, "Cell association and interference coordination in heterogeneous lte-a cellular networks," *IEEE Journal on selected areas in communications*, vol. 28, no. 9, pp. 1479–1489, 2010.

[5] Y.Gu and S.Aissa, "Rf-based energy harvesting in decode-and-forward relaying systems: Ergodic and outage capacities," *IEEE Transactions on Wireless Communications*, vol. 14, no. 11, pp. 6425–6434, 2015.

[6] J.Mitola and G.Q.Maguire, "Cognitive radio: making software radios more personal," *IEEE personal communications*, vol. 6, no. 4, pp. 13–18, 1999.

[7] S.Haykin, "Cognitive radio: brain-empowered wireless communications," *IEEE journal on selected areas in communications*, vol. 23, no. 2, pp. 201–220, 2005.

[8] A.Goldsmith, S.A.Jafar, I.Maric, and S.Srinivasa, "Breaking spectrum gridlock with cognitive radios: An information theoretic perspective," *Proceedings of the IEEE*, vol. 97, no. 5, pp. 894–914, 2009.

[9] Z.Ding, X.Lei, G.K.Karagiannidis, R.Schober, J.Yuan, and V.K.Bhargava, "A survey on non-orthogonal multiple access for 5g networks: Research challenges and future trends," *IEEE Journal on Selected Areas in Communications*, vol. 35, no. 10, pp. 2181–2195, 2017.

[10] T.L.Nguyen and D.T.Do, "Exploiting impacts of intercell interference on swipt-assisted non-orthogonal multiple access," *Wireless Communications and Mobile Computing*, vol. 2018, 2018.

[11] L.Dai, B.Wang, Y.Yuan, S.Han, I.Chih-Lin, and Z.Wang, "Non-orthogonal multiple access for 5g: solutions, challenges, opportunities, and future research trends," *IEEE Communications Magazine*, vol. 53, no. 9, pp. 74–81, 2015.

[12] S.M.R.Islam, N.Avazov, O.A.Dobre, and K.S.Kwak, "Power-domain non-orthogonal multiple access (noma) in 5g systems: Potentials and challenges," *IEEE Communications Surveys & Tutorials*, vol. 19, no. 2, pp. 721–742, 2016.

[13] H.Chingoska, Z.Hadzi-Velkov, I.Nikoloska, and N.Zlatanov, "Resource allocation in wireless powered communication networks with non-orthogonal multiple access," *IEEE Wireless Communications Letters*, vol. 5, no. 6, pp. 684–687, 2016.

[14] P.D.Diamantoulakis, K.N.Pappi, G.K.Karagiannidis, H.Xing, and A.Nallanathan, "Joint downlink/uplink design for wireless powered networks with interference," *IEEE Access*, vol. 5, pp. 1534–1547, 2017.

[15] D.T.Do and C.B.Le, "Application of noma in wireless system with wireless power transfer scheme: Outage and ergodic capacity performance analysis," *Sensors*, vol. 18, no. 10, p. 3501, 2018.

[16] D.T.Do, C.B.Le, H.N.Nguyen, T.N.Kieu, S.P.Le, N.L.Nguyen, N.T.Nguyen, and M.Voznak, "Wireless power transfer enabled noma relay systems: two sic modes and performance evaluation," *Telkomnika*, vol. 17, no. 6, pp. 2697–2703, 2019.

[17] G.Maral, M.Bousquet, and Z.Sun, *Satellite communications systems: systems, techniques and technology*. John Wiley & Sons, 2020.

[18] D.T.Do and A.T.Le, "Noma based cognitive relaying: Transceiver hardware impairments, relay selection policies and outage performance comparison," *Computer Communications*, vol. 146, pp. 144–154, 2019.

[19] D.T.Do, A.T.Le, and B.M.Lee, "Noma in cooperative underlay cognitive radio networks under imperfect sic," *IEEE Access*, vol. 8, pp. 86180–86195, 2020.

[20] X.Zhang, D.Guo, K.An, Z.Chen, B.Zhao, Y.Ni, and B.Zhang, "Performance analysis of noma-based cooperative spectrum sharing in hybrid satellite-terrestrial networks," *IEEE Access*, vol. 7, pp. 172321–172329, 2019.

[21] Z.Lin, M.Lin, W.P.Zhu, J.B.Wang, and J.Cheng, "Robust secure beamforming for wireless powered cognitive satellite-terrestrial networks," *IEEE Transactions on Cognitive Communications and Networking*, 2020.

[22] M.Joseph III, "Cognitive radio architecture: The engineering foundation of radio xml," *New Jersey US: John Wiley & Sons*, 2006.

[23] W.Liang, S.X.Ng, and L.Hanzo, "Cooperative overlay spectrum access in cognitive radio networks," *IEEE Communications Surveys & Tutorials*, vol. 19, no. 3, pp. 1924–1944, 2017.

[24] Y.Liu, Y.Zhang, R.Yu, and S.Xie, "Integrated energy and spectrum harvesting for 5g wireless communications," *IEEE Network*, vol. 29, no. 3, pp. 75–81, 2015.

[25] A.A.Nasir, X.Zhou, S.Durrani, and R.A.Kennedy, "Relaying protocols for wireless energy harvesting and information processing," *IEEE Transactions on Wireless Communications*, vol. 12, no. 7, pp. 3622–3636, 2013.

[26] A.Zahedi, M.Ergen, and I.Shayea, "Optimum time/power fraction of energy harvesting in tsr/psr swipt-based cooperative communications with effective capacity maximization approach," *AEU-International Journal of Electronics and Communications*, vol. 111, p. 152889, 2019.

[27] A. Gupta and R. K. Jha, "A survey of 5g network: Architecture and emerging technologies," *IEEE access*, vol. 3, pp. 1206–1232, 2015.

[28] A.Nosratinia, T.E.Hunter, and A.Hedayat, "Cooperative communication in wireless networks," *IEEE communications Magazine*, vol. 42, no. 10, pp. 74–80, 2004.

[29] D.J.Love, R.W.Heath, and T.Strohmer, "Grassmannian beamforming for multiple-input multiple-output wireless systems," *IEEE transactions on information theory*, vol. 49, no. 10, pp. 2735–2747, 2003.

[30] J.N.Laneman, D.NC.Tse, and G.W.Wornel, "Cooperative diversity in wireless networks: Efficient protocols and outage behavior," *IEEE Transactions on Information theory*, vol. 50, no. 12, pp. 3062–3080, 2004.

[31] J.N.Laneman, G.W.Wornell, and D.NC.Tse, "An efficient protocol for realizing cooperative diversity in wireless networks," in *Proceedings. 2001 IEEE International Symposium on Information Theory (IEEE Cat. No. 01CH37252)*, p. 294, 2001.

[32] T.E.Hunter and A.Nosratinia, "Diversity through coded cooperation," *IEEE transactions on wireless communications*, vol. 5, no. 2, pp. 283–289, 2006.

[33] C.Peng, Q.Zhang, M.Zhao, and Y.Yao, "On the performance analysis of network-coded cooperation in wireless networks," in *IEEE INFOCOM 2007-26th IEEE International Conference on Computer Communications*, pp. 1460–1468, 2007.

[34] Z.Zheng, X.Zhang, LX.Cai, R.Zhang, and X.Shen, "Sustainable communication and networking in two-tier green cellular networks," *IEEE Wireless Communications*, vol. 21, no. 4, pp. 47–53, 2014.

[35] H.S.Nguyen, D.T. Do, and M.Voznak, "Two-way relaying networks in green communications for 5g: Optimal throughput and tradeoff between relay distance on power splitting-based and time switching-based relaying swipt," *AEU-International Journal of Electronics and Communications*, vol. 70, no. 12, pp. 1637–1644, 2016.

[36] M.-L. Ku, W. Li, Y. Chen, and K. R. Liu, "Advances in energy harvesting communications: Past, present, and future challenges," *IEEE Communications Surveys & Tutorials*, vol. 18, no. 2, pp. 1384–1412, 2015.

[37] D.T.Do and H.S.Nguyen, "A tractable approach to analyzing the energy-aware two-way relaying networks in the presence of co-channel interference," *EURASIP Journal on Wireless Communications and Networking*, vol. 2016, no. 1, p. 271, 2016.

[38] T.N.Kieu, D.T.Do, X.N.Xuan, T.N.Nhat, and H.H.Duy, "Wireless information and power transfer for full duplex relaying networks: performance analysis," in *AETA 2015: Recent Advances in Electrical Engineering and Related Sciences*, pp. 53–62, Springer, 2016.

[39] F. Hu, B. Chen, and K. Zhu, "Full spectrum sharing in cognitive radio networks toward 5g: A survey," *IEEE Access*, vol. 6, pp. 15754–15776, 2018.

[40] M. Amjad, M. H. Rehmani, and S. Mao, "Wireless multimedia cognitive radio networks: A comprehensive survey," *IEEE Communications Surveys & Tutorials*, vol. 20, no. 2, pp. 1056–1103, 2018.

[41] F. A. Awin, Y. M. Alginahi, E. Abdel-Raheem, and K. Tepe, "Technical issues on cognitive radio-based internet of things systems: A survey," *IEEE access*, vol. 7, pp. 97887–97908, 2019.

[42] C. Jiang, H. Zhang, Y. Ren, Z. Han, K.-C. Chen, and L. Hanzo, "Machine learning paradigms for next-generation wireless networks," *IEEE Wireless Communications*, vol. 24, no. 2, pp. 98–105, 2016.

[43] Z. Wei, J. Yuan, D. W. K. Ng, M. Elkashlan, and Z. Ding, "A survey of downlink non-orthogonal multiple access for 5g wireless communication networks," *arXiv preprint arXiv:1609.01856*, 2016.

[44] S. Arzykulov, G. Nauryzbayev, T. A. Tsiftsis, B. Maham, and M. Abdallah, "On the outage of underlay cr-noma networks with detect-and-forward relaying," *IEEE Transactions on Cognitive Communications and Networking*, vol. 5, no. 3, pp. 795–804, 2019.

[45] P.D.Diamantoulakis, K.N.Pappi, Z.Ding, and G.K.Karagiannidis, "Wireless-powered communications with non-orthogonal multiple access," *IEEE Transactions on Wireless Communications*, vol. 15, no. 12, pp. 8422–8436, 2016.

[46] S.Arzykulov, T.A.Tsiftsis, G.Nauryzbayev, and M.Abdallah, "Outage performance of cooperative underlay cr-noma with imperfect csi," *IEEE Communications Letters*, vol. 23, no. 1, pp. 176–179, 2019.

[47] W. Zhao, R. She, and H. Bao, "Security energy efficiency maximization for two-way relay assisted cognitive radio noma network with self-interference harvesting," *IEEE Access*, vol. 7, pp. 74401–74411, 2019.

[48] D.T.Do, H.S.Nguyen, M.Voznak, and T.S.Nguyen, "Wireless powered relaying networks under imperfect channel state information: System performance and optimal policy for instantaneous rate," *Radioengineering*, vol. 26, no. 3, 2017.

[49] Y. Wang, Y. Xu, Y. Zhang, and P. Zhang, "Hybrid satellite-aerial-terrestrial networks in emergency scenarios: a survey," *China Communications*, vol. 14, no. 7, pp. 1–13, 2017.

[50] T. Wei, W. Feng, Y. Chen, C.-X. Wang, N. Ge, and J. Lu, "Hybrid satellite-terrestrial communication networks for the maritime internet of things: key technologies, opportunities, and challenges," *IEEE Internet of Things Journal*, vol. 8, no. 11, pp. 8910–8934, 2021.

[51] X. Fang, W. Feng, T. Wei, Y. Chen, N. Ge, and C.-X. Wang, "5g embraces satellites for 6g ubiquitous iot: Basic models for integrated satellite terrestrial networks," *arXiv preprint arXiv:2011.03182*, 2020.

[52] Y. Ruan, Y. Li, R. Zhang, W. Cheng, and C. Liu, "Cooperative resource management for cognitive satellite-aerial-terrestrial integrated networks towards iot," *IEEE Access*, vol. 8, pp. 35759–35769, 2020.

[53] R. Ge, D. Bian, K. An, J. Cheng, and H. Zhu, "Performance analysis of cooperative nonorthogonal multiple access scheme in two-layer geo/leo satellite network," *IEEE Systems Journal*, 2021.

[54] T. Teng, X. Yu, M. Li, and G. Wang, "Performance analysis of satellite-terrestrial network of weibull fading channel," *Wireless Personal Communications*, pp. 1–19, 2021.

[55] Y. Akhmetkaziyev, G. Nauryzbayev, S. Arzykulov, A. M. Eltawil, K. M. Rabie, and X. Li, "Performance of noma-enabled cognitive satellite-terrestrial networks with non-ideal system limitations," *IEEE Access*, vol. 9, pp. 35932–35946, 2021.

[56] S. Vassaki, M. I. Poulakis, and A. D. Panagopoulos, "Optimal isinr-based power control for cognitive satellite terrestrial networks," *Transactions on Emerging Telecommunications Technologies*, vol. 28, no. 2, p. e2945, 2017.

[57] K. An, M. Lin, J. Ouyang, and W.-P. Zhu, "Secure transmission in cognitive satellite terrestrial networks," *IEEE Journal on Selected Areas in Communications*, vol. 34, no. 11, pp. 3025–3037, 2016.

[58] M.Lin, Z.Lin, W.P.Zhu, and J.B.Wang, "Joint beamforming for secure communication in cognitive satellite terrestrial networks," *IEEE Journal on Selected Areas in Communications*, vol. 36, no. 5, pp. 1017–1029, 2018.

[59] W.Cao, Y.Zou, Z.Yang, and J.Zhu, "Relay selection for improving physical-layer security in hybrid satellite-terrestrial relay networks," *IEEE Access*, vol. 6, pp. 65275–65285, 2018.

[60] X.Zhang, B.Zhang, K.An, Z.Chen, S.Xie, H.Wang, L.Wang, and D.Guo, "Outage performance of noma-based cognitive hybrid satellite-terrestrial overlay networks by amplify-and-forward protocols," *IEEE Access*, vol. 7, pp. 85372–85381, 2019.

[61] B.Li, Z.Fei, Z.Chu, F.Zhou, K.K.Wong, and P.Xiao, "Robust chance-constrained secure transmission for cognitive satellite terrestrial networks," *IEEE Transactions on Vehicular Technology*, vol. 67, no. 5, pp. 4208–4219, 2018.

[62] V.Singh, V.Bankey, and P.K.Upadhyay, "Underlay cognitive hybrid satellite-terrestrial networks with cooperative-noma," in *2020 IEEE Wireless Communications and Networking Conference (WCNC)*, pp. 1–6, 2020.

[63] V.Singh, P.K.Upadhyay, and M.Lin, "On the performance of noma-assisted overlay multiuser cognitive satellite-terrestrial networks," *IEEE Wireless Communications Letters*, vol. 9, no. 5, pp. 638–642, 2020.

[64] S.P.Le, M.S.Van Nguyen, D.T.Do, H.N.Nguyen, N.L.Nguyen, N.T.Nguyen, and M.Voznak, "Enabling wireless power transfer and multiple antennas selection to iot network relying on noma," *Elektronika ir Elektrotechnika*, vol. 26, no. 5, pp. 59–65, 2020.

[65] S.Arzykulov, G.Nauryzbayev, T.A.Tsiftsis, and B.Maham, "Performance analysis of underlay cognitive radio nonorthogonal multiple access networks," *IEEE Transactions on Vehicular Technology*, vol. 68, no. 9, pp. 9318–9322, 2019.

[66] A.Kumar and K.Kumar, "Relay sharing with df and af techniques in noma assisted cognitive radio networks," *Physical Communication*, p. 101143, 2020.

[67] D.T.Do, M.S.Van Nguyen, F.Jameel, R.Jantti, and I.S.Ansari, "Performance evaluation of relay-aided cr-noma for beyond 5g communications," *IEEE Access*, vol. 8, pp. 134838–134855, 2020.

[68] H.S.Nguyen, A.H.Bui, D.T.Do, and M.Voznak, "Imperfect channel state information of af and df energy harvesting cooperative networks," *China Communications*, vol. 13, no. 10, pp. 11–19, 2016.

[69] T. N. Nguyen, D.-T. Do, P. T. Tran, and M. Voznak, "Time switching for wireless communications with full-duplex relaying in imperfect csi condition," *KSII Transactions on Internet and Information Systems (TIIS)*, vol. 10, no. 9, pp. 4223–4239, 2016.

[70] T.L.Nguyen and D.T.Do, "A new look at af two-way relaying networks: energy harvesting architecture and impact of co-channel interference," *Annals of Telecommunications*, vol. 72, no. 11-12, pp. 669–678, 2017.

[71] G. Zhu and K. Huang, "Analog spatial cancellation for tackling the near-far problem in wirelessly powered communications," *IEEE Journal on Selected Areas in Communications*, vol. 34, no. 12, pp. 3566–3576, 2016.

[72] Y.Ma, H.Chen, Z.Lin, Y.Li, and B.Vucetic, "Distributed and optimal resource allocation for power beacon-assisted wireless-powered communications," *IEEE Transactions on Communications*, vol. 63, no. 10, pp. 3569–3583, 2015.

[73] S.Bi and R.Zhang, "Placement optimization of energy and information access points in wireless powered communication networks," *IEEE transactions on wireless communications*, vol. 15, no. 3, pp. 2351–2364, 2015.

[74] P.Sun, K.G.Shin, H.Zhang, and L.He, "Transmit power control for d2d-underlaid cellular networks based on statistical features," *IEEE Transactions on Vehicular Technology*, vol. 66, no. 5, pp. 4110–4119, 2017.

[75] C.Zhong, X.Chen, Z.Zhang, and G.K.Karagiannidis, "Wireless-powered communications: Performance analysis and optimization," *IEEE Transactions on Communications*, vol. 63, no. 12, pp. 5178–5190, 2015.

[76] I.S.Gradshteyn and I.M.Ryzhik, *Table of integrals, series, and products*. Academic press, 2014.

[77] A.Ghosh, N.Mangalvedhe, R.Ratasuk, B.Mondal, M.Cudak, E.Visotsky, T.A.Thomas, J.G.Andrews, P.Xia, H.S.Jo, *et al.*, "Heterogeneous cellular networks: From theory to practice," *IEEE communications magazine*, vol. 50, no. 6, pp. 54–64, 2012.

[78] J.G.Andrews, H.Claussen, M.Dohler, S.Rangan, and M.C.Reed, "Femtocells: Past, present, and future," *IEEE Journal on Selected Areas in communications*, vol. 30, no. 3, pp. 497–508, 2012.

[79] Z.Wang, Z.Chen, L.Luo, Z.Hu, B.Xia, and H.Liu, "Outage analysis of cognitive relay networks with energy harvesting and information transfer," in *2014 IEEE international conference on communications (ICC)*, pp. 4348–4353, 2014.

[80] A.Goldsmith, S.A.Jafar, I.Maric, and S.Srinivasa, "Breaking spectrum gridlock with cognitive radios: An information theoretic perspective," *Proceedings of the IEEE*, vol. 97, no. 5, pp. 894–914, 2009.

[81] M.Namdar and A.Basgumus, "Outage performance analysis of underlay cognitive radio networks with decode-and-forward relaying," *Cognitive Radio*, pp. 25–38, 2017.

[82] A.Ghasemi and E.S.Sousa, "Fundamental limits of spectrum-sharing in fading environments," *IEEE Transactions on Wireless Communications*, vol. 6, no. 2, pp. 649–658, 2007.

[83] L. Wang, K. J. Kim, T. Q. Duong, M. Elkashlan, and H. V. Poor, "Security enhancement of cooperative single carrier systems," *IEEE Transactions on Information Forensics and Security*, vol. 10, no. 1, pp. 90–103, 2014.

[84] L. J. Rodriguez, N. H. Tran, T. Q. Duong, T. Le-Ngoc, M. Elkashlan, and S. Shetty, "Physical layer security in wireless cooperative relay networks: State of the art and beyond," *IEEE Communications Magazine*, vol. 53, no. 12, pp. 32–39, 2015.

[85] L. Sun, T. Zhang, L. Lu, and H. Niu, "On the combination of cooperative diversity and multiuser diversity in multi-source multi-relay wireless networks," *IEEE Signal Processing Letters*, vol. 17, no. 6, pp. 535–538, 2010.

[86] M. Ju, H.-K. Song, and I.-M. Kim, "Joint relay-and-antenna selection in multi-antenna relay networks," *IEEE Transactions on Communications*, vol. 58, no. 12, pp. 3417–3422, 2010.

[87] T.-D. Le and O.-S. Shin, "Wireless energy harvesting in cognitive radio with opportunistic relays selection," in *2015 IEEE 26th annual international symposium on personal, indoor, and mobile radio communications (PIMRC)*, pp. 949–953, IEEE, 2015.

[88] A. Banerjee, A. Paul, and S. P. Maity, "Joint power allocation and route selection for outage minimization in multihop cognitive radio networks with energy harvesting," *IEEE Transactions on Cognitive Communications and Networking*, vol. 4, no. 1, pp. 82–92, 2017.

[89] M. Wakaiki, K. Suto, K. Koiwa, K.-Z. Liu, and T. Zanma, "A control-theoretic approach for cell zooming of energy harvesting small cell networks," *IEEE Transactions on Green Communications and Networking*, vol. 3, no. 2, pp. 329–342, 2018.

[90] H.Wang, J.Wang, G.Ding, L.Wang, T.A.Tsiftsis, and P. K. Sharma, "Resource allocation for energy harvesting-powered d2d communication underlaying uav-assisted networks," *IEEE Transactions on Green Communications and Networking*, vol. 2, no. 1, pp. 14–24, 2018.

[91] L. Fan, N. Yang, T. Q. Duong, M. Elkashlan, and G. K. Karagiannidis, "Exploiting direct links for physical layer security in multiuser multirelay networks," *IEEE Transactions on Wireless Communications*, vol. 15, no. 6, pp. 3856–3867, 2016.

[92] J. Ye, Z. Liu, H. Zhao, G. Pan, Q. Ni, and M.-S. Alouini, "Relay selections for cooperative underlay cr systems with energy harvesting," *IEEE Transactions on Cognitive Communications and Networking*, vol. 5, no. 2, pp. 358–369, 2019.

[93] G.Im and J.H.Lee, "Outage probability for cooperative noma systems with imperfect sic in cognitive radio networks," *IEEE Communications Letters*, vol. 23, no. 4, pp. 692–695, 2019.

[94] X.Yue, Y.Liu, S.Kang, A.Nallanathan, and Z.Ding, "Exploiting full/half-duplex user relaying in noma systems," *IEEE Transactions on Communications*, vol. 66, no. 2, pp. 560–575, 2017.

[95] S.Lee, D.B.da Costa, and T.Q.Duong, "Outage probability of non-orthogonal multiple access schemes with partial relay selection," in *2016 IEEE 27th Annual International Symposium on Personal, Indoor, and Mobile Radio Communications (PIMRC)*, pp. 1–6, IEEE, 2016.

[96] L.Lv, J.Chen, and Q.Ni, "Cooperative non-orthogonal multiple access in cognitive radio," *IEEE Communications Letters*, vol. 20, no. 10, pp. 2059–2062, 2016.

[97] X.Kang, Y.C.Liang, A.Nallanathan, H.K.Garg, and R.Zhang, "Optimal power allocation for fading channels in cognitive radio networks: Ergodic capacity and outage capacity," *IEEE Transactions on Wireless Communications*, vol. 8, no. 2, pp. 940–950, 2009.

[98] Y.Pei, Y.C.Liang, K.C.Teh, and K.H.Li, "Secure communication in multiantenna cognitive radio networks with imperfect channel state information," *IEEE Transactions on Signal Processing*, vol. 59, no. 4, pp. 1683–1693, 2011.

[99] Z.Li, T.Jing, X.Cheng, Y.Huo, W.Zhou, and D.Chen, "Cooperative jamming for secure communications in mimo cooperative cognitive radio networks," in *2015 IEEE International Conference on Communications (ICC)*, pp. 7609–7614, 2015.

[100] P.H.Lin, F.Gabry, R.Thobaben, E.A.Jorswieck, and M.Skoglund, "Multi-phase smart relaying and cooperative jamming in secure cognitive radio networks," *IEEE Transactions on Cognitive Communications and Networking*, vol. 2, no. 1, pp. 38–52, 2016.

[101] Y.Y.He, J.Evans, and S.Dey, "Secrecy rate maximization for cooperative overlay cognitive radio networks with artificial noise," in *2014 IEEE International Conference on Communications (ICC)*, pp. 1663–1668, 2014.

[102] X.X.Nguyen and D.T.Do, "Optimal power allocation and throughput performance of full-duplex df relaying networks with wireless power transfer-aware channel," *EURASIP Journal on Wireless Communications and Networking*, vol. 2017, no. 1, p. 152, 2017.

[103] X.X.Nguyen and D.T.Do, "Maximum harvested energy policy in full-duplex relaying networks with swipt," *International Journal of Communication Systems*, vol. 30, no. 17, p. e3359, 2017.

[104] D.T.Do, MS.Van Nguyen, T.A.Hoang, and M.Voznak, "Noma-assisted multiple access scheme for iot deployment: Relay selection model and secrecy performance improvement," *Sensors*, vol. 19, no. 3, p. 736, 2019.

[105] K.An, M.Lin, and T.Liang, "On the performance of multiuser hybrid satellite-terrestrial relay networks with opportunistic scheduling," *IEEE Communications Letters*, vol. 19, no. 10, pp. 1722–1725, 2015.

[106] D.T.Do, "Optimal throughput under time power switching based relaying protocol in energy harvesting cooperative networks," *Wireless Personal Communications*, vol. 87, no. 2, pp. 551–564, 2016.

[107] V.Bankey, P.K.Upadhyay, D.B.Da Costa, P.S.Bithas, A.G.Kanatas, and U.S.Dias, "Performance analysis of multi-antenna multiuser hybrid satellite-terrestrial relay systems for mobile services delivery," *IEEE Access*, vol. 6, pp. 24729–24745, 2018.

[108] S.K.Sharma, S.Chatzinotas, and B.Ottersten, "Cognitive radio techniques for satellite communication systems," in *2013 IEEE 78th vehicular technology conference (VTC Fall)*, pp. 1–5, IEEE, 2013.

[109] S.Vassaki, M.I.Poulakis, A.D.Panagopoulos, and P.Constantinou, "Power allocation in cognitive satellite terrestrial networks with qos constraints," *IEEE Communications Letters*, vol. 17, no. 7, pp. 1344–1347, 2013.

[110] Z.Li, F.Xiao, S.Wang, T.Pei, and J.Li, "Achievable rate maximization for cognitive hybrid satellite-terrestrial networks with af-relays," *IEEE Journal on Selected Areas in Communications*, vol. 36, no. 2, pp. 304–313, 2018.

[111] X.Zhang, K.An, B.Zhang, Z.Chen, Y.Yan, and D.Guo, "Vickrey auction-based secondary relay selection in cognitive hybrid satellite-terrestrial overlay networks with non-orthogonal multiple access," *IEEE Wireless Communications Letters*, vol. 9, no. 5, pp. 628–632, 2020.

[112] P.Lai, H.Bai, Y.Huang, Z.Chen, and T.Liu, "Performance evaluation of underlay cognitive hybrid satellite–terrestrial relay networks with relay selection scheme," *IET Communications*, vol. 13, no. 16, pp. 2550–2557, 2019.

[113] K.Guo, K.An, B.Zhang, Y.Huang, and G.Zheng, "Outage analysis of cognitive hybrid satellite-terrestrial networks with hardware impairments and multi-primary users," *IEEE Wireless Communications Letters*, vol. 7, no. 5, pp. 816–819, 2018.

[114] D.T.Do, A.T.Le, C.B.Le, and B.M.Lee, "On exact outage and throughput performance of cognitive radio based non-orthogonal multiple access networks with and without d2d link," *Sensors*, vol. 19, no. 15, p. 3314, 2019.

[115] W.Shin, M.Vaezi, B.Lee, D.J.Love, J.Lee, and H.V.Poor, "Non-orthogonal multiple access in multi-cell networks: Theory, performance, and practical challenges," *IEEE Communications Magazine*, vol. 55, no. 10, pp. 176–183, 2017.

[116] Z.Ding, Z.Yang, P.Fan, and H.V.Poor, "On the performance of non-orthogonal multiple access in 5g systems with randomly deployed users," *IEEE signal processing letters*, vol. 21, no. 12, pp. 1501–1505, 2014.

[117] X.Wang, J.Wang, L.He, and J.Song, "Outage analysis for downlink noma with statistical channel state information," *IEEE Wireless Communications Letters*, vol. 7, no. 2, pp. 142–145, 2017.

[118] H.E.TZheng, A.S.Madhukumar, R.P.Sirigina, and A.K.Krishna, "An outage probability analysis of full-duplex noma in uav communications," in *2019 IEEE Wireless Communications and Networking Conference (WCNC)*, pp. 1–5, IEEE, 2019.

[119] I.Cosandal, M.Koca, E.Biglieri, and H.Sari, "Noma-2000 vs. pd-noma: An outage probability comparison," *IEEE Communications Letters*, vol. 25, 2020.

[120] J.A.Oviedo and H.R.Sadjadpour, "A fair power allocation approach to noma in multiuser siso systems," *IEEE Transactions on Vehicular Technology*, vol. 66, no. 9, pp. 7974–7985, 2017.

[121] Y.Ji, W.Duan, M.Wen, P.Padidar, J.Li, N.Cheng, and P.H.Ho, "Spectral efficiency enhanced cooperative device-to-device systems with noma," *IEEE Transactions on Intelligent Transportation Systems*, 2020.

[122] A.Anwar, B.C.Seet, S.F.Hasan, X.J.Li, P.H.J.Chong, and M.Y.Chung, "An analytical framework for multi-tier noma networks with underlay d2d communications," *IEEE Access*, vol. 6, pp. 59221–59241, 2018.

[123] L.Zhang, J.Liu, M.Xiao, G.Wu, Y.C.Liang, and S.Li, "Performance analysis and optimization in downlink noma systems with cooperative full-duplex relaying," *IEEE Journal on Selected Areas in Communications*, vol. 35, no. 10, pp. 2398–2412, 2017.

[124] D.T.Do and M.S.Van Nguyen, "Device-to-device transmission modes in noma network with and without wireless power transfer," *Computer Communications*, vol. 139, pp. 67–77, 2019.

[125] Z.Na, Y.Liu, J.Shi, C.Liu, and Z.Gao, "Uav-supported clustered noma for 6g-enabled internet of things: Trajectory planning and resource allocation," *IEEE Internet of Things Journal*, 2020.

[126] W.Mei and R.Zhang, "Uplink cooperative noma for cellular-connected uav," *IEEE Journal of Selected Topics in Signal Processing*, vol. 13, no. 3, pp. 644–656, 2019.

[127] D.Hu, Q.Zhang, Q.Li, and J.Qin, "Joint position, decoding order, and power allocation optimization in uav-based noma downlink communications," *IEEE Systems Journal*, vol. 14, no. 2, pp. 2949–2960, 2019.

[128] L.Bariah, S.Muhaidat, and A.Al-Dweik, "Error performance of noma-based cognitive radio networks with partial relay selection and interference power constraints," *IEEE Transactions on Communications*, vol. 68, no. 2, pp. 765–777, 2019.

[129] L.Lv, L.Yang, H.Jiang, T.H.Luan, and J.Chen, "When noma meets multiuser cognitive radio: Opportunistic cooperation and user scheduling," *IEEE Transactions on Vehicular Technology*, vol. 67, no. 7, pp. 6679–6684, 2018.

[130] W.Xu, X.Li, C.H.Lee, M.Pan, and Z.Feng, "Joint sensing duration adaptation, user matching, and power allocation for cognitive ofdm-noma systems," *IEEE Transactions on Wireless Communications*, vol. 17, no. 2, pp. 1269–1282, 2017.

[131] V.Singh, S.Solanki, P.K.Upadhyay, D.B.da Costa, and J.M.Moualeu, "Performance analysis of hardware-impaired overlay cognitive satellite–terrestrial networks with adaptive relaying protocol," *IEEE Systems Journal*, vol. 15, no. 1, 2020.

[132] P.K.Upadhyay and P.KSharma, "Max-max user-relay selection scheme in multiuser and multirelay hybrid satellite-terrestrial relay systems," *IEEE Communications Letters*, vol. 20, no. 2, pp. 268–271, 2015.

[133] K.An, J.Ouyang, M.Lin, and T.Liang, "Outage analysis of multi-antenna cognitive hybrid satellite-terrestrial relay networks with beamforming," *IEEE Communications Letters*, vol. 19, no. 7, pp. 1157–1160, 2015.

[134] D.BDa Costa and S.Aissa, "Cooperative dual-hop relaying systems with beamforming over nakagami-m fading channels," *IEEE Transactions on Wireless Communications*, vol. 8, no. 8, pp. 3950–3954, 2009.

[135] X.Li, J.Li, and L.Li, "Performance analysis of impaired swipt noma relaying networks over imperfect weibull channels," *IEEE Systems Journal*, vol. 14, no. 1, pp. 669–672, 2019.

[136] V. Adamchik and O. Marichev, "The algorithm for calculating integrals of hypergeometric type functions and its realization in reduce system," in *Proceedings of the international symposium on Symbolic and algebraic computation*, pp. 212–224, 1990.

[137] L.Yang and M.O.Hasna, "Performance analysis of amplify-and-forward hybrid satellite-terrestrial networks with cochannel interference," *IEEE Transactions on Communications*, vol. 63, no. 12, pp. 5052–5061, 2015.

[138] M.K.Arti, "Channel estimation and detection in hybrid satellite–terrestrial communication systems," *IEEE Transactions on Vehicular Technology*, vol. 65, no. 7, pp. 5764–5771, 2015.

[139] V.Singh, S.Solanki, and P.K.Upadhyay, "Cognitive relaying cooperation in satellite-terrestrial systems with multiuser diversity," *IEEE Access*, vol. 6, pp. 65539–65547, 2018.

[140] X.Zhu, C.Jiang, L.Kuang, N.Ge, S.Guo, and J.Lu, "Cooperative transmission in integrated terrestrial-satellite networks," *IEEE network*, vol. 33, no. 3, pp. 204–210, 2019.

[141] F.Li, K.Y.Lam, N.Zhao, X.Liu, K.Zhao, and L.Wang, "Spectrum trading for satellite communication systems with dynamic bargaining," *IEEE Transactions on Communications*, vol. 66, no. 10, pp. 4680–4693, 2018.

[142] K.An, M.Lin, W.P.Zhu, Y.Huang, and G.Zheng, "Outage performance of cognitive hybrid satellite–terrestrial networks with interference constraint," *IEEE Transactions on Vehicular Technology*, vol. 65, no. 11, pp. 9397–9404, 2016.

[143] Z.Chen, D.Guo, G.Ding, X.Tong, H.Wang, and X.Zhang, "Optimized power control scheme for global throughput of cognitive satellite-terrestrial networks based on non-cooperative game," *IEEE Access*, vol. 7, pp. 81652–81663, 2019.

[144] P.K.Sharma, P.K.Upadhyay, D.B.Da Costa, P.S.Bithas, and A.G.Kanatas, "Performance analysis of overlay spectrum sharing in hybrid satellite-terrestrial systems with secondary network selection," *IEEE Transactions on Wireless Communications*, vol. 16, no. 10, pp. 6586–6601, 2017.

[145] D.T.Do, "Time power switching based relaying protocol in energy harvesting mobile node: optimal throughput analysis," *Mobile Information Systems*, vol. 2015, pp. 1–8, 2015.

[146] Z.Song, X.Wang, Y.Liu, and Z.Zhang, "Joint spectrum resource allocation in noma-based cognitive radio network with swipt," *IEEE Access*, vol. 7, pp. 89594–89603, 2019.

[147] J.Du, F.R.Yu, G.Lu, J.Wang, J.Jiang, and X.Chu, "Mec-assisted immersive vr video streaming over terahertz wireless networks: A deep reinforcement learning approach," *IEEE Internet of Things Journal*, vol. 7, no. 10, pp. 9517–9529, 2020.

[148] J.Du, L.Zhao, X.Chu, F.R.Yu, J.Feng, and I.Chih-Lin, "Enabling low-latency applications in lte-a based mixed fog/cloud computing systems," *IEEE Transactions on Vehicular Technology*, vol. 68, no. 2, pp. 1757–1771, 2018.

[149] H.Wu, Y.Zou, J.Zhu, X.Xue, and T.Tsiftsis, "Secrecy performance of hybrid satellite-terrestrial relay systems with hardware impairments," in *ICC 2019-2019 IEEE International Conference on Communications (ICC)*, 2019.

[150] V.Bankey and P.K.Upadhyay, "Ergodic secrecy capacity analysis of multiuser hybrid satellite-terrestrial relay networks with multiple eavesdroppers," in *2019 IEEE International Conference on Communications Workshops (ICC Workshops)*, pp. 1–6, 2019.

[151] V.Bankey and P.K.Upadhyay, "Physical layer security of multiuser multirelay hybrid satellite-terrestrial relay networks," *IEEE Transactions on Vehicular Technology*, vol. 68, no. 3, pp. 2488–2501, 2019.

[152] P.K.Sharma and D.I.Kim, "Secure 3d mobile uav relaying for hybrid satellite-terrestrial networks," *IEEE Transactions on Wireless Communications*, vol. 19, no. 4, pp. 2770–2784, 2020.

[153] N.I.Miridakis, D.D.Vergados, and A.Michalas, "Dual-hop communication over a satellite relay and shadowed rician channels," *IEEE Transactions on Vehicular Technology*, vol. 64, no. 9, pp. 4031–4040, 2014.

[154] M.K.Arti and M.R.Bhatnagar, "Beamforming and combining in hybrid satellite-terrestrial cooperative systems," *IEEE Communications Letters*, vol. 18, no. 3, pp. 483–486, 2014.

[155] M.K.Simon and M.S.Alouini, *Digital communication over fading channels*, vol. 95. John Wiley & Sons, 2005.

[156] X.Li, M.Zhao, X.C.Gao, L.Li, D.T.Do, K.M.Rabie, and R.Kharel, "Physical layer security of cooperative noma for iot networks under i/q imbalance," *IEEE Access*, vol. 8, pp. 51189–51199, 2020.

[157] Y.Liu, Z.Ding, M.Elkashlan, and H.V.Poor, "Cooperative non-orthogonal multiple access with simultaneous wireless information and power transfer," *IEEE Journal on Selected Areas in Communications*, vol. 34, no. 4, pp. 938–953, 2016.

Candidate's Results Cited in the Dissertation

The list of results achieved within my Ph.D. study, where individual ideas of the dissertation are published.

[NHN01] **Nguyen, H.-N.**, Nguyen, N.-L., Nguyen, N.-T., Le A.-T., et al. *Reliable and Secure Transmission in Multiple Antennas Hybrid Satellite-Terrestrial Cognitive Networks Relying on NOMA*. IEEE Access, (2020), 8, pp. 215044-215056, DOI: 10.1109/ACCESS.2020.3041680. IF 3.367 (2020).

[NHN02] Nguyen, N.-L., **Nguyen, H.-N.**, Le, A.-T., Do, D.-T., et al. *On Performance Analysis of NOMA-Aided Hybrid Satellite Terrestrial Relay With Application in Small-Cell Network*. IEEE Access, (2020), 8, pp. 188526–188537, DOI: 10.1109/ACCESS.2021.3069247. IF 3.367 (2020).

[NHN03] Nguyen, N.-T., **Nguyen, H.-N.**, Nguyen, N.-L., Le, A.-T., et al. *Enhancing spectrum efficiency for multiple users in hybrid satellite-terrestrial networks*. IEEE Access, (2021), 9, pp. 50291–50300, 9388646, DOI: 10.1109/ACCESS.2021.3069247. IF 3.367 (2020).

[NHN04] **Nguyen, H.-N.**, Dang, H.-P., Le, S.-P., et al. *Enabling D2D Transmission Mode with Energy Harvesting and Information Transfer in Heterogeneous Networks*. Advances in Electrical and Electronic Engineering, (2018), 16(2), pp. 178–184, DOI: 10.15598/aeee.v16i2.2393.

[NHN05] **Nguyen, H.-N.**, Van, C.-H., Phan, V.-D., Nguyen, N.-T., et al. *Outage Performance of Underlay Cognitive Radio Networks over Mix Fading Environment*. International Journal of Electrical and Computer Engineering, (2021), 11(3), pp. 2019–2026, DOI: 10.11591/ijece.v11i3.pp2019-2026.

[NHN06] Le, S.-P., Van Nguyen, M.-S., Do, D.-T., **Nguyen, H.-N.**, et al. *Enabling Wireless Power Transfer and Multiple Antennas Selection to IoT Network Relying on NOMA*. Elektronika ir Elektrotechnika, (2020), 26(5), pp. 59–65, https://doi.org/10.5755/ j01.eie.26.5.27889. IF 0.684 (2018).

[NHN07] Dao, T.-T.T., Nguyen, N.-L., **Nguyen, H.-N.**, Le, S.-P., et al. *Exploiting Secure Performance of Full-Duplex Decode and Forward in Optimal Relay Selection Networks*. Elektronika ir Elektrotechnika, (2018), 24(4), pp. 72-76, DOI: 10.5755/j01. eie.24.4.21483. IF 0.684 (2018).

[NHN08] Do, D.-T., Le, C.-B., **Nguyen, H.-N.**, Tam, N.-K., et al. *Wireless power transfer enabled NOMA relay systems: two SIC modes and performance evaluation*. Telkomnika (Telecommunication Computing Electronics and Control), (2019), 17(6), pp. 2697–2703, DOI: 10.12928/Telkomnika.v17i6.12218.

[NHN09] Viet, N.-X., Thuy, D.T.-T., Phu, L.-S., **Nguyen, H.-N.**, et al. *Secure performance analysis of adaptive energy harvesting enabled relaying network*. Journal of Engineering Science and Technology, (2018), 13(12), pp. 4039-4052.

[NHN10] **Nguyen, H.-N.**, Nguyen NL., Nguyen, N.-T., Nguyen, N.-L., et al. *Outage Probability of CR-NOMA Schemes with Multiple Antennas Selection and Power Transfer Approach*. Advances in Networked-

Based Information Systems (NBiS), (2021), Springer, vol 313, pp 131-142, https://doi.org/10.1007/978-3-030-84913-9_12.

[**NHN11**] **Nguyen, H.-N.**, Le, S.-P., Le, C.-B., Nguyen, N.-L., et al. *Cognitive Radio Assisted Non−Orthogonal Multiple Access: Outage Performance.* 42nd International Conference on Telecommunications and Signal Processing (TSP), (2019), IEEE, pp. 449-453, DOI: 10.1109/TSP.2019. 8768873.

[**NHN12**] **Nguyen, H.-N.**, Dang, H.-P., Le, T.-D., Le, S.-P., et al. *On the Outage Probability of Device-to-Device Communication Enabled NOMA.* Advances in Intelligent Systems and Computing (IMIS), (2017), Springer, pp. 629–635, https: //doi.org/10.1007/978-3-319-61542-4_62, pp. 629-635.

[**NHN13**] Nguyen, N.-L., **Nguyen, H.-N.**, Nguyen, N.-T., Le, A.-T., et al. *On Secure Cognitive Radio Networks with NOMA: Design of Multiple-Antenna and Performance Analysis.* Proceedings of 2020 IEEE Workshop on Microwave Theory and Techniques in Wireless Communications (MTTW), (2020), IEEE, pp. 1–6, DOI: 10.1109/ MTTW51045.2020.9245070.

[**NHN14**] Le, S.-P., Le, C.-B., **Nguyen, H.-N.**, Nguyen, N.-L., et al. *Exploitting Performance Of Miso Based Non-Orthogonal Multiple Access.* 42nd International Conference on Telecommunications and Signal Processing (TSP), (2019), IEEE, pp. 454-458, DOI: 10.1109/TSP.2019.8768834.

[**NHN15**] Le, S.-P., **Nguyen, H.-N.**, Nguyen, N.-L., Do, D.-T., et al. *Device-to-Device Network with MISO Scheme for Wireless Power Transfer: Outage Performance Analysis.* 41st International Conference on Telecommunications and Signal Processing (TSP), (2018), IEEE, pp. 1-4, DOI: 10.1109/TSP.2018. 8441401.

[**NHN16**] Nguyen, N.-T., Le, T.T.-T., **Nguyen, H.-N.**, et al. *Cognitive Radio Architecture for WBAN in e-Health Applications: An Overview.* 6th NAFOSTED Conference on Information and Computer Science (NICS), (2019), IEEE, pp. 546–551, 9023802, DOI: 10.1109/NICS48868.2019.9023802.

About the Candidate

Research activities

I provide the following overview of indexed results in relevant scientific databases, in order to document my research activities within the entire period of my doctoral studies:

- Articles in journals indexed in WoS/Scopus: 8.
- Conference papers indexed in WoS/Scopus: 9.
- Citations: 28 in Scopus and 14 in Web of Science.
- ORCID: 0000-0002-3094-4454
- Research ID: ABC-6180-2020

Participation in Research Project

The research leading to the results shown in the dissertation received funding from:

- Proj. reg. no. SP2018/59 - Networks and Communications Technologies for Smart Cities I., Student Grant Competition of VSB-TUO (2018).
- Proj. reg. no. SP2019/41 - Networks and Communications Technologies for Smart Cities II., Student Grant Competition of VSB-TUO (2019).
- Proj. reg. no. SP2020/65 - Networks and Communications Technologies for Smart Cities III., Student Grant Competition of VSB-TUO (2020).
- Proj. reg. no. SP2021/25 - Networks and Communications Technologies for Smart Cities IV., Student Grant Competition of VSB-TUO.(2021)